SYNTHESIS AND SELF-ASSEMBLY OF FUNCTIONAL BOTTLEBRUSH DIBLOCK COPOLYMERS

by

Yonghui Wang

B.Eng., Sichuan University, 2016

A THESIS SUBMITTED IN PARTIAL FULFILLMENT OF

THE REQUIREMENTS FOR THE DEGREE OF

MASTER OF SCIENCE

in

THE FACULTY OF GRADUATE AND POSTDOCTORAL STUDIES

(Chemistry)

THE UNIVERSITY OF BRITISH COLUMBIA

(Vancouver)

January 2019

The following individuals certify that they have read, and recommend to the Faculty of Graduate and Postdoctoral Studies for acceptance, a thesis/dissertation entitled:

SYNTHESIS AND SELF-ASSEMBLY OF FUNCTIONAL BOTTLEBRUSH DIBLOCK COPOLYMERS

submitted by Yonghui Wang in partial fulfillment of the requirements for

the degree of Master of Science

in Chemistry

Examining Committee:

Prof. Zachary M. Hudson
Supervisor

Prof. Parisa Mehrkhodavandi
Supervisory Committee Member

Prof. Derek P. Gates
Supervisory Committee Member

Prof. Michael D. Fryzuk
Supervisory Committee Chair

Abstract

Bottlebrush copolymers have shown promise as building blocks for self-assembled nanomaterials due to their reduced chain entanglement relative to linear polymers and their ability to self-assemble with remarkably low critical micelle concentrations (CMCs). Concurrently, the preparation of bottlebrush polymers from organic electronic materials has recently been described, allowing multiple optoelectronic functions to be incorporated along the length of single bottlebrush strands. Here we successfully synthesized well-defined bottlebrush diblock copolymers containing soluble n-butyl acrylate blocks and carbazole-based organic semiconductors with control over the backbone length ratio. Then the successful incorporation of highly fluorescent dye molecules into the BBCP was achieved by using the CzBA polymer as an organic semiconductor host to facilitate energy transfer.

We also describe the self-assembly of these molecular bottlebrushes, which self-assemble in selective solvent to give spherical micelles with CMCs below 54 nM. These narrowly dispersed structures were stable in solution at high dilution over periods of months, and could further be functionalized with fluorescent dyes to give micelles with quantum yields of unity. These results demonstrate that bottlebrush-based nanostructures can be formed from organic semiconductor building blocks, opening the door to the preparation of fluorescent or redox-active micelles from giant polymeric surfactants.

Lay Summary

Bottlebrush polymers are large molecules consisting of molecular side chains attached to a central molecular chain. This type of molecule has shown promise for use in self-forming nanomaterials. Recently, it has been shown that organic electronic materials can be used to prepare these bottlebrush polymers. This allows for different types of electronic functions to be incorporated along the length of a single molecular strand. Here we describe the successful formation of bottlebrush polymers from organic semiconductor molecules. We then incorporate highly fluorescent dye molecules into the polymer. The organic semiconductors are used to transfer energy to the fluorescent dye. We also describe the self-formation of spherical molecular assemblies (micelles) from the bottlebrush polymers in solution. These molecular assemblies are stable for months and their fluorescence can be further modified. The formation of such structures from organic semiconductors paves the way for fluorescent or electronically active micelles from giant polymeric molecules.

Preface

All experiments described herein were performed by me except as noted below. This thesis was revised and edited by my supervisor Prof. Zachary M. Hudson. Dr. Feng Shao obtained the TEM images of bottlebrush diblock copolymers. Ethan Sauvé conducted the reaction for synthesizing **poly(CzBA)$_{15}$-Br** and obtained the AFM images after I prepared the samples on HOPG. Chris Tonge synthesized the blue fluorescent acrylic dye **PAPOMA** as well as **CzBA** monomers, and obtained the quantum yield of (**nBuA-MM)-*b*-(CzBA-*co*-PAPOMA-MM)**.

Table of Contents

List of Tables

List of Figures

List of Schemes

List of Symbols and Abbreviations

χ	the Flory-Huggins parameter
AFM	atomic force microscopy
ATRP	atom transfer radical polymerization
BBCPs	bottlebrush copolymers
BCPs	block copolymers
BHT	butylated hydroxytoluene
CMC	critical micelle concentration
CPR	controlled living radical polymerization
Cryo-TEM	cryogenic transmission electron microscopy
Cu(0)-RDRP	copper(0) reversible-deactivation radical polymerization
CuAAC	copper-catalyzed alkyne-azide cycloaddition
CzBA	4-(9H-carbazol-9-yl)benzyl acrylate
DLS	dynamic light scattering
DMF	dimethylformamide
DSC	differential scanning calorimetry
EBiB	ethyl α-bromoisobutyrate
EPR	enhanced permeability and retention
f	volume fraction of each block
F	free energy
G1	1st generation Grubbs catalyst
G2	2nd generation Grubbs catalyst
G3	3rd generation Grubbs catalyst
HOPG	highly oriented pyrolytic graphite
l	segment length
Me	methyl
Me_6TREN	tris[2-(dimethyl-amino)ethyl]amine
MEHQ	4-hydroxyanisole
MMs	macromonomers
M_n	number-average weight molecular weight

MWs	molecular weights
n	refractive index
N	the degree of polymerization
nBuA	n-butyl acrylate
NHC	*N*-heterocyclic carbene
nM	nanomolarity
NMP	nitroxide-mediated polymerization
NMR	nuclear magnetic resonance spectroscopy
ODT	order-to-disorder transition
OLED	organic light emitting diode
p	packing parameter
P3HT-*b*-PCBM	poly(3-hexylthiophene):[6,6]-phenyl C61-butyric acid methyl ester
PAA	poly(acrylic acid)
PAPOMA	(4'-(5-(4-(bis(4-(tert-butyl)phenyl)amino)phenyl)-1,3,4-oxadiazol-2-yl)-[1,1'-biphenyl]-4-yl)methyl acrylate
PB	poly(butadiene)
PDI or Đ	polydispersity
PFS	polyferrocenyldimethylsilane
PI	polyisoprene
PMA	poly(methyl acrylate)
PS	poly(styrene)
R_A	the micelle core radius
RAFT	reversible addition-fragmentation chain transfer
R_B	the thickness of the shell
RDRP	reversible-deactivation radical polymerization
RIE	reactive ion etching
ROMP	ring opening metathesis polymerization
ROP	ring opening polymerization
SANS	small angle neutron scattering
SAXS	small angle X-ray scattering
SCMF	self-consistent mean-field theory

SEC	size exclusion chromatography
SSL	strong segregation limit
T	temperature
TEM	transmission electron microscopy
TFE	trifluoroethanol
T_g	glass transition temperature
THF	tetrahydrofuran
UV-vis	ultraviolet-visible spectroscopy
WSL	weak segregation limit

Acknowledgements

First of all, I would like to thank my supervisor Prof. Zachary M. Hudson for always being there to help me throughout my graduate school career, not only as an excellent research advisor but also as an encouraging teacher and mentor. I have been very lucky to have a supervisor who is a passionate, brilliant scientist that cares a lot about my progress and career. His passion and work ethic will always inspire me.

I would also like to thank my wonderful labmates for their support and friendship, including Dr. Feng Shao, Ethan Sauvé, Zoë Hackett, Cheyenne Christopherson, Donny Mayder, Chris Tonge, Kyle Thompson, Nathan Paisley, Jade Poisson, and Alex Polgar. I'm very grateful for the constructive suggestions from Ethan and Chris as well as their generous help with my project. I also appreciate that Cheyenne taught me how to operate DSC and analyze the data. My deep thanks go to our postdoctoral fellow Dr. Feng Shao for being a great friend and a supportive coworker, who helped me with TEM and DLS characterization and made research life more enjoyable.

I would like to thank people who helped me from other group and facilities. Brad Ross from the Bioimaging Facility helped me optimize the TEM conditions with great patience. Dr. Charlotte E. Boott, postdoctoral fellow from the MacLachlan group, gave me valuable advice on self-assembly techniques and characterization. My friends Wenxuan Zhang and Arvind Soni from the Tanner group helped me with Mass Spectroscopy. I also thank Mitacs for providing me the graduate student fellowship.

Finally, words can't even express my thanks to my family, my friends, and my dearest boyfriend Brendan. They supported me through the toughest of times and shared every special moment in my life. Their love made me a better person.

To my parents and my grandparents,

For their unconditional love and support

Chapter 1: Introduction

Self-assembly is a process by which an ordered complex structure spontaneously forms from basic units, based on specific interactions among the units. Biological systems depend on a variety of functional nanoscale structures that are constructed by the self-assembly of molecular components. For example, the cell membrane is self-assembled by structurally unique amphiphilic phospholipids into a well-defined bilayer, which provides a selective gate between the cell and its environment.[1] DNA stores biological information in the double helix structure from self-assembly of nucleotides, stabilized by hydrogen bonding and aromatic base stacking.[2] Also, enzyme function is well-controlled in living cells by means of compartmentalization and positional assembly of proteins.[3,4] In fact, the phenomenon of self-assembly may have been responsible for the origins of life.[5-6] The complexity and precision of self-assembled structures exhibited by biological systems are derived from self-stabilization through tensegrity, which describes an internal balance between continuous tension and local compression in a three-dimensional structure.[6]

To exploit nature's self-assembly principles, small amphiphilic molecules have been synthesized to create nanomaterials with hierarchical structures and tailored properties. Small molecule amphiphiles, also known as surfactants, consist of hydrophobic tails less than 10-carbon atoms in length and a hydrophilic head group. Their unique chemical structure and associated self-assembly behaviour motivate the studies on molecular self-assembly principles, theories, structures, and properties of assemblies. After many decades of study, various assembly morphologies have been observed in bulk and in aqueous solution.[7-11] The morphologies include spherical micelles (spheres), cylindrical micelles (cylinders), bicontinuous structures, lamella, and vesicles, among others. These surfactant micelles can be used for various applications. The most common commercial applications are personal care and cleaning products in our homes, which

generate bubbles originating from the self-assembly of small-molecule surfactants such as sodium lauryl sulfate (SLS) and sodium dodecyl sulfate (SDS). Also self-assembly of surfactants at the monomer/water interface has been used to generate multi-scale topographical features on polymer substrates for stem cell growth and differentiation.[12] There is growing interest in developing self-assembly of amphiphiles for applications in nanotechnologies including biosensors, medical imaging, drug delivery, and nanoreactors.[3,13-15]

Macromolecular amphiphiles are analogous to amphiphilic small molecules with hydrophobic and hydrophilic regions increased in size by 1~2 orders of magnitude. Amphiphilic polymers which have already been studied extensively include block copolymers of the AB, ABA or ABC types, as well as different graft copolymers. Compared to small molecule aggregates, polymer aggregates display higher stability and durability due to their mechanical and physical properties.[16] Also due to their synthetic versatility, tunable self-assembly, and favorable solution properties, macromolecular amphiphiles have attracted considerable attention toward their potential applications in many fields, such as medicine, microelectronics, photoelectric materials, diagnostic imaging, and emulsion stabilizers.[17-21]

Accordingly, this chapter will focus on the self-assembly of block copolymers, from fundamental theories to morphology characterization and potential applications. Then molecular polymer brushes, also known as graft copolymers, will be introduced, including relevant synthetic strategies and potential applications. The last section will overview the importance and purpose of the current work.

1.1 Self-assembly of block copolymers (BCPs)

Block copolymers consist of two or more homopolymer subunits connected by covalent bonds. Each incompatible block displays different physical and chemical properties, which enable block copolymers to assemble into micellar structures in selective solvent and to form ordered films on the surface of substrates. The morphologies, functionalities and sizes obtained can be tuned by a combination of polymer compositions and self-assembly conditions.[18,22-26] This provides opportunities to develop self-assembly strategies for block copolymers to build nanostructures with complex functionalities.

1.1.1 Fundamental theories

1.1.1.1 Block copolymers in bulk

In bulk, block copolymers will microphase separate due to the incompatibility of different blocks. An unfavorable mixing enthalpy coupled with a small mixing entropy drives the self-assembly behaviors, while the covalent bond connecting the different blocks prevent macroscopic phase separation.[27] The microphase separation of block copolymers depends on three parameters: (1) the volume fractions of each block; such as a diblock (f_A and f_B, with $f_A + f_B = 1$) or triblock (f_A, f_B and f_C, with $f_A + f_B + f_C = 1$); (2) the total degree of polymerization (N); and (3) the Flory-Huggins parameter, χ_{AB} for diblocks, or χ_{AB}, χ_{AC}, and χ_{BC} for triblocks.[28,29] The χ-parameter defines the degree of incompatibility between each pair of blocks, which reflects the interaction energy between different blocks and is the driving force of microphase separation. For diblock copolymers, the relationship between χ_{AB} and temperature (T) is given in equation (1): [16,30]

$$\chi_{AB} = \left(\frac{z}{k_B T}\right)\left[\varepsilon_{AB} - \frac{1}{2}(\varepsilon_{AA} + \varepsilon_{BB})\right] \quad (1)$$

where z is the number of nearest neighbors per repeat unit in the polymer, k_B is Boltzmann's constant, and k_BT represents the available thermal energy. ε_{AB}, ε_{AA}, and ε_{BB} are the interaction energies per repeat unit of *A*-*B*, *A*-*A*, and *B*-*B*, respectively. As temperature increases, the value of χ_{AB} decreases, which indicates the incompatibility between the constituent blocks decreases. A negative value of χ_{AB} results from a favorable energy of mixing, which means the average of contact energies of *A*-*A* and *B*-*B* segment-segment interactions is larger than the contact energy of *A*-*B* segment-segment interactions. Usually when there are no strong specific interactions between *A*-*B* segments, such as hydrogen bonding, ionic charges or host-guest interactions, χ_{AB} is small and positive. When $\chi_{AB} > 0$ a decrease in *A*-*B* contacts in an AB diblock copolymer reduces the system enthalpy *H*. While the enthalpy contribution to Gibbs energy is related to χ, the configurational entropy contribution to the Gibbs energy is proportional to N^{-1}. Therefore, the segregation product (χN) is important for determining the microstructures of diblocks.[27,31,32]

Here is an example for the symmetric case (f_A = 0.5). For $\chi N \ll 10$, diblocks exist in a disordered homogeneous state and *A*-*B* interactions are relatively weak.[33] The balance of Gibbs free energy can be shifted by increasing N or χ, which leads to microphase separation.[34] As χN increases to 10, a delicate balance between energetic and entropic factors produces a disorder-to-order phase transition.[27] When $\chi N \gg 10$, energetic factors dominate and ordered microstructures are formed (see Figure 1.1). Changes in f_A mainly affect the shape and packing symmetry of the ordered microstructure. f_A is almost independent of χN, except near the order-to disorder transition (ODT).[35]

In terms of χN, two theories have been developed to study the phase behaviour of diblock

copolymers in bulk, which are the weak segregation limit (WSL) ($\chi N \leq 10$) and strong segregation limit (SSL) ($\chi N \gg 10$). In SSL theories, sharp boundaries appear among well-ordered microdomain structures as result of chain stretching. In WSL theories, the ordered composition profile is approximately sinusoidal with lower amplitude, which is based on unperturbed Gaussian coils as result of weak *A*-*B* segment-segment interactions[27] Mean-field SSL theories successfully predict how microdomain symmetry, size, and periodicity depend on *N*, *f*, and χ away from ODT, while WSL theories simplify calculations for order-to-disorder transition (ODT) theories.[36] To span the range, self-consistent mean-field (SCMF) theory has been developed. Figure 1.2 shows morphology changes of diblock copolymers predicted by SCMF theory when $f_A < 0.5$. The order-to-disorder transition (ODT) starts from closely packed spheres (CPS), passing through body-centered cubic spheres (S), hexagonally packed cylinders (C) and bicontinuous gyroids (G), to lamellae (L), when f_A increases at a fixed χN above 10.5.[33,37,38] Morphology inversion occurs with increasing f_A when $f_A > 0.5$ (L $\rightarrow$ G $\rightarrow$ C $\rightarrow$ S $\rightarrow$ CPS $\rightarrow$ disordered). The morphologies and their transitions have been verified experimentally through polystyrene-polyisoprene diblock copolymers (PS-*b*-PI).[30]

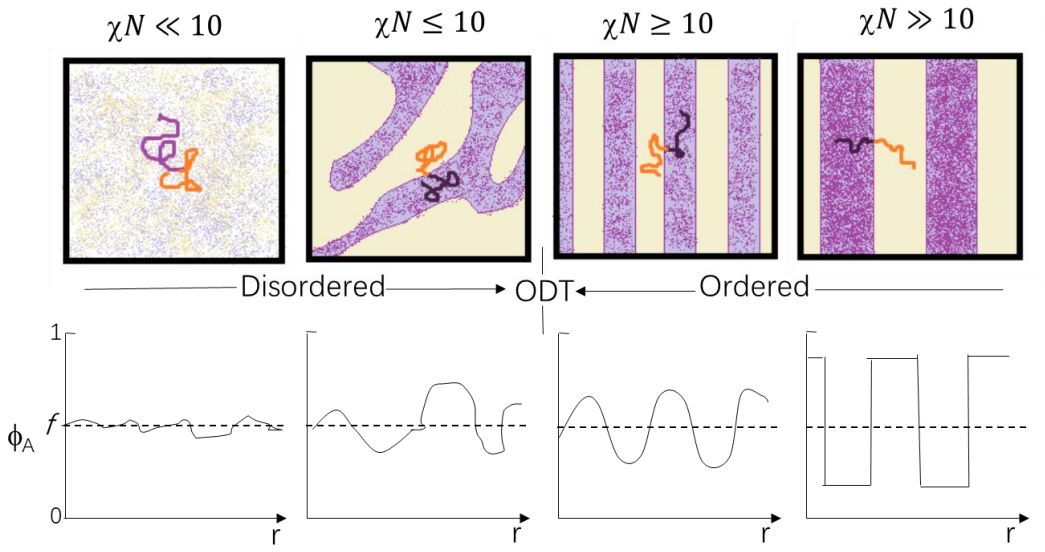

Figure 1.1. Change of structure according to the combined parameter χN for a symmetric, diblock copolymer with f_A = 0.5. ϕ_A and f refer to the local and stoichiometric (i.e. macroscopic) A-block volume fractions, respectively. When $\chi N \sim 10$, small variations in system entropy ($\sim N^{-1}$) or energy (χ) leads to ordered ($\chi N \geq 10$) or disordered ($\chi N \leq 10$) states. Adapted from reference [30].

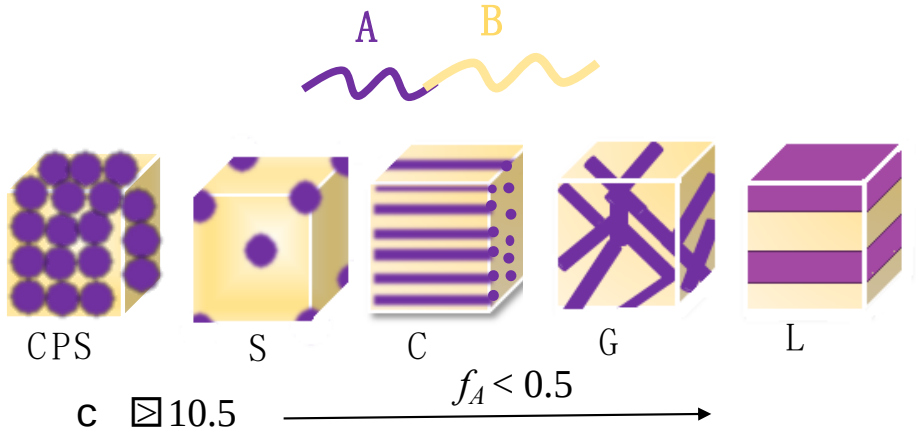

Figure 1.2. Morphology transitions of AB diblock copolymers in bulk: CPS = closely packed spheres, S = body-centered cubic spheres, C = hexagonally packed cylinders, G = bicontinuous gyroid, L= lamellae. Adapted from reference [16].

To summarize the above, morphological transitions depend on two competing factors: an enthalpic contribution from interfacial energy between two blocks, and an entropic contribution

from chain stretching. Microphase separation occurs because chains stretch away from preferred random coils to minimize interfacial area between two blocks in order to lower the interfacial energy.[33] The degree of chain stretching depends on the volume fraction of one block relative to that of the diblock. When f_A is small, the A blocks tend to aggregate into spheres, with the B blocks surrounded outside as coronas. As f_A increases, the corona volume fraction decreases and interfaces with lower curvature are formed. This leads to cylinders and lamellae.[35,39-41]

1.1.1.2 Block copolymers in solution

Compared to BCP self-assembly in bulk, self-assembly of diblock copolymers in solution is more complicated. As for *A*-*B* diblock copolymers, its self-assembly process involves six Flory-Huggins solvent/polymer interaction parameters χ, namely χ_{AB}, χ_{AG}, χ_{AS}, χ_{BG}, χ_{BS}, χ_{GS}, where *A* and *B* represent the two blocks, *G* stands for the good solvent for both blocks, and *S* expresses the selective solvent for one of the blocks.[42] The complexity of a self-assembly process depends on the number of components present in the solution. These parameters are furthermore directly correlated with the solubility parameter δ of the compounds. Knowing the "solubility parameter" (δ) of solvents and polymers is helpful for the selection of selective solvents, which is important to induce the self-assembly of block copolymers in solution.

Similar with small molecule amphiphiles, block copolymers also self-assemble into spherical micelles, cylindrical micelles, and vesicles in aqueous solution or organic solvent.[43-45] The morphology can be controlled by varying block copolymer compositions, and is determined by the packing parameter p ($p = \frac{v}{a_0 l_c}$, where v is the volume of the hydrophobic segment, a_0 is the

contact area of the head group, and l_c is the length of the hydrophobic segment).[46] Figure 1.3 shows the relationship between micelle structures and packing parameter p. When $p < \frac{1}{3}$, spherical micelles are formed; when $\frac{1}{3} < p < \frac{1}{2}$, cylindrical micelles; when $\frac{1}{2} < p < 1$, vesicles and lamellae; when $p = 1$, lamellae.[47]

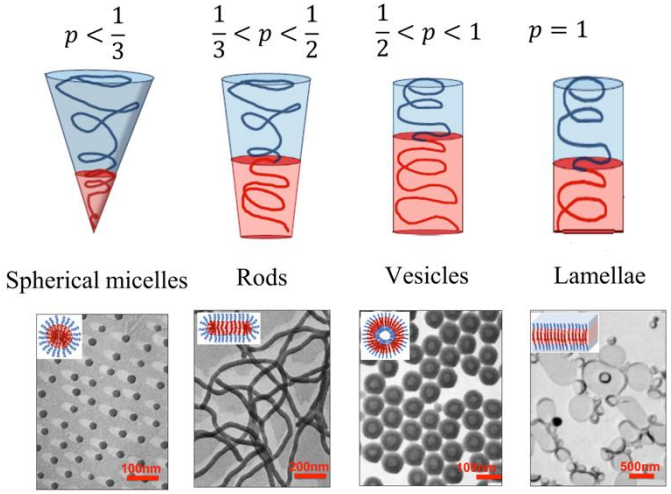

Figure 1.3. Representation of micelle structures formed by block copolymers. The structure depends on the packing parameter *p*. Reproduced from reference [47].

Thermodynamics of block copolymer micelles

Micelle morphologies of block copolymers are determined by a balance among the free energy contributions of the interfacial energy, core chain stretching, and corona chain repulsion at equilibrium. The balance is described by two theories: scaling approaches and mean-field theories.[48] The scaling approaches provide us with useful and simple relations of how the size of the micellar core and corona depend on the degree of polymerization of the different blocks. Mean field theories apply a potential field to the configurations of chain molecules, to effectively study how the degree of polymerization of different blocks and polymer/solvent interaction parameters

χ influence the micelle aggregation number, domain sizes, micellar volume fraction, and critical micelle concentration.[46,49] Scaling theories work best for systems with strong excluded volume interactions, while mean field theories work best for systems with weak polymer-solvent interactions and excluded volume interactions.[49]

In scaling theories, micellization of AB-diblock copolymers is discussed. It assumes that the micelles are monodisperse and their concentration is too low for the micelles to interact with each other. A micelle consists of an incompressible spherical core from A blocks and a spherical shell from B blocks (corona). The total free energy of a micelle is approximated according to the interfacial tension (enthalpic) and the chain stretching (entropic): $F = F_{interface} + F_{core} + F_{shell}$, where $F_{interface}$ describes the interfacial free energy, F_{core} represents the stretching free energy of A blocks in the core, and F_{shell} is the repulsion free energy of B blocks in the shell. Minimization of $F_{interface}$ is the driving force to form micelles. $F_{interface}$ is determined by the following equation (2):

$$F_{interface} \approx \gamma {R_A}^2 \tag{2}$$

in which R_A is the micelle core radius, γ is the interfacial tension, and the symbol $\approx$ denotes equal within a numerical factor of one order of magnitude. F_{core} is due to chains uniformly stretching in the core and is expressed as the following equation (3);

$$\frac{F_{core}}{kT} \approx p\left(\frac{R_A}{{N_A}^{1/2} l}\right)^2 \tag{3}$$

in which k is Boltzmann's constant, T is temperature, l is the segment length, p represents the aggregation number and N_A is the degree of polymerization of A blocks (core). F_{shell} is due to the repulsion of chains in the shell, which is different for two limiting cases: the large core case for $N_A \gg N_B$ ("crew cut micelles") and the small core case for $N_A \ll N_B$ ("hairy micelles") (see Figure

1.4). In the case of the large core, the volume fraction of B segments is constant in the shell, while in the case of small core, the volume fraction of B segments is assumed to decrease with increasing distance from the core.[46] Therefore, for crew cut micelles,

$$\frac{F_{shell}}{kT} \approx p\left(\frac{R_B}{{N_B}^{1/2}l}\right)^2 \quad (4)$$

in which R_B is the thickness of the shell.[46,49] As for hairy micelles,

$$\frac{F_{shell}}{kT} \approx p^{3/2} \quad (5)$$

R_A, R_B are also correlated to N_A, N_B, p, and l,

$${R_A}^3 \approx pN_A l^3 \quad (6)$$

$$R_B \approx p^{1/5}{N_B}^{3/5}l \quad (7)$$

Substitution of $F_{interface}$, F_{core}, F_{shell} in $F = F_{interface} + F_{core} + F_{shell}$ using equations (2-5) and elimination of R_A, R_B by employing equations (6-7) leads to two free energy expressions of a single micelle for two limiting cases respectively, where the aggregation number p is the only unknown parameter. The aggregation number can be determined by minimization of the free energy per polymer chain, *F/p*. For the case of large cores ($N_A \gg N_B$), $F_{core} \gg F_{shell}$,

$$p \approx \gamma N_A \quad (8)$$

$$R_A \approx \gamma^{1/3}{N_A}^{2/3}l \quad (9)$$

In the opposite limit with small cores ($N_A \ll N_B$), $F_{core} \ll F_{shell}$,

$$p \approx \gamma^{6/5}{N_A}^{4/5} \quad (10)$$

$$R_A \approx \gamma^{2/5}{N_A}^{3/5}l \quad (11)$$

$$R_B \approx \gamma^{6/25}{N_A}^{4/25}{N_B}^{3/5}l \quad (12)$$

To summarize the scaling approaches, the aggregation number and size are dependent on the degree of polymerization of the core and corona block ($N_{A,}N_B$), interfacial tension (γ), and the segment length (l).[50-52] It provides theoretical proof of tuning micelle structures by controlling the composition of block copolymer and solvent selectivity. Scaling theories have been proven experimentally by PS-*b*-PAA copolymers.[53]

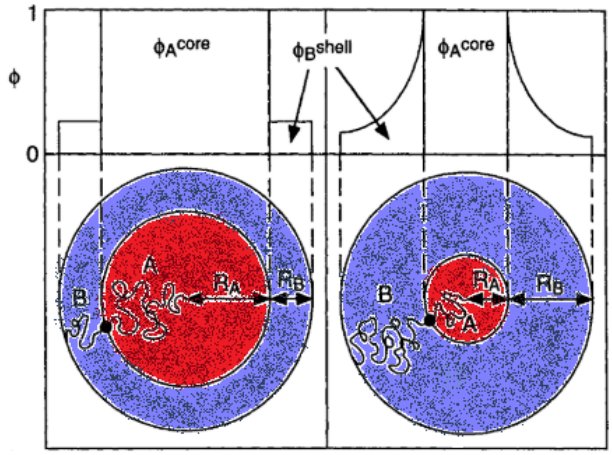

Figure 1. 4. Schematic representation of crew-cut micelles (left) and hairy micelles (right) of AB-diblock copolymers as considered by scaling theories. The volume faction profiles ($\phi_{B,}\phi_{A)}$ are attached for the large core case ($\boldsymbol{N_A \gg N_B}$) and the small core case ($\boldsymbol{N_A \ll N_B}$). Adapted from reference [46].

In mean-field theories, the various interactions described by Flory-Huggins χ-parameters are considered. Similar with scaling approaches, core-shell models are applied, which assumes the physical separation of the two different blocks of the copolymer into two domains, the core and the shell (corona). Based on this separation, a free energy expression represents the free energy of the micelle with respect to some reference state as the following equation (13):

$$F = \left(F_{interface} + F_{elastic} - TS_{shell}\right) + F_{solution} - TS_{mixing} \quad (13)$$

where $F_{interface}$ denotes the interfacial free energy of the interface between the core (A-blocks) and the shell (B-blocks), $F_{elastic}$ arises from the elastic deformation of the copolymers in the micelle, TS_{shell} represents the mixing free energy of solvent molecules with the B-blocks in the shell, $F_{solution}$ and TS_{mixing} stand for the free energy of the homogeneous solution outside the micelles and the free energy of mixing the micellar aggregates in the micellar solution. These free energy variables are dependent on a few parameters, such as Flory-Huggins χ-parameter, domain sizes, and micellar volume fraction. After minimizing *F* with respect to these parameters, the equilibrium properties of the micellar solution can be obtained. The detailed math will not be discussed here.[46]

Kinetics of block copolymer micelles

Micelle structure and morphology depend on not only thermodynamic factors, but also kinetic factors, such as copolymer concentration, solvent changes, pressure/temperature jumps, and the presence of additives. In general, two kinetic mechanisms are responsible for changes in micelle size and structure: single chain exchange and micelle fusion/fission (Figure 1.5).[54-56] In single chain exchange, a polymer chain diffuses through solution after being discharged from one micelle, and then rejoins into another micelle. Fusion occurs when two micelles collide and recombine into a larger micelle. Fission is the reverse process where a larger micelle breaks into two smaller micelles.

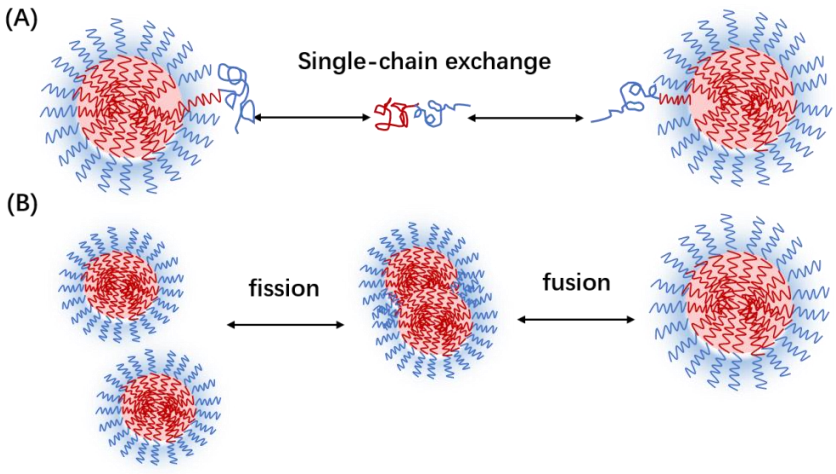

Figure 1. 5. Schematic representation of single chain exchange (A) and fusion/fission (B). Adapted from ref. [57,58].

Near equilibrium, single chain exchange dominates the dynamics in block copolymer micelles.[59] The rate of chain exchange is dependent on the solvent selectivity for each of the block copolymers. Chain exchange is relatively slower in highly selective solvents than in mildly selective solvents.[60,61] On the other hand, the length of corona blocks and micelle sizes can also influence the chain exchange rate.[62-65]

Before equilibrium, the dominant dynamic process in micellar systems is still unclear. Choi monitored the chain exchange events in the spherical micelle formation of diblock copolymers by time-resolved small-angle neutron scattering (TR-SANS).[57] In contrast, Dormidontova suggested that fusion is the preferred growth mechanism in micelles.[66] Cui applied fusion to explain the sphere-to-cylinder morphological transition of PAA_{94}-*b*-PMA_{103}-*b*-PS_{44} when THF was introduced to an aqueous solution of the polymer micelles.[54] Recently, Sun described the new morphology of dumbbells of tubules formed by fusion of tubules, which originate from the self-assembly of P4VP-*b*-PS.[67] Ren also observed the fusion of adjacent vesicles when photosensitive micelles were irradiated with green light.[68] However, Rharbi argued that fusion may also occur at

equilibrium as well as single chain exchange, although the fusion is much slower.[58] Thus, the mechanisms governing micelle structure evolution are still unsolved and a better understanding of macromolecular assemblies are required.

1.1.2 Morphology characterization

Various morphologies have been obtained by BCP self-assembly in solution, some of which are thermodynamically induced, while others are kinetically controlled. These morphologies have been studied by the following characterization techniques: dynamic light scattering (DLS), small angle X-ray and neutron scattering (SAXS and SANS), transmission electron microscopy (TEM and Cryo-TEM), scanning electron microscopy (SEM), and atomic force microscopy (AFM).

Although with the drawback that it is model-dependent, DLS provides quantitative information on the micelle sizes and size distribution, as well as critical micelle concentration (CMC). DLS can be used to screen the effects of processing techniques on BCPs and select samples for further studies. More detailed nanostructure characterizations are performed using both SAXS and SANS, which can distinguish the different shapes of micelles by q-range, and analyze the core and corona of the micelles separately using a contrast variation method.[69] TEM, SEM and AFM can provide direct visualization of block copolymer micelles. Recently, nanoscale coronal segregation in rod-like micelles was visualized by TEM.[70] As for Cryo-TEM, it even allows direct observation of micelles in a glassy water phase and accordingly determines the characteristic dimensions of both the core and swollen corona.

However, TEM requires stain techniques to improve the electronic contrast of block copolymer micelles containing light elements (such as C, H, N, O). Drying and staining can influence the resulting morphology of micelles, leading to misinterpretation of solution assemblies.

And Cryo-TEM is most frequently performed in water instead of in organic solvents. AFM may deform micelles by tip-convolution effects, or by specific interactions between the substrate and some moieties of the block copolymer. The selectivity of suitable techniques to characterize the macromolecular assemblies requires consideration of BCP composition and self-assembly conditions.

Alongside the development of the above characterization techniques, a wide range of nanoscale structures has been identified from the self-assembly of BCPs. For example, crew-cut aggregates include more than 20 morphologies, such as spherical micelles, rods, bicontinuous structures, lamellae, vesicles, large compound micelles (LCMs), large compound vesicles (LCVs), tubules, "onions", "eggshells", etc.[47,71] Among these morphologies, some are thermodynamically controlled, such as spheres, rods, bicontinuous rods, lamellae, and vesicles. Others are kinetically controlled, such as LCVs and tubules. The most commonly observed morphologies will be described further here.

Spherical micelles consist of a spherical hydrophobic/solvophobic core surrounded by hydrophilic/solvophilic coronal chains. It is required that the longest hydrophobic/solvophobic chain in its planar zigzag configuration must always be longer than the radius of the core. Spherical micelles have been applied extensively to study thermodynamics of BCP assemblies, such as the "crew cut micelle" model and "hairy micelle" model for scaling theories.[30] They also can be considered as the starting morphology for other aggregates.[72,73] For example, David J. Kinning proved that structural transitions can occur from spherical to non-spherical micelles by increasing the molecular weight of homopolymer additives.[74] In addition, spherical micelles are able to carry dyes and hydrophobic drugs in their hydrophobic cores, while the surrounding hydrophilic shell allows for high solubility and stability of the micelles themselves.[75,76]

Rods (cylindrical or wormlike micelles) are composed of a cylindrical core and a corona surrounding the core. Since long cylinders allow uniform curvature across the entire aggregate, they are generally more energetically favoured than shortened cylinders.[77] Recently developed "living self-assembly" strategies have achieved good control of the rod length in cylindrical micelles as well, as the crystalline nature of polyferrocenyldimethylsilane (PFS) is a key feature that promotes the formation of cylinders.[78,79] Moreover, worm-like micelles have shown a high drug loading capacity and increased *in vivo* circulation time by overcoming biological processes responsible for clearance of nanocarriers.[80] Therefore, cylindrical micelles are ideal for flow-intensive drug delivery applications.

Bilayers (lamellae and vesicles) occur in the next stage due to the change of block compositions or environment parameters, such as solvent contents and solvent polarity. Lamellae are flat or slightly curved bilayers, while vesicles are closed bilayers, namely hollow spheres with a bilayer wall sandwiched by internal and external coronas. Vesicles are more frequently seen than lamellae owing to their higher thermodynamic stability.[16,81-83] Upon manipulating one block length, initial copolymer concentration, organic co-solvent and water content, a wide range of vesicles have been discovered, such as multi-compartment vesicles, Janus vesicles, onion-like vesicles, tubule-like vesicles, etc.[84]

1.1.3 Potential applications of macromolecular assemblies

Studies towards fundamental theories (thermodynamics and kinetics) and characterization techniques allow us to explore the various morphologies of macromolecular assemblies. By controlling the composition of individual block components and self-assembly conditions, the nanostructures of macromolecular assemblies can be tailored to some specific applications, such

as drug delivery,[85] diagnostic imaging,[21] photonic crystals,[19] emulsion stabilizers,[86] nanoreactors,[87] oil recovery,[88] nanopatterning,[89] etc. Recently, Choudhury developed a facile way of preparing porous carbon cathodes for lithium-sulfur batteries by using a self-assembled nanostructured block copolymer as template.[90] Moreover, Tamate summarized the BCP self-assembly in a new media (ionic liquids), which can be further applied to electric double layer capacitors, lithium-ion batteries, and electroactive soft actuators.[91] Described below is the detailed motivation and background for several well-developed block copolymer nanomaterials towards specific potential applications.

Nanomedicines

Over 100 years ago, 'drug delivery' was defined as a 'magic bullet' by Nobel Laureate Paul Ehrlich, which describes a therapeutic concept that the effective dose of active drug must be maintained until it reaches the site of action.[92] However, for most drugs, several barriers exist in such a process, including the fast degradation of many drugs in the complex *in vivo* environment, inadequate pharmacokinetics, lack of selectivity for the targeted tissues, and widespread biodistribution after systemic administration, which is a potential cause of toxicity.[93]

To solve these problems, some of the earliest nanomedicines were developed based on self-assembled liposomes, in which water-soluble drugs are encapsulated within the hydrophilic cores of vesicles, and hydrophobic drugs are entrapped in the phospholipid bilayer. Using liposomes to trap drugs can allow their stable circulation in the blood compartment, avoid harmful interactions with blood cells, and effectively eliminate accidental extravasation.[94] However, some problems have limited the manufacture and development of liposomes, such as stability issues, batch-to-batch reproducibility, and particle size control.

The use of amphiphilic block copolymers to develop drug nanocarriers has been pioneered by Kabanov and Kataoka to overcome the problems of liposome nanomedicines.[95,96] Polymer-based drug nanocarriers are advantageous in the following aspects: synthetic versality, tunable sizes, larger drug payload capacity, extremely low CMC, and stability against dissociation under highly diluted conditions in bodily fluids. Some details about specific advantages of polymeric nanomedicines will be discussed in the following section: size control and low CMC.

Nanomedicine sizes are directly related to the enhanced permeability and retention (EPR) effect, which results in the accumulation of drug carriers in target tissues and is based on the high permeability of malignant vasculatures to macromolecules.[97,98] Accordingly, the size of assemblies should be large enough to allow 'passive targeting' of tissues such as tumors by the EPR effect, but not so large to limit deep penetration through the tumor tissues. The most effective size has been reported to be between 10 and 100 nm in diameter, although for tumors with low permeability, nanomedicines with size below 50 nm should be favourable.[99] Moreover, extremely low CMC indicates the stability of polymeric micelles derived from the greater interfacial free energy of the larger insoluble segments, compared to low molecular weight surfactants.[100] The segregation of blocks in the micellar core can generate a variety of intermolecular forces to further lower the CMC. Drug payloads can also stabilize the micellar core through their interactions with the core-forming segments.

To design a good drug delivery vehicle, several criteria need to be considered. First, polymers must be biocompatible, nontoxic and biodegradable. Second, corona blocks need to achieve effective steric stabilization of micelles with the aim of extending the half-life of proteins in blood, reducing their immunogenicity, and avoiding proteolytic degradation. Third, hydrophobic core-forming segments must have interactions with hydrophobic drugs, which is the driving force for

the formation of micelles and drug encapsulation efficiency. These interactions include hydrogen bonding, host-guest interactions, π-π stacking, electrostatic interactions, etc. The core blocks can be further designed to trigger the release of the drug load in response to the specific signals in bodily fluids, such as pH and redox potential.

For example, polyethylene glycol (PEG) has been used widely as the corona-forming segment in biocompatible BCPs because of its hydrophilicity, linearity, chain flexibility, and availability in a wide range of MWs with low PDI.[101] Other than PEG, other choices typically involve the use of biocompatible hydrophilic polymers, including poly(glycerol) (PG)[102], poly(N-vinyl-2-pyrolidone) (PVP)[103], poly(vinyl alcohol) (PVA)[104], poly(acrylamide) (PAAm)[105], poly[N-(2-hydroxy-propyl) methacrylamide] (PHPMA)[106], poly(oxazolines) (POxs)[107], poly(acrylic acid)[108], polysaccharides.[109] For core-forming segments, the most commonly used polymers are polyethers[110], polyesters, and polyamino acids[111]. Some polyesters and polyamino acids have been clinically approved because of their biodegradability and high loading capacity, such as poly(*D, L*-lactide) and poly(glutamic acid).

Nanoreactors

In biological systems, chemical reactions happen in a confined environment and are closely connected to each other such that the product of one reaction is the catalyst of another. To create a well-defined reaction environment for the coupling of reactions in time and space, synthetic nanoreactors have been developed, which are capable of encapsulating reagents inside. Self-assembled block copolymers have attracted great attention in the field of nanoreactors. Hydrophobic substrates and catalysts can be effectively entrapped in the cores of macromolecular assemblies, which can increase the solubility of reagents while protecting them from degradation.

Specifically, amphiphilic block copolymers can form micelles to stabilize and synthesize metal colloids or metal oxides, since the polymeric shell around the metal particles can prevent their agglomeration and precipitation.

To obtain metal nanoparticles from metal-containing BCPs, there are mainly two approaches. One is to first complex the metal ions to the monomers, which will be polymerized and then form aggregates of polymer-metal hybrids. Another is to synthesize block copolymers first, then form micelles to entrap metal salts, where chemical reactions happen and products (metal particles) aggregate to larger size by nucleation and growth. Stable hybrid materials of BCPs and inorganic compounds are very important for the process, which requires sufficient adhesion between the polymer chains and the metal particles. Therefore, BCPs have been synthesized with functional blocks, such as acidic, basic coordinating blocks or neutral ligands. The chemical reactions occurring in the micellar core usually are reduction reactions for forming metal colloids, are oxidation reactions for forming metal oxides, or involve the addition of H_2S to form metal sulfides. For example, it has been reported that Pd particles were successfully synthesized inside diblock copolymer micelles of polystyrene-*b*-poly(4-vinylpridine) from anionic polymerization.[112]

Polymeric micelles can also be applied in the hydrogenation of olefins and acetylenes, C-C coupling reactions, and enzymatic reactions. Catalytically active metal colloids or enzymes are buried inside the micelle core and the reactants must pass through the shell to reach the interior. It is advantageous because catalyst recovery is straightforward by performing ultrafiltration or precipitation in poor solvents for the polymer. For the hydrogenation of olefins and acetylenes, advances have been made in chemo-, stereo-, and regioselective hydrogenations of various substrates. For example, the Tao group used Pt nanoparticles stabilized by PVP to reduce the carbonyl group in cinnamaldehyde to cinnamic alcohol, while leaving the double bond intact.[113]

For C-C coupling reactions, a good example was presented by El-Sayed and coworkers, who used the Suzuki coupling as a test reaction to investigate the effect of the polymeric stabilizers on both the catalytic activity and the stability of Pd colloids.[114] For enzyme reactions, one example has been reported by Meier that a pH-sensitive enzyme proved to be catalytically active within the vesicles, yielding an insoluble fluorescent product from a soluble non-fluorescent substrate.[115]

Nanopatterning

Nanopatterning is a fundamental technology for semiconductor device fabrication. Self-assembly of block copolymers have attracted a great deal of attention in this field because they can form ordered, periodic arrays of spheres, cylinders, or lamellae with a typical feature size in the 3-50 nm region.[116-118] Compared to traditional photolithography, self-assembly nanopatterning has a variety of benefits, including molecular scale pattern precision, ultrafine line edge roughness, and low-cost processing.[119]

Here is a classic example of nanopatterning using BCPs.[120] Park et al. developed periodic arrays of similar 10^{11} holes/cm^2 using pattern transfer from spherical microdomains in PS-*b*-PB or PS-*b*-PI to an underlying semiconductor substrate by dry etching. First, a block-copolymer film (PS-*b*-PB or PS-*b*-PI) solution was coated on the surface of silicon nitride. In bulk, PS-*b*-PB microphase separates into a cylindrical morphology and produces hexagonally ordered PB cylinders embedded in a PS matrix; PS-*b*-PI exhibits a spherical morphology and produces PI spheres in a PS matrix with body-centered-cubic order. To produce holes in silicon nitride, PB (or PI) spherical microdomains in the film were etched away by ozonation. Then the patterns were transferred into silicon nitride using CF_4 RIE on the mask of the hole structure in a PS matrix. On

the other hand, to produce dots in silicon nitride, the PS matrix was etched away using OsO_4 staining after cross-linking the PB. The morphology was transferred into silicon nitride by RIE.

1.2 Introduction to molecular polymer brushes

Bottlebrush copolymers (BBCPs) are a type of branched or graft polymer with polymeric side-chains attached to a linear backbone. Due to the steric interactions among the densely grafted side chains, the backbone usually adopts entropically unfavored extended chains, which leads to worm-like morphologies of molecular polymer brushes if the backbone is longer than the side chains. Therefore, BBCPs do not entangle, and can self-assemble into ordered nanostructures with large domain sizes, up to several hundred nanometers. In solution, BBCPs can form micelles with a much lower critical micelle concentration compared with linear block copolymers, which enables applications such as detection or sensing in biological media that requires dilute conditions. Bottlebrush polymer side-chains can also be functionalized by elements for specific properties, such as introducing fluorescent groups for bioimaging and adding target groups for recognition.

1.2.1 Strategies for the synthesis of molecular brushes

Bottlebrush polymers were first synthesized in the early 1980s, and early work was primarily focused on the development of synthetic strategies.[121] Using living polymerizations and ring-opening polymerizations, the lengths of backbone and side-chain as well as the compositions of BBCPs can be controlled precisely. Generally, there are three strategies to synthesize molecular brushes: grafting from, grafting to, and grafting through, as shown by Figure 1.6. The grafting-from method is used to grow side chains by the polymerization of monomers using a polyinitiator as a backbone. Grafting-to methods attach the side chains to a backbone which was synthesized

separately. Grafting-through methods polymerize the functionalized chain end groups of pre-polymerized macromonomers. Each method has its own advantages and drawbacks, as will be discussed in the following section. The selection or the combination of these strategies depend on the targeted structures of molecular brushes.

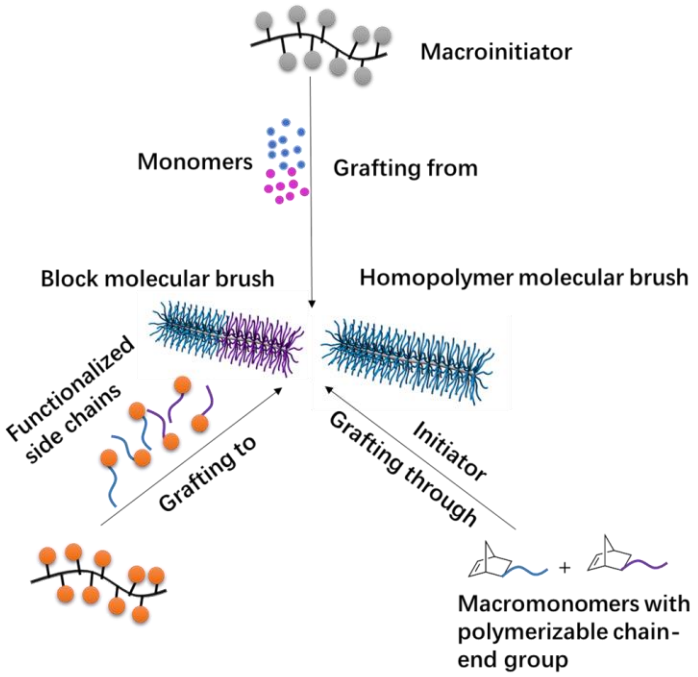

Figure 1. 6. Three strategies to construct bottlebrush copolymers: "grafting-from", "grafting-to", and "grafting-through".

The grafting-from strategy requires the synthesis of a backbone macroinitiator with multiple initiation sites which is subsequently used to polymerize the monomers of side chains. The initiator groups can be directly polymerized into the polymer backbone or protected and introduced later after the backbone polymerization. The grafting-from strategy is favorable when bottlebrush copolymers with very long backbones need to be prepared. The grafting density can also be controlled by co-polymerizing more than one monomer during backbone synthesis.[122] In addition,

core-shell type bottlebrushes can be synthesized by a sequential polymerization of different monomers used in constructing the side-chains. However, several drawbacks also need to be considered for the selection of the grafting-from strategy. First, there are significant steric effects from the initiation groups close to each other along the backbone, which might lead to low conversions of side-chain monomers. Second, it can sometimes require multiple protection and deprotection steps, which increases the complexity of the synthetic process.[123]

The grafting-to approach involves the synthesis of the bottlebrush backbone and side chain separately, followed by a coupling reaction that attaches the side-chains to the backbone. This allows for good control over the compositions and lengths of BBCPs and leads to well-defined architectures. However, the limitations of the grafting-to strategy are obvious. With increasing grafting density, steric hindrance along the backbone may impede the attachment of side-chains, which is already entropically unfavorable as random coiled side-chains are forced to stretch. Therefore, high grafting densities are difficult to achieve, and they are usually lower than 60%, although some exceptions have been reported.[124,125] Also, incomplete coupling of side chains may also result in difficult purifications for brushes prepared in this manner.

The grafting-through strategy requires the preparation of macromonomers as side-chains, of which the functionalized end groups will be polymerized into a backbone of bottlebrush copolymer. Usually, different lengths of side chains can be obtained by varying the mole ratio of monomers and initiators, while changing the mole ratio of macromonomers and catalyst can precisely control the lengths of the bottlebrush backbones. Controlled radical polymerizations and living anionic polymerizations have been widely applied to the synthesis of macromonomers. Details will be discussed in the next section 1.2.2. To enable the polymerization of macromonomers in very dilute solution, avoiding high solution viscosities due to the high MW of macromonomers, highly active

catalysts are needed to achieve high conversion and control over molecular weight. Fortunately, Grubbs catalysts have been developed as a perfect fit to finish the second step of bottlebrush copolymer synthesis, which can polymerize norbornenyl macromonomers by ring opening metathesis polymerization (ROMP) with high efficiency.[126,127] Ring opening polymerizations can also be used for the polymerization of macromonomers.[128]

The pros and cons of each synthetic approach are related to specific requirements and applications of bottlebrush copolymers. For applications involving bulk materials or bottlebrush coatings, the grafting-from strategy would be optimal. The grafting-to strategy produces BBCPs with lower grafting densities and less stretched side chains, which may benefit coatings and additives. The grafting-through strategy can precisely control over the lengths of backbones and side-chains with high grafting densities, which contributes to fundamental studies of structure and function and has been used for imaging and detection.[129,130]

1.2.2 Polymerization techniques for "grafting-through" bottlebrush synthesis

The grafting-through strategies are divided into two steps: macromonomer synthesis and bottlebrush copolymer synthesis. To obtain macromonomers with polymerizable end groups, either initiators with functional groups must be used, or chain ends should be modified after polymerization. Living/controlled polymerization techniques have been used widely to obtain bottlebrush copolymers, such as, for the macromonomer synthesis step: reversible-deactivation radical polymerizations (RDRP) and living anionic polymerization, and for the bottlebrush copolymer synthesis step: ring opening polymerization (ROP) and ring opening metathesis polymerization (ROMP). RDRP includes nitroxide-mediated polymerizations (NMP), atom transfer radical polymerizations (ATRP), copper (0) reversible-deactivation radical

polymerization (Cu(0)-RDRP), and reversible addition-fragmentation chain transfer (RAFT). Together, these methods can be applied to a wide range of monomers, and many have good functional group tolerance and use simple reaction conditions. Some of these polymerization techniques will be discussed in detail here, as well as their mechanisms.

RAFT Polymerization

Scheme 1.1 shows the general mechanism of RAFT polymerization.[131] The process is achieved by a chain transfer agent in the form of a thiocarbonylthio compound, which initiates and propagates radicals. In the early stages of the polymerization, addition of a propagating radical ($P_n\cdot$) to the thiocarbonylthio compound followed by the formation of an intermediate radical generates a polymeric thiocarbonylthio compound and a new radical ($R\cdot$). The new radical combines with monomers to form another propagating radical ($P_m\cdot$). Chain equilibrium between the active propagating radicals ($P_n\cdot$ or $P_m\cdot$) and the polymeric thiocarbonylthio compound provides equal probability for all chains to grow into narrow dispersity polymers.

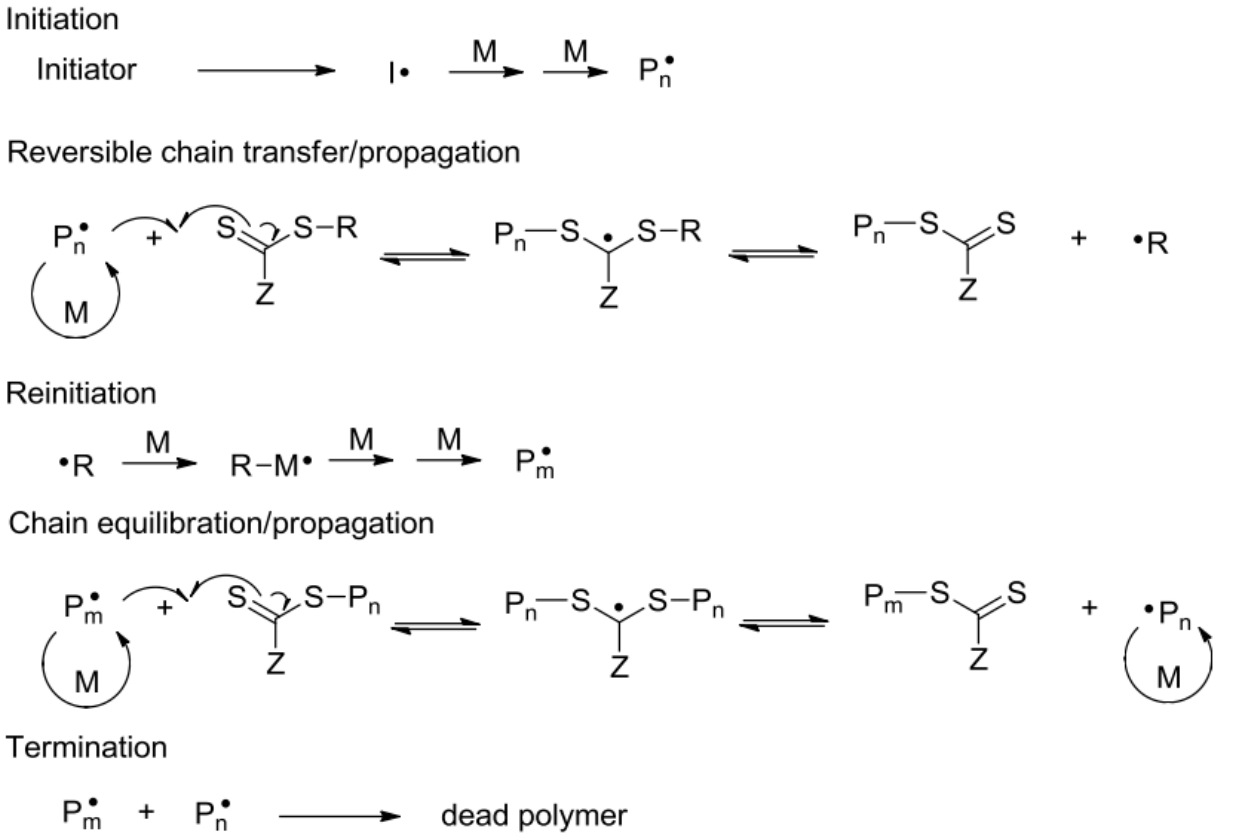

Scheme 1. 1. General mechanism of RAFT polymerizations. Adopted from reference [131].

ATRP & Cu(0)-RDRP

Scheme 1.2 shows the general mechanism of ATRP, which was discovered by Matyjaszewski.[132] The initiating radicals are generated from alkyl halides through a reversible redox process by a transition metal complex (Mt^m/L represents the transition metal species in oxidation state m and L is a ligand). ATRP is controlled by an equilibrium between propagating radicals (P_n·) and dormant species, mainly in the form of initiating alkyl halides or macromolecular species (P_nX).

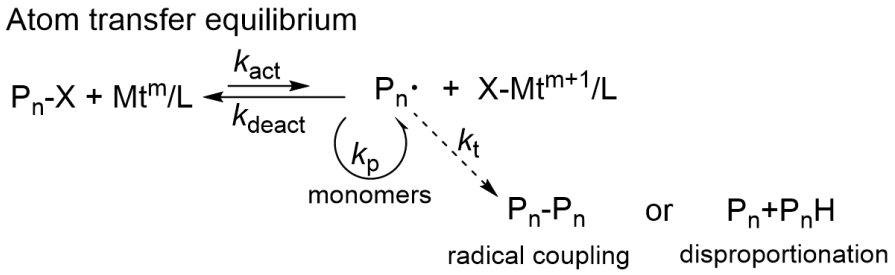

Scheme 1.2. General mechanism of transition-metal-catalyzed ATRP. Adopted from reference [133].

Based on the activation-deactivation equilibrium of ATRP, a transition metal complex in the lower oxidation state can be Cu^I/L or Cu^0/L. In this case, Cu(0)-RDRP has been developed, and it is also called SET-LRP or SARA ATRP, which is mainly used to polymerize acrylic polymers. The SET-LRP mechanism assumes essentially exclusive activation by Cu^0 species with deactivation by Cu^{II}. In contrast, the SARA ATRP mechanism indicates that the activation of radicals by Cu^I and deactivation of radicals by Cu^{II} take responsibility for the process, and Cu^0 is a supplemental activator and reducing agent. However, there remains significant debate about the true nature of the Cu(0)-RDRP mechanism.[134]

ROMP

Ring opening metathesis polymerization (ROMP) has been developed to polymerize strained cyclic olefins to produce low-dispersity polymers and copolymers.[135] Scheme 1.3 shows the general mechanism of ROMP. ROMP uses metal-alkylidene complexes as well-defined olefin-metathesis catalysts, such as molybdenum-based complexes (Schrock's catalysts) or ruthenium-based complexes (Grubbs' catalysts). Metal-alkylidene complexes coordinate with strained cyclic olefins to form a four-membered metallacyclobutane intermediate through [2+2]-cycloaddition. This intermediate provides a new metal alkylidene by a cycloreversion reaction. The increasing

size of the new metal complex does not influence its reactivity towards cyclic olefins. Analogous catalytic cycles occur continuously until all the monomers are consumed. ROMP reactions are commonly quenched through the addition of ethyl vinyl ether. The driving force of ROMP reactions is the enthalpy released from the release of ring strain, and thus the polymerization is irreversible.

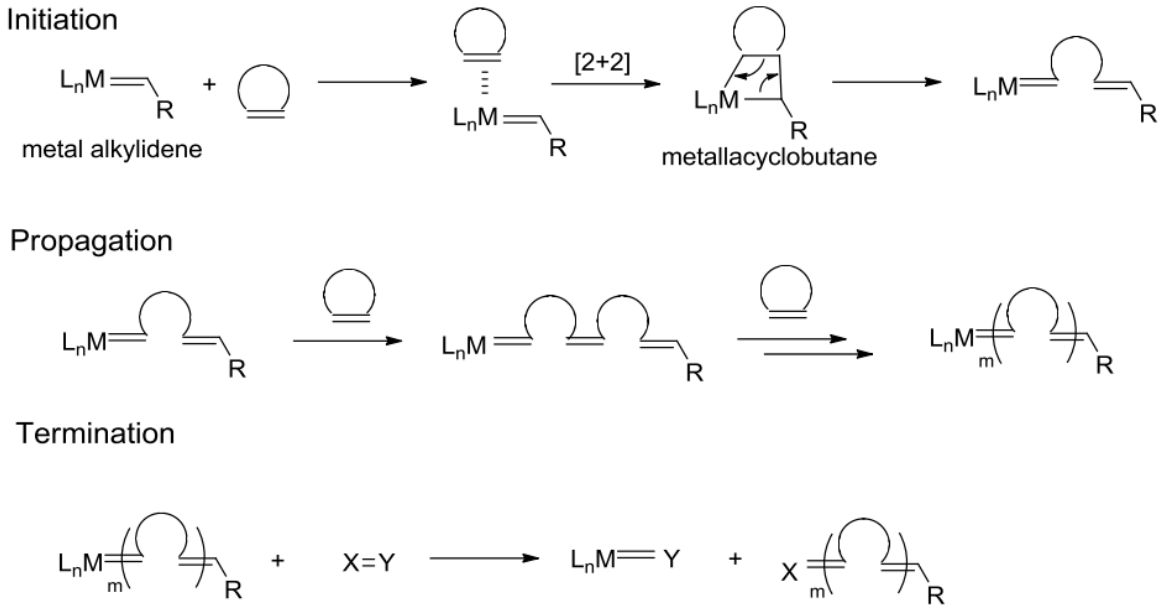

Scheme 1.3. A general mechanism to a typical ROMP reaction. Adapted from reference [136].

1.2.3 Potential applications of bottlebrush copolymers

The advances in synthetic methods discussed above enabled the self-assembly of molecular brushes to develop as a precise and tunable approach for preparing various nanostructures. Their unique worm-like structures result in a number of potentially useful properties, such as high molecular weight, lack of entanglement, large domain sizes of self-assembled structures and dense functionality of bottlebrush side-chains. Therefore, the self-assembly of bottlebrush copolymers

has emerged as a promising strategy for advanced applications, such as the preparation of photonic crystals,[137] lithographic patterning,[138] bioimaging[139] and drug delivery.[140]

Photonic crystals

Photonic crystals, which are ordered composite structures with periodicity comparable to the wavelengths of visible light, require good control over their bandwidths and center frequencies. Traditional fabrication of photonic crystals uses "top-down" techniques, such as layer-by-layer stacking[141] and electrochemical etching[142], which can meet the requirements but are very complicated to process. However, self-assembly of bottlebrush block copolymers has been discovered as a simple way to prepare photonic crystals under mild processing conditions. It is advantageous because of the efficient synthesis process, the ability to access large domain spacings, and fast self-assembly kinetics.

The simplest photonic crystals consist of alternating layers of high and low-refractive-index materials. At each interface of these structures, some light at certain wavelength can be reflected. The intensity of the reflected light (R) depends on the refractive index contrast (n_2/n_1) and the number of layers of the multilayer film, as shown by Equation 14.

$$R = \left[\frac{1-\left(\frac{n_2}{n_1}\right)^{2N}}{1+\left(\frac{n_2}{n_1}\right)^{2N}}\right]^2 \quad (14)$$

While the refractive index contrast between each layer in a BBCP film is relatively small, increasing the number of layers can be helpful to obtain a large reflectivity. Blending with high-index components, such as linear homopolymers and nanoparticles, can also increase the reflectivity by increasing the refractive index contrast.[143] Moreover, the wavelength of reflected light depends on the optical thickness of each layer in the BBCP films for a normal incident beam

(θ = 0), which is a product of the refractive index and the thickness of the layer, as shown by Equation 15.

$$\lambda = 2(n_1 d_1 + n_2 d_2) \quad (15)$$

These equations provide guidance for designing photonic crystals with the desired properties by controlling the thickness and the number of layers in BBCP films.

There are several ways to tune the nanostructures of BBCP films. Xia et al. investigated the influence of polymer sequence (*i.e.*, random or block) on domain spacing in brush copolymer nanostructures. They found that a domain spacing of 116 nm was measured by SAXS for symmetric block copolymers while a domain spacing of 14 nm was determined for random polymers, which consist of polylactide and poly(n-butyl acrylate) side chains.[144] On the other hand, the Grubbs group has studied the effects of BBCP molecular weight and assembly method on the photonic properties of BBCP films constructed from poly(hexyl-isocyanate) and poly(4-phenyl-butyl-isocyanate). They concluded that the film preparation method plays an important role in photonic properties, from the fact that films of one sample cast from CH_2Cl_2, THF, or that were thermally annealed appeared blue, green, or red respectively. They also found that the maximum reflectance wavelength was a linear function of molecular weight for all self-assembly techniques analyzed.[145]

Bottlebrush block copolymers have been demonstrated as promising materials for preparing photonic crystals, although opportunities still exist in understanding the thermodynamics of ordering and optimizing protocols for their self-assembly.

Polymeric sufactants

Polymeric surfactants containing lyophilic and lyophobic segments are ideally suited to explore the compartmentalization of soft-matter nanosystems, with lower critical micelle concentrations (CMCs) and more easily controlled solvophilic/solvophobic interactions relative to their small-molecule counterparts.[69] As a result, thermodynamically stable polymeric assemblies with remarkable complexity can now be prepared which can draw on the immense diversity of techniques available for polymer functionalization to create tailor-made assemblies. Such hierarchical assemblies are increasingly finding applications in drug delivery,[140] bioimaging and detection.

More recently, molecular polymer brushes have emerged as a powerful building block for the assembly of soft matter. Characterized by pendant polymer chains protruding from a central polymer chain, these structures favor extended cylindrical morphologies owing to the steric repulsion between side chains.[146] As a result, bottlebrush polymers experience limited chain entanglement compared to traditional linear polymers, significantly reducing the entropic cost of reorganization into larger assemblies. Amphiphilicity can be readily incorporated into a bottlebrush structure either radially in a core-shell structure, side-by-side along the length of the bottlebrush to create a 'Janus-type' structure, or in a block-by-block fashion along the length of the backbone chain. This versatility has led researchers to prepare amphiphilic bottlebrushes for use as giant surfactants.

For example, Johnson *et al.* developed a series of functionalized bottlebrushes as responsive water-soluble drug nanocarriers, where anticancer drugs doxorubicin (DOX) and camptothecin (CT) were attached to bottlebrush copolymers via photocleavable linkers.[140] Miki *et al.* designed water-soluble bottlebrush copolymers with near-infrared fluorescence dye and targeting agents

covalently attached to the bottlebrush backbone, which can be used to image malignant tumors.[139] Sleiman and coworkers prepared bottlebrush copolymers containing a hydrophilic PEG block, biotin functionality for binding to streptavidin, and luminescent ruthenium, iridium, or osmium polypyridine complexes, of which the assemblies can be used as biodetection assays.[147]

Although work with bottlebrush polymeric surfactants has advanced greatly, a more comprehensive understanding of the phase behavior, kinetics, and stability of micelles is needed to prepare well-defined nanomaterials with desired properties for biomedical applications.

1.3 Scope of the thesis

Our group recently demonstrated that multiblock bottlebrush copolymers (BBCPs) could be prepared from organic semiconductors, giving nanomaterials with well-defined interfaces analogous to p-n junctions on single macromolecules.[148] This strategy was used to prepare multiblock nanofibers with the hierarchical structure of multilayer organic light-emitting diodes (OLEDs) on single polymer chains, providing new opportunities for the study of charge transport at nanoscale junctions. We then reasoned that similar organic semiconductors could be incorporated into amphiphilic BBCPs, giving giant polymeric surfactants capable of building complex optoelectronic function into larger assemblies. These BBCPs can be further modified for some potential applications, such as bioimaging and detection.

In this dissertation, we describe the synthesis of amphiphilic BBCPs composed of a soluble *n*-butyl acrylate (nBuA) macromonomer block and a carbazole-based benzyl acrylate (CzBA) organic semiconductor block, and their self-assembly to give micellar structures in selective solvents. Carbazole moieties are found in many of the most common host materials used in OLEDs, capable of efficient energy transfer to a wide range of luminescent dopant molecules. Based on

this principle, we then incorporate a deep-blue emitting acrylic dye molecule into the carbazole segment of an amphiphilic bottlebrush polymer, giving giant polymer micelles with a quantum yield of unity after self-assembly.

More specifically, a highly efficient, versatile "grafting through" synthetic methodology is shown in **Chapter 2** by combining Cu(0)-reversible deactivation radical polymerization, ring opening metathesis polymerization, chain end modification (azide exchange) and "click chemistry" (CuAAC). We have achieved the preparation of diblock molecular brushes with well-defined structures and compositions. In **Chapter 3**, we optimized the self-assembly conditions to obtain spherical micelles with various sizes. Their size distribution and morphology were characterized by dynamic light scattering (DLS) and transmission electron microscopy (TEM). Their polymeric properties and fluorescent properties were also investigated. **Chapter 4** will discuss the conclusions from this work and the outlook for future studies.

Chapter 2: Synthesis and characterization of bottlebrush diblock copolymers

This chapter describes experimental procedures for the synthesis of well-defined diblock bottlebrush copolymers using a "grafting-through" strategy, as well as techniques to characterize the resulting materials, including ^{1}H-NMR, SEC, DSC, and AFM. These procedures allow for accurate control over the BBCP composition, which enable the further investigation of their self-assembly behaviors in solution and thin films.

2.1 Introduction

Bottlebrush copolymers (BBCPs) have shown promise as building blocks for self-assembled nanomaterials due to their reduced chain entanglement relative to linear polymers and their ability to self-assemble with remarkably low critical micelle concentrations (CMCs). Concurrently, the preparation of bottlebrush polymers from organic electronic materials has recently been described, allowing multiple optoelectronic functions to be incorporated along the length of single bottlebrush strands.[148] For example, Sivula *et al.* developed donor-acceptor copolymer brushes (P3HT-*b*-PCBM) via a sequential grafting-through polymerization for solar cell applications.[149]

To enable the successful incorporation of semiconducting functionalities into bottlebrush copolymers, an appropriate synthetic route is necessary. The two-step "grafting through" strategy is ideally suited to the synthesis of bottlebrush block copolymers as it gives high grafting densities with good functional group tolerance. This procedure requires two principal steps: first, macromonomers are synthesized incorporating a polymerizable functional group at the chain end. Next, these chain ends undergo a second "grafting through" polymerization to give the BBCP. For the first step, living/controlled radical polymerization (CRP) has been used extensively in literature due to its precise control over molecular weight, although the polymerization is usually quenched

at moderate conversions (50-70%)when norbornenyl end groups are used to prevent side reactions such as radical addition across the norbornene olefin.[150] In some cases, the separation of unreacted monomers from macromonomers at this stage can also present a challenge if the solubilities of the macromonomer and monomer are similar. Scheme 2.1 depicts several examples of macromonomer synthesis. The second "grafting through" step to give BBCPs is more challenging due to the low concentration of polymerizable end groups and high level of steric hindrance of the macromonomers. Ring opening metathesis polymerization (ROMP) is ideally suited to these reactions, as high catalyst activity and relief of ring strain can drive the reaction to high conversion. The degree of polymerization of ROMP can be easily tuned by controlling the ratio of macromonomer to catalyst.

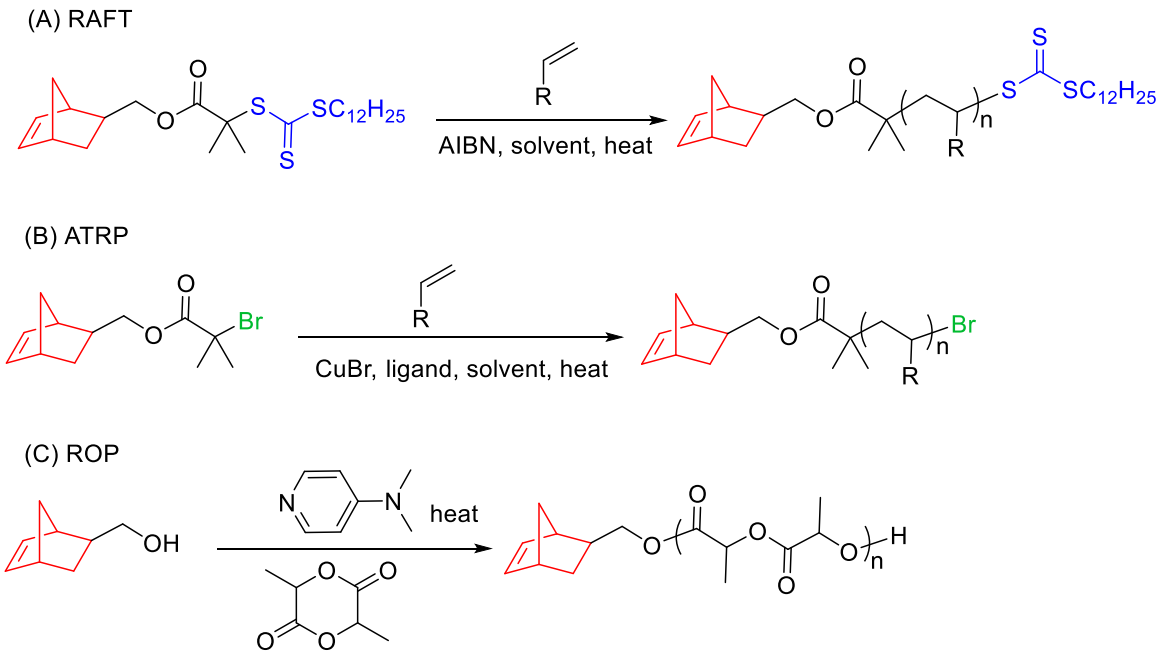

Scheme 2.1. Examples of the direct synthesis of norbornenyl macromonomers by (A) RAFT, (B) ATRP, and (C) ROP. Adapted from reference [136].

In an alternative strategy, the chain ends of well-defined polymers synthesized from CRP can also be capped with norbornenyl or other polymerizable units through post polymerization

modification. This is usually achieved by substituting ATRP-initiating (or Cu(0)-RDRP-initiating) halides with azides, followed by copper-catalyzed alkyne-azide cycloaddition (CuAAC) with alkynyl-functionalised norbornenes to yield macromonomers.[144,151,152] The CuAAC reaction is efficient and highly functional group tolerant, and can also be conducted in a wide variety of solvents. Scheme 2.2 represents the mechanism of the CuAAC generating the 1,4-regiosiomer of the distributed triazole compound.

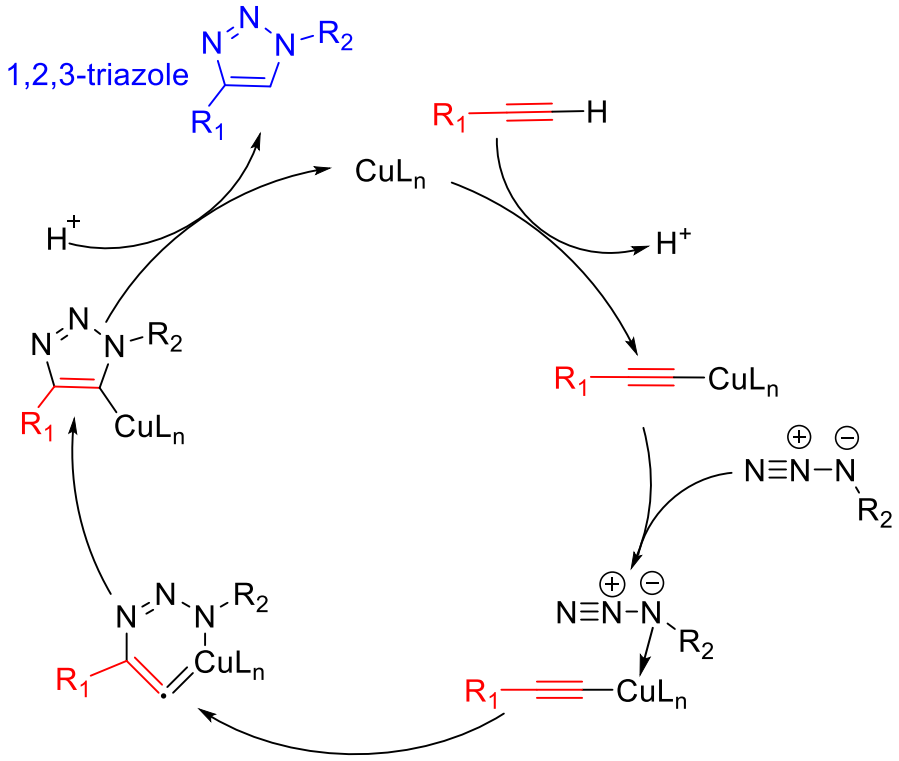

Scheme 2.2. Mechanism of the copper-catalyzed azide-alkyne cycloaddition. Adapted from reference [151].

For the second polymerization step to give BBCPs, the selection of an appropriate catalyst for ROMP is critical. Most of the well-defined olefin-metathesis catalysts are molybdenum-based Schrock's catalysts or ruthenium-based Grubbs' catalysts. Figure 2.1 shows the three generations of Grubbs catalysts. Wooley and coworkers found that the propagation in ROMP of

macromonomers is often terminated unexpectedly when using first-generation Grubbs (**G1**) catalyst.[136] The activity of G1 is low because of the similar association and dissociation rate at equilibrium. For second-generation Grubbs catalyst (**G2**), an *N*-heterocyclic carbene (NHC) ligand takes the place of one of the phosphine ligands, leading to enhanced activity. NHC ligands are stronger σ-donors, such that phosphine ligands are more likely to dissociate due to trans effect.[153] However, Wooley also found that ROMP was poorly controlled using **G2** because it initiates slowly and propagates fast.[136] As such, third-generation Grubbs catalyst (**G3**) is ideally suited to ROMP as it initiates rapidly as a result of substitution of the phosphine in **G2** with weakly bound heterocyclic ligands such as pyridine.[154]

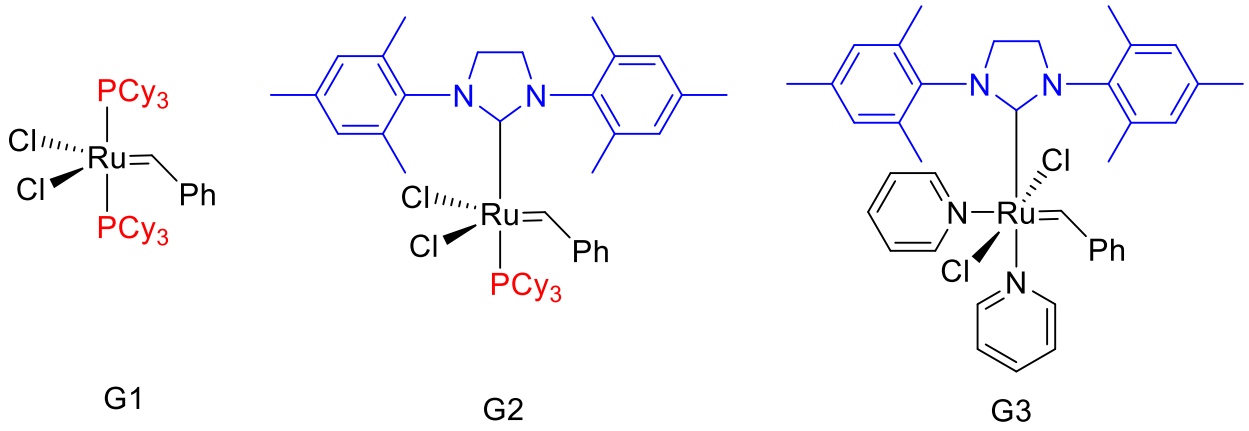

Figure 2.1. Grubbs catalysts of first (G1), second (G2), and third (G3) generations. Adapted from reference [155].

In this chapter, synthetic routes are developed to access functional diblock bottlebrush copolymers containing π-conjugated materials, due to their high fluorescence quantum yields and photochemical stability, which are of interest in labeling and imaging. More specifically, carbazole and their derivatives were examined as they have been well-studied as host materials capable of efficient intramolecular electron transfer in optoelectronic devices.[156]

2.2 Results and Discussion

Direct-Growth Synthesis of Macromonomers

The synthesis of macromonomers of *n*-butyl acrylate **(nBuA)** was first attempted using norbornenyl-functionalized initiators through copper(0) reversible-deactivation radical polymerization (Cu(0)-RDRP), as shown in scheme 2.3. This method has the advantage of giving polymers in which every chain is functionalized with a norbornene handle at the α-terminus, but it was necessary to quench the reactions at very low conversions (< 40%) to prevent biradical coupling or atom-transfer radical addition. The latter side reaction additionally results in α,ω-dinorbornenyl telechelic macromonomers,[150] which can act as crosslinkers during ROMP and resulted in bottlebrush polymers with a high-molecular weight shoulder and/or broadened molecular weight distribution following the grafting-through step. It was also found that the configuration of atoms linking the polymer to a polymerizable norbornene handle has influence on the kinetics of ROMP.[157] To maximize the conversion of macromonomers (MMs) in ROMP, rapid propagation rates are required in order to maximize conversion during the lifetime of the active catalyst species. Since MMs functionalized with an *exo*-norbornene anhydride derivative have been shown to propagate more slowly than simple functionalized norbornenes, the polymerizable norbornenyl chain end was substituted for *exo*-5-norbornylmethylpent-4-ynoate, as shown in Scheme 2.4.

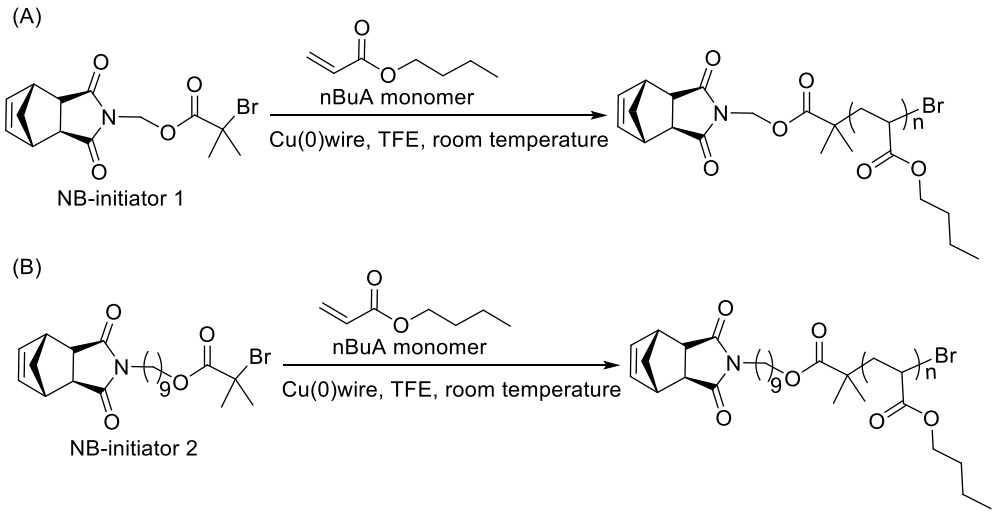

Scheme 2.3. Unsuccessful synthesis of **nBuA** macromonomers using short-spacing (A) and long-spacing (B) norbornenyl-functionalized initiators. Using NB-initiator 2 (B) is supposed to increase the flexibility of side-chains and reduce the steric hindrance of macromonomer polymerization.

Synthesis of Macromonomers by Post-Polymerization Functionalization

To avoid atom-transfer radical addition, a two-step synthesis of macromonomers was then identified in which azide-functionalized polymers synthesized by Cu(0)-RDRP could be functionalized with norbornenyl units via CuAAC (Scheme 2.4). Unfortunately, polymerizable macromonomers with a bimodal molecular weight distribution were obtained, as shown in Figure 2.2. Since the catalysts used for CuAAC are similar to those used in ATRP or Cu(0)-RDRP, it is likely that biradical combination of prepolymers occurred during the CuAAC reaction due to the reactivity of the bromine chain end. The modification of the polymer ω-terminus was then attempted to prevent this undesired reactivity.

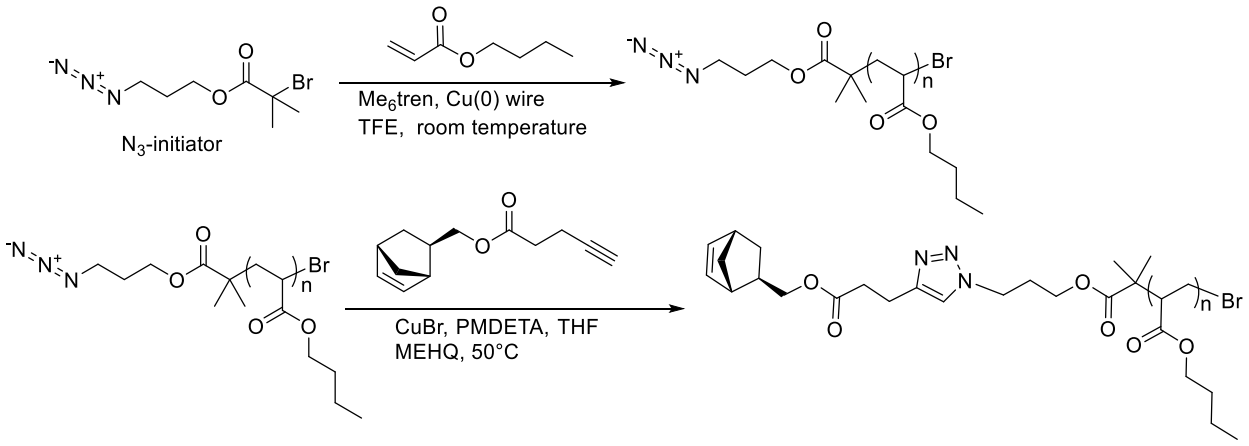

Scheme 2.4. Unsuccessful synthesis of **nBuA** macromonomers via post polymerization modification (CuAAC).

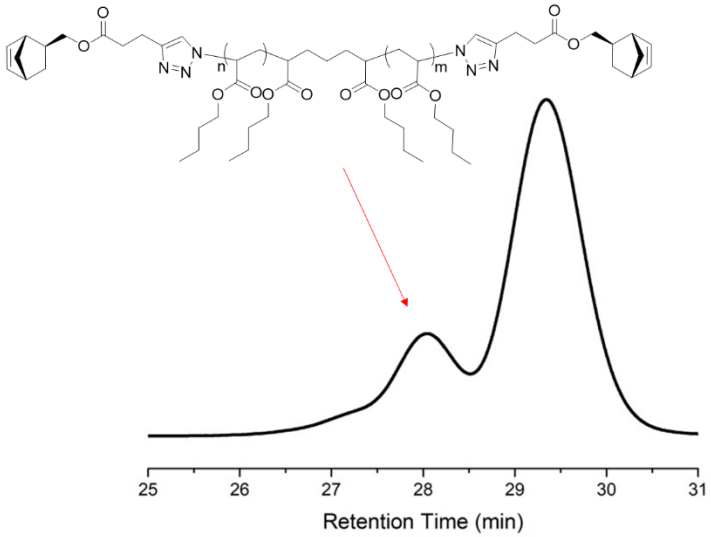

Figure 2.2. Bimodal molecular weight distribution of **nBuA** macromonomers by scheme 2.4.

Macromonomers of **nBuA** and **CzBA** were then successfully synthesized by Cu(0)-RDRP, (Scheme 2.5). Alternatively termed SET-LRP or SARA-ATRP, these room-temperature polymerization reactions make use of simple Cu(0) wire as catalyst, providing scalable routes to multigram quantities of both materials. Using ethyl-α-bromoisobutyrate (EBiB) as initiator, bromine-terminated polymers **poly(nBuA)-Br** (M_n = 5200, Đ = 1.16) and **poly(CzBA)-Br** (M_n = 4800, Đ = 1.16) were prepared. While **poly(nBuA)-Br** can be easily purified by reprecipitation

from CH_2Cl_2 into 80:20 MeOH:H_2O, the solubility characteristics of the π-conjugated **CzBA** monomer and its corresponding polymer are very similar, making reprecipitation unsuitable in a wide range of solvent combinations. Fortunately, residual **CzBA** monomer can be easily removed from **poly(CzBA)-Br** by passing the crude product over a reusable polystyrene-co-divinylbenzene resin to give pure polymer product.

These bromine-terminated polymers were then converted into norbornene-containing macromonomers suitable for grafting-through bottlebrush synthesis via ring-opening metathesis polymerization (ROMP).[144] The bromine end groups were first exchanged for azide groups by stirring with sodium azide in dry DMF at room temperature, after which a norbornene group could be added using CuAAC and a norbornene-functionalized alkyne.

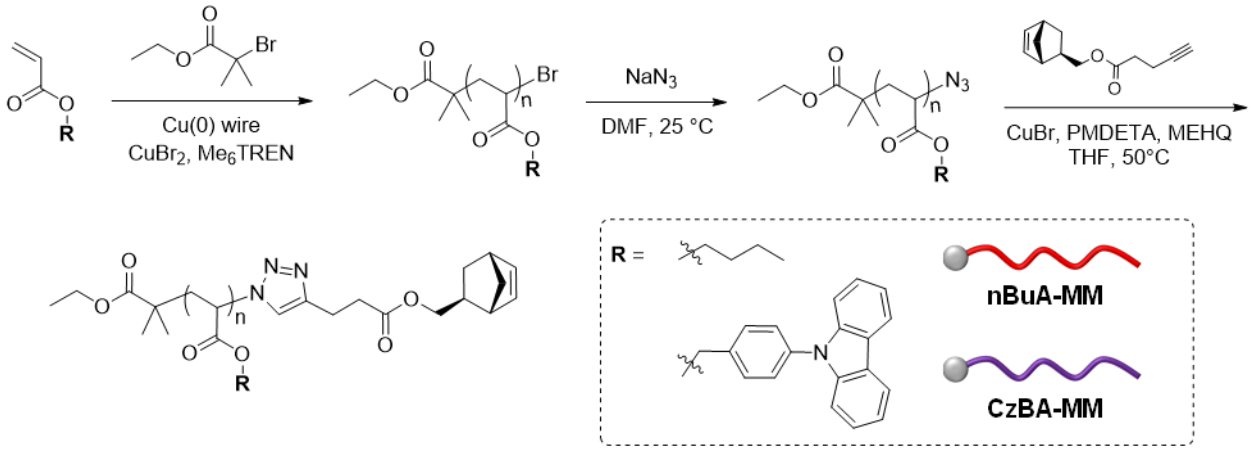

Scheme 2.5. Successful synthesis of macromonomers **nBuA-MM** and **CzBA-MM**.

Xia and coworkers have recently shown that this 'growth then coupling' strategy for controlled radical macromonomer synthesis can reduce molecular weight broadening during ROMP compared to directly grafting a polymer chain from a norbornene-functionalized initiator.[150] By adding the norbornene group to the polymer ω-terminus after the polymerization

reaction, any chain-chain coupling events during the radical polymerization simply result in unreactive chains during ROMP, as the terminal bromine atoms are no longer available for substitution. This is in contrast to direct grafting methods, in which chain-chain coupling would instead result in bifunctional polymers with norbornene groups at both ends, and thus able to act as crosslinkers.[158,159] As such, a growth-then-coupling approach was used for macromonomer synthesis here, though we note that direct growth methods can also be used in the preparation of low-dispersity bottlebrushes if chain-chain coupling events can be minimized during the initial radical polymerization step.[31] Notably, both the azide exchange and CuAAC reactions proceeded with no significant change in the SEC trace of either polymer after both reactions (Figure 2.3). The polymeric properties of prepolymers and macromonomers by scheme 2.5 are shown in the Table 2.1 and Table 2.2. Their molecular weights were controlled around 5000 Da with a narrow polydispersity (PDI ~1.1), which contributed to the synthesis of well-defined diblock BBCPs. The DP of **poly(CzBA)$_{15}$-Br** (or **poly(CzBA-*co*-PAPOMA)$_{15}$-Br**) calculated by SEC was higher than the one we expected from its [M/I] at 78% (or 73%) conversion , which may be due to systematic errors and experimental errors such as the quality of solvent (THF).

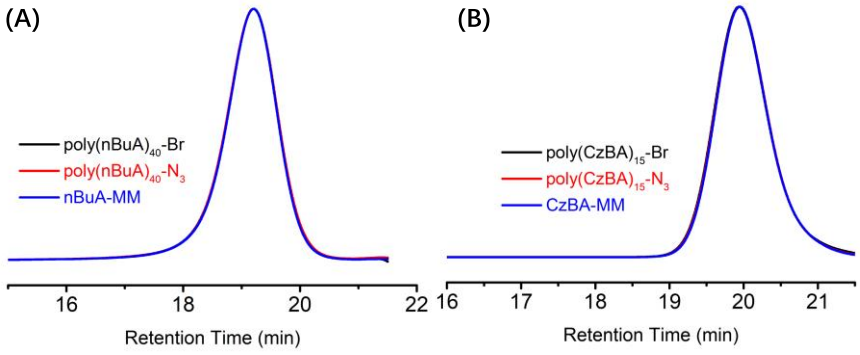

Figure 2.3. SEC refractive index (RI) traces for **poly(nBuA)-Br**, **poly(CzBA)-Br**, and their azide- and norbornene-functionalized analogues.

Table 2.1. Synthesis of prepolymers.

Entry	M_n[a] (Da)	DP[a]	[M/I][b]	$Đ$	Conv. (%)[c]
Poly(nBuA)$_{40}$-Br	5200	39	40	1.16	95
Poly(CzBA)$_{15}$-Br	4800	13	15	1.16	78
Poly(CzBA-*co*-PAPOMA)$_{15}$-Br	5700	14	15	1.12	73

[a]Determined by SEC in THF
[b]Monomer to initiator ratio.
[c]Determined using ^{1}H NMR.

Table 2.2. Synthesis of macromonomers.

Entry	M_n (Da)	$Đ$
nBuA-MM	5600	1.14
CzBA-MM	5200	1.15
(CzBA-co-PAPOMA)-MM	6000	1.12

A grafting-through approach via ROMP was then used to give diblock copolymers with backbone degrees of polymerization between 72 and 110, varying the ratio of **nBuA** and **CzBA** macromonomer units in the chain from ~1:3 to ~7:1 (Table 2.3). Narrow dispersities of 1.08-1.11 were obtained for these diblock copolymers with tailing at low molecular weights likely due to a small percentage of chain death after growth of the first block. Unreacted macromonomer is easily removed by filtering the BBCPs through a column of hydroxylated methacrylic resin, giving pure BBCPs suitable for self-assembly studies. The short, cylindrical morphology of the bottlebrush copolymers can also be observed by atomic force microscopy (AFM) on highly-oriented pyrolytic graphite (HOPG), with heights of approximately 1.8 nm when dried (Figure 2.4 (C)).

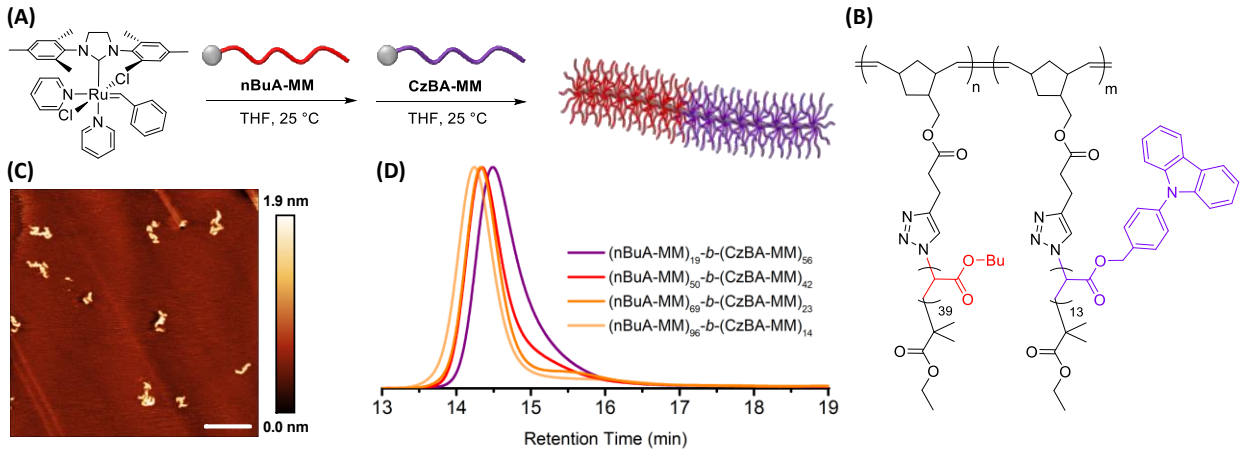

Figure 2.4. (A, B) Synthesis of amphiphilic bottlebrush copolymers via ROMP. (C) Atomic force microscopy image of **(nBuA-MM)$_{19}$-*b*-(CzBA-MM)$_{56}$** on HOPG, scale bar = 120 nm. (D) SEC RI traces for four **(nBuA-MM)-*b*-(CzBA-MM)** diblock BBCPs.

Table 2.3. Synthesis of bottlebrush diblock copolymers.

Polymer	$M_{n,\ nBuA}$[a] (kDa)	$M_{n,\ total}$ (kDa)[a]	$Đ$	wt.% nBuA
(nBuA-MM)$_{19}$-*b*-(CzBA-MM)$_{56}$	104	454	1.09	23%
(nBuA-MM)$_{50}$-*b*-(CzBA-MM)$_{42}$	276	692	1.09	40%
(nBuA-MM)$_{69}$-*b*-(CzBA-MM)$_{23}$	345	640	1.11	54%
(nBuA-MM)$_{96}$-*b*-(CzBA-MM)$_{14}$	538	853	1.10	63%

[a]Determined by SEC in THF. DP=degree of polymerization of poly(norbornene) backbone

We then sought to use these techniques to incorporate low concentrations of highly fluorescent dye molecules directly into the BBCP using the **CzBA** polymer as an organic semiconductor host to facilitate energy transfer. We synthesized a blue fluorescent acrylic dye

PAPOMA ((4'-(5-(4-(bis(4-(tert-butyl)phenyl)amino)phenyl)-1,3,4-oxadiazol-2-yl)-[1,1'-biphenyl]-4-yl)methylacrylate) including a triphenylamine-based donor and oxadiazole-based acceptor, as similar donor-acceptor pairs have been used previously to give high quantum yield materials used for emitters in OLEDs.[160,161] Copolymerization of **CzBA** with 10 wt.% **PAPOMA** by Cu(0)-RDRP gave **poly(CzBA-*co*-PAPOMA)$_{15}$-Br** (M_n = 5700, Đ = 1.12, Table 2.1), which was then converted to macromonomer **(CzBA-*co*-PAPOMA)-MM** (Table 2.2) by azide substitution and CuAAC with a norbornene-functionalized alkyne (Figure 2.5). This macromonomer was then used to synthesize a diblock BBCP (**nBuA-MM)$_{41}$-*b*-(CzBA-*co*-PAPOMA-MM)$_{39}$** via ROMP M_n = 689,000, Đ = 1.08, 34 wt.% **nBuA**). The short, cylindrical morphology of the diblock can be observed by atomic force microscopy (AFM) on highly-oriented pyrolytic graphite (HOPG), with heights of approximately 1.8 nm when dried (Figure 2.6).

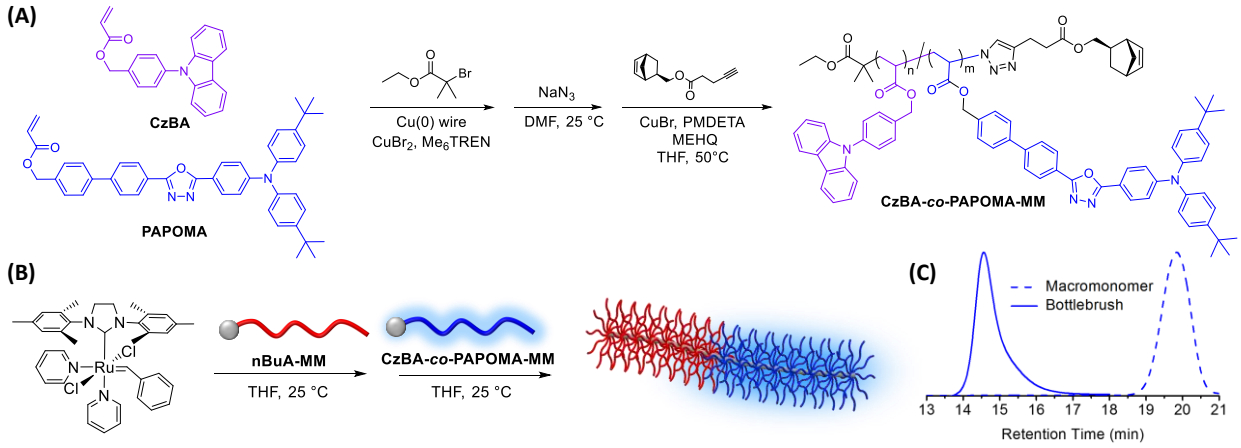

Figure 2.5. (A) Synthesis of CzBA macromonomer doped with 10 wt.% fluorescent PAPOMA dye. (B) Schematic representation of the ROMP of **nBuA-MM** with **(CzBA-*co*-PAPOMA)-MM** to give giant fluorescent polymer surfactants. (C) SEC RI traces of **(CzBA-*co*-PAPOMA)-MM** and the corresponding diblock bottlebrush copolymer.

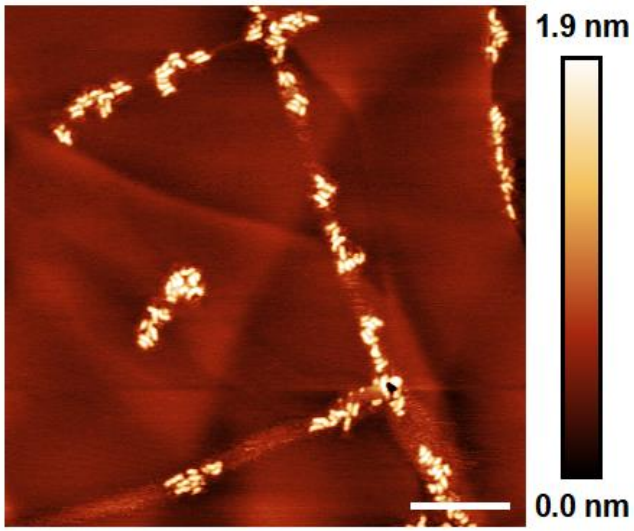

Figure 2. 6. AFM images for **nBuA$_{41}$-b-(CzBA-co-PAPOMA)$_{39}$** on HOPG substrate. Scale Bar = 120 nm.

The thermal properties of these macromonomers and diblock copolymers were then investigated by differential scanning calorimetry (DSC), which is important for understanding the annealing process when preparing self-assembled films of diblock BBCPs. This is essential as these polymers should be annealed above the glass transition temperatures (T_gs) of both blocks, to ensure that side-chains are flexible enough to allow ordered structures to form from microphase separation.[143] For the macromonomers, the T_g of **nBuA-MM** and **CzBA-MM** were found to be -53 °C and 103 °C respectively. After being polymerized into diblock bottlebrush copolymers, the Tg of the **nBuA** blocks and **CzBA** blocks all increased, to different extents (Table 2.4 and Figure 2.8), although the T_g of **the CzBA** blocks could not be observed for diblock BBCPs with a large weight percentage of **nBuA,** such as **(nBuA-MM)$_{69}$-*b*-(CzBA-MM)$_{23}$** and **(nBuA-MM)$_{96}$-*b*-(CzBA-MM)$_{14}$**.

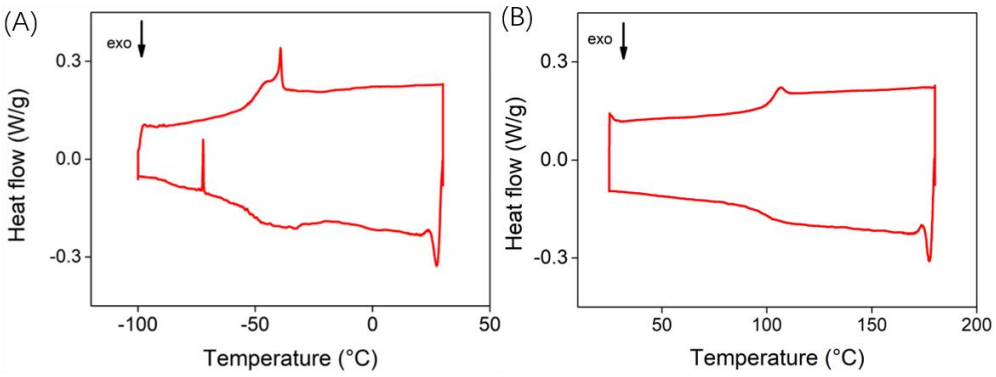

Figure 2.7. DSC traces of macromonomers (A) **nBuA-MM** and (B) **CzBA-MM** run at a rate of 10 °C min^{-1} under a 60 mL min^{-1} flow of nitrogen. Two consecutive heating and cooling cycles were performed, the second is shown.

Table 2.4. Glass transition temperatures of bottlebrush diblock copolymers.

Entry	Tg, nBuA (°C)	Tg, CzBA (°C)
(nBuA-MM)$_{19}$-*b*-(CzBA-MM)$_{56}$	–27.9	112.5
(nBuA-MM)$_{50}$-*b*-(CzBA-MM)$_{42}$	–22.4	109.2
(nBuA-MM)$_{69}$-*b*-(CzBA-MM)$_{23}$	–25.7	—[a]
(nBuA-MM)$_{96}$-*b*-(CzBA-MM)$_{14}$	–32.6	—[a]
(nBuA-MM)$_{41}$-*b*-((CzBA-*co*-PAPOMA)-MM)$_{39}$	–26.3	119.3

[a]Not observed.
[a]Not observed.

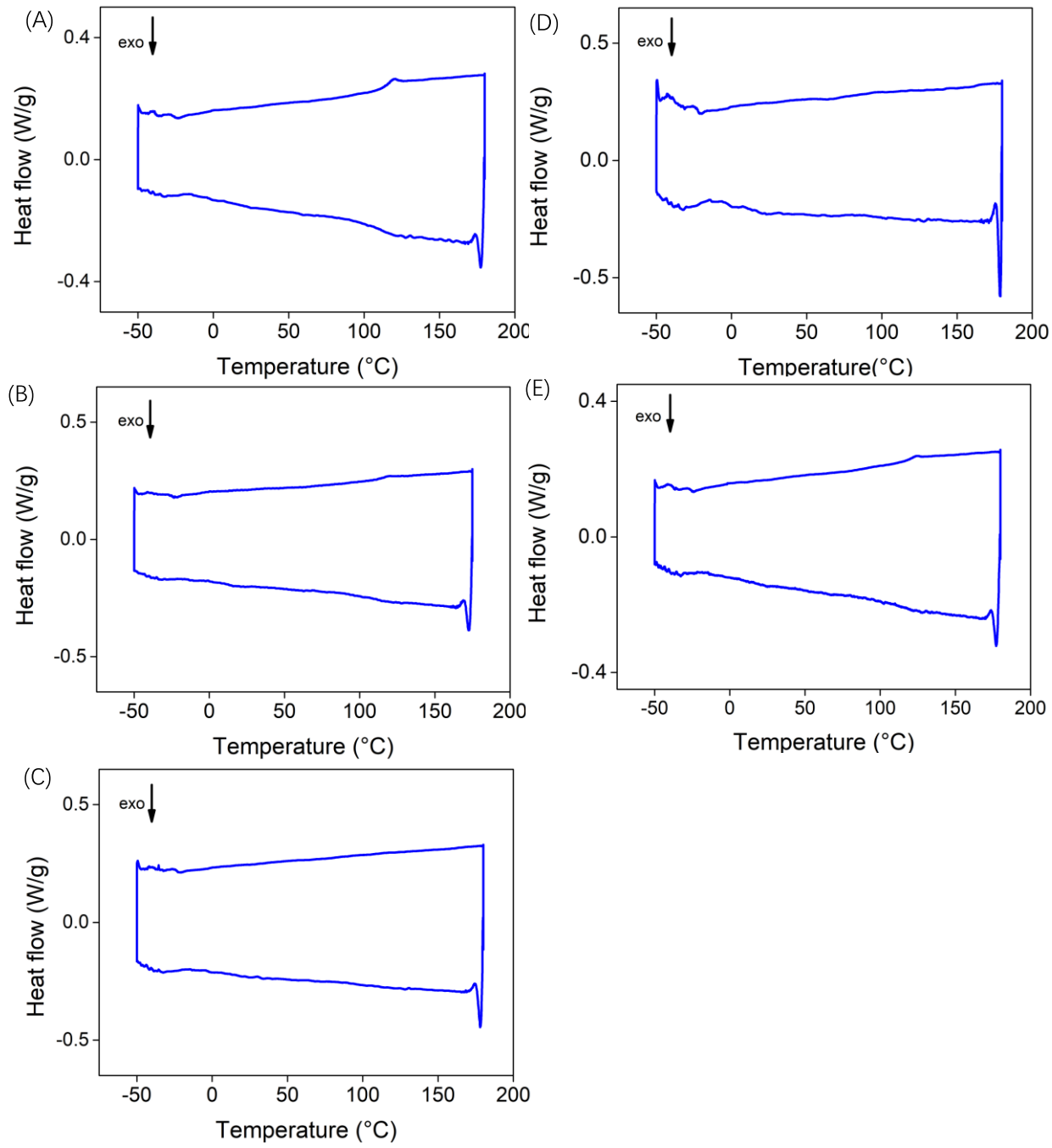

Figure 2.8. DSC traces of bottlebrush diblock copolymers (A) **(nBuA-MM)$_{19}$-*b*-(CzBA-MM)$_{56}$,** (B) **(nBuA-MM)$_{50}$-*b*-(CzBA-MM)$_{42}$,** (C) **(nBuA-MM)$_{69}$-*b*-(CzBA-MM)$_{23}$,** (D) **(nBuA-MM)$_{96}$-*b*-(CzBA-MM)$_{14}$,** (E) **(nBuA-MM)$_{41}$-*b*-(CzBA-*co*-PAPOMA-MM)$_{39}$**

2.3 Conclusions

A scalable and efficient synthetic route using "grafting through" strategy was successfully developed to synthesis well-defined diblock bottlebrush copolymers with low dispersity (PDI from 1.08 to 1.11), high grafting density and well controlled compositions. This synthetic route was achieved by two steps, which are macromonomer synthesis and bottlebrush copolymer synthesis. The first step used the growth-then-coupling method by combining Cu(0)-RDRP and two high yield reactions (azide exchange and CuAAC), which successfully removed the active bromine chain ends of prepolymers and efficiently prevented bifunctional macromonomers with norbornene groups at both ends from chain-chain coupling. In the second step, diblock bottlebrush copolymers with well-defined side chains were obtained by sequent ROMP, of which the advantages include time efficiency and functional group tolerance. The backbone length ratio of **nBuA** and **CzBA** block in diblocks was well controlled from ~1:3 to ~7:1 by varying the ratio of macromonomer and catalyst (G3). To ensure the high purity of diblock BBCPs for next step investigation of self-assembly behaviors, we also developed an efficient purification method to remove the unreacted macromonomers by filtering the BBCPs through a size exclusion column packed with hydroxylated methacrylic resin.

Using the same synthetic route, we also successfully incorporated low concentrations of highly fluorescent dye molecules directly into the BBCP using the **CzBA** polymer as an organic semiconductor host to facilitate energy transfer. The structures and compositions of macromonomers and diblock bottlebrush copolymers were fully characterized by ^{1}H-NMR, SEC and AFM. The short, cylindrical morphology of the bottlebrush copolymers can be observed by AFM, with heights of approximately 1.8 nm when dried. The thermal properties of BBCPs were

investigated using DSC, which provided us the values of T_gs to ensure the annealing temperature for BBCP self-assembly in film.

2.4 Experimental details

2.4.1 General considerations

Dry solvents were purchased from Caledon Laboratories, dried using an Innovative Technologies Inc. solvent purification system, collected under vacuum, and stored under a nitrogen atmosphere over 4 Å molecular sieves. All reagents were obtained from Sigma-Aldrich or Alfa Aesar and used as received unless otherwise stated. Tris[2-(dimethyl-amino)ethyl]amine (Me_6TREN), ethyl α-bromoisobutyrate (EBiB), mesitylene, dry tetrahydrofuran (THF), trifluoroethanol

(TFE) and dry dimethylformamide (DMF) were degassed by three freeze-pump-thaw cycles, then stored under a nitrogen atmosphere. *N*-butyl acrylate (**nBuA**) was passed through a short column of basic alumina to remove inhibitors, degassed by three freeze-pump-thaw cycles, then stored under a nitrogen atmosphere. *N*-methyl-2-pyrrolidone (NMP) was distilled, then degassed and stored under N_2 atmosphere. Dichloro[1,3-bis(2,4,6-trimethylphenyl)-2-imidazolidinylidene](benzylidene)bis(pyridine) ruthenium(II) (**G3**) was prepared according to literature procedures.[162] 4-(9H-carbazol-9-yl)benzyl acrylate (**CzBA**) and (4'-(5-(4-(bis(4-(tert-butyl)phenyl)amino)phenyl)-1,3,4-oxadiazol-2-yl)-[1,1'-biphenyl]-4-yl)methyl acrylate (**PAPOMA**) were synthesized according to previous literatures (see structures below).[163, 164] The ^{1}H nuclear magnetic resonance (NMR) spectra were measured on a Bruker AV III HD 400 MHz spectrometer with chloroform-*d* ($CDCl_3$) or benzene-d_6 (C_6D_6) as the solvent.

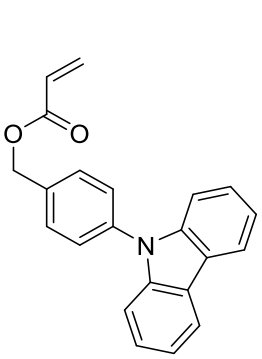

CzBA

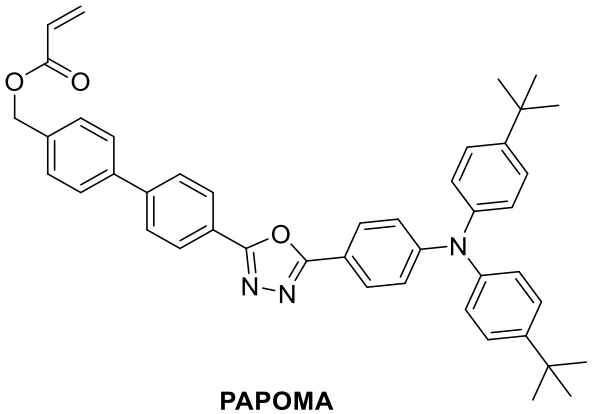

PAPOMA

Size Exclusion Chromatography (SEC)

SEC experiments were conducted in chromatography-grade THF at concentrations of 1 – 10 mg mL^{-1} using a Malvern OMNISEC GPC instrument equipped with a Viscotek TGuard guard column (CLM3008), and Viscotek T3000 (CLM3003) and T6000 (CLM3006) GPC columns packed with porous poly(styrene-*co*-divinylbenzene) particles regulated at a temperature of 35 °C. Signal response was measured using differential viscometer, differential refractive index, photodiode array and right-angle and low angle light scattering detectors. Calibration of interdetector distances was performed using a polystyrene standard from Malvern Inc. Refractive index increments (d*n*/d*c*) were determined using 100% mass recovery methods from Malvern OMNISEC software version 10.2 with each polymer sample being run at least five times to ensure reproducibility of the calculated refractive index increment.

Thermal Analysis

Glass transition temperatures were determined using differential scanning calorimetry (DSC) on a NETZSCH DSC 214 Polyma instrument. The diblock copolymer samples were placed in an aluminum pan and heated from –50 to 180 °C at 10 °C min^{-1} under a flow of nitrogen for 2

heating/cooling cycles, while nBuA and CzBA macromonomers were heated from –30 to 100 °C and 25 to 180 °C respectively.

Atomic Force Microscopy (AFM)

Atomic force microscopy (AFM) images were obtained using an Asylum Instruments Cypher S AFM system in tapping mode at scan rates of 0.30 Hz. Samples were prepared by spin-coating solutions of polymer onto freshly cleaved highly-oriented pyrolytic graphite (HOPG) at 4000 rpm for 30 s at concentrations of ~0.001 mg mL–1. For best results, 1,2-dichloroethane was used as the solvent for nBuA19-b-CzBA56 and nBuA41-b-(CzBA-co-PAPOMA)39. Samples were placed in a vacuum oven (60 ºC) for at least 2 h before images were obtained using Mikromasch HQ:NSC14/No Al or HQ:NSC19/No Al probes, with typical resonance frequencies f and spring constants k of (f = 160 kHz, k = 5 N/m) and (f = 65 kHz, k = 0.5 N/m) respectively.

2.4.2 Synthetic procedures of macromonomers

Synthesis of poly(nBuA)$_{40}$-Br by Cu(0)-RDRP

Modified from a previously reported procedure.[165] In a nitrogen atmosphere glovebox, a 20 mL vial equipped with a magnetic stir bar was filled with **nBuA** (4.00 g, 31.2 mmol, 40.0 eq.), EBiB (115 μL, 0.780 mmol, 1.00 eq.), 1.00 mL of a solution of Me_6TREN in TFE (20.0 μL mL^{-1}; Me_6TREN: 1.80×10^{-2} g, 7.80×10^{-2} mmol, 0.100 eq.). Following the addition of TFE (half the volume of monomer, 2.2 ml), the mixture was stirred at room temperature for 10 minutes to allow all reagents to fully dissolve. Concurrently, a 10 cm piece of 18 gauge copper (0) wire was soaked in concentrated HCl for 15 minutes to remove surface impurities, then washed with water followed by acetone three times each, dried in an oven at 60 °C for 5 minutes and transferred to the glovebox.

The wire was added to the mixture to initiate the polymerization. The polymerization was stirred at 25 °C in the glove box for 5 hours, then quenched by removing the copper wire and passing the solution through a short column of neutral alumina in CH_2Cl_2. The solution was concentrated *in vacuo*, then precipitated into 20% water in MeOH three times. The final product was dried *in vacuo* overnight. Yield = 2.8 g. M_n (SEC) = 5200 Da (dn/dc = 0.057), Đ = 1.16. ^{1}H NMR: see Figure 2.9.

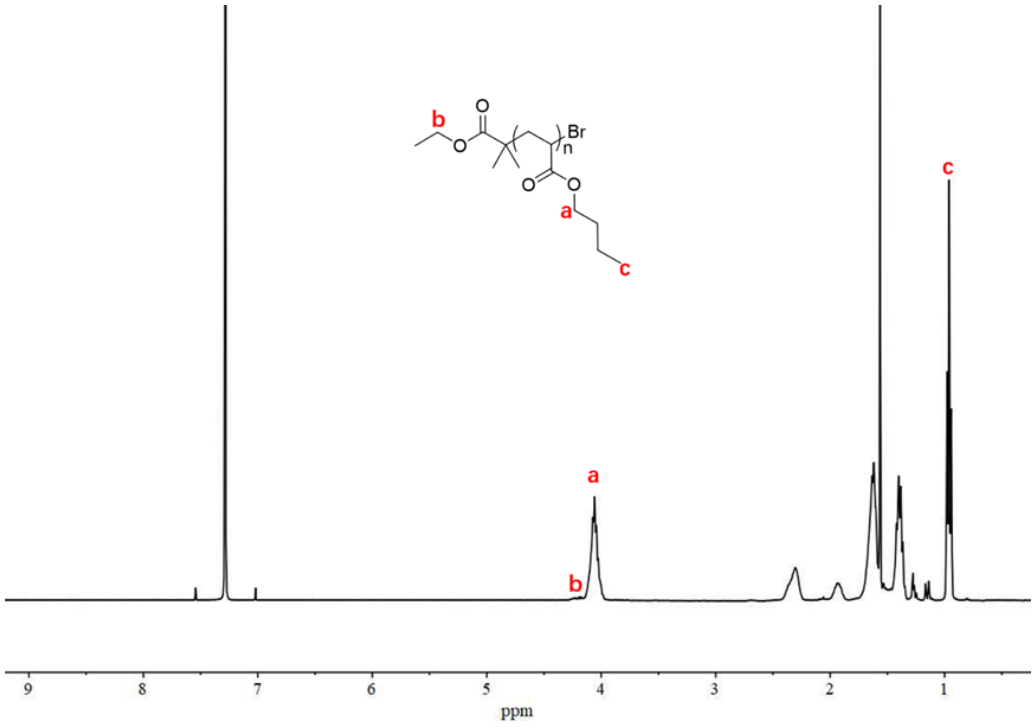

Figure 2.9. ^{1}H NMR spectrum of **poly(nBuA)$_{40}$-Br** in $CDCl_3$.

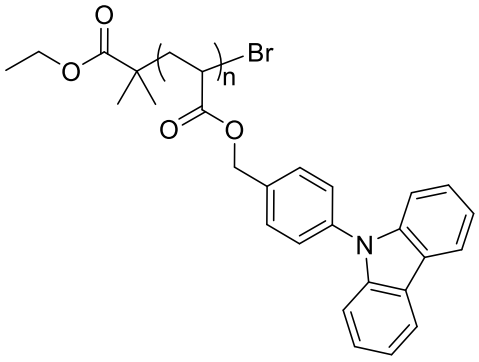

Synthesis of poly(CzBA)$_{15}$-Br by Cu(0)-RDRP

Prepared according to a modified literature procedure.[163] In a nitrogen atmosphere glovebox, **CzBA** (2.00 g, 6.11 mmol, 15.2 eq.), 59 μL of a solution of EBiB in NMP (C_{EBiB} =50 mg mL^{-1}; EBiB: 78 mg, 0.40 mmol, 1.0 eq.), and 1.5 mL of a solution of $CuBr_2$/$MeTREN_6$ in NMP (C_{Cu} = 3.75 mg mL^{-1}; $CuBr_2$: 5.8 mg, 2.6 × 10^{-2} mmol, 0.065 eq.; Me_6TREN: 6.3 mg, 2.7 × 10^{-2} mmol, 0.068 eq.) was added to a 20 mL vial. 8.4 mL of NMP was then added to dissolve the mixture. Concurrently, a 20 cm piece of 18 gauge copper (0) wire was soaked in concentrated HCl for 15 minutes to remove surface impurities, then washed with water followed by acetone, dried *in vacuo* and taken into the glovebox. The wire was added to the mixture to initiate the polymerization. The reaction was stirred at 25 °C in the glove box. After 6.5 hours, a 25 μL aliquot was taken and diluted with $CDCl_3$, and the conversion monitored by ^{1}H NMR. At approximately 78 % conversion (after 8 hours), the polymerization was quenched by removing the copper wire and adding deionized water, then the crude polymer was isolated by centrifugation. Further purification was done by preparatory size exclusion chromatography (Bio-Rad Bio-Beads S-X1 Support) in THF to remove residual monomer. The fractions containing polymer were determined by SEC analysis. All fractions containing polymer were collected and dried *in vacuo* overnight. Yield = 1.73 g. M_n (SEC) = 4600 Da (dn/dc = 0.1946), Đ = 1.16. ^{1}H NMR: see Figure 2.10.

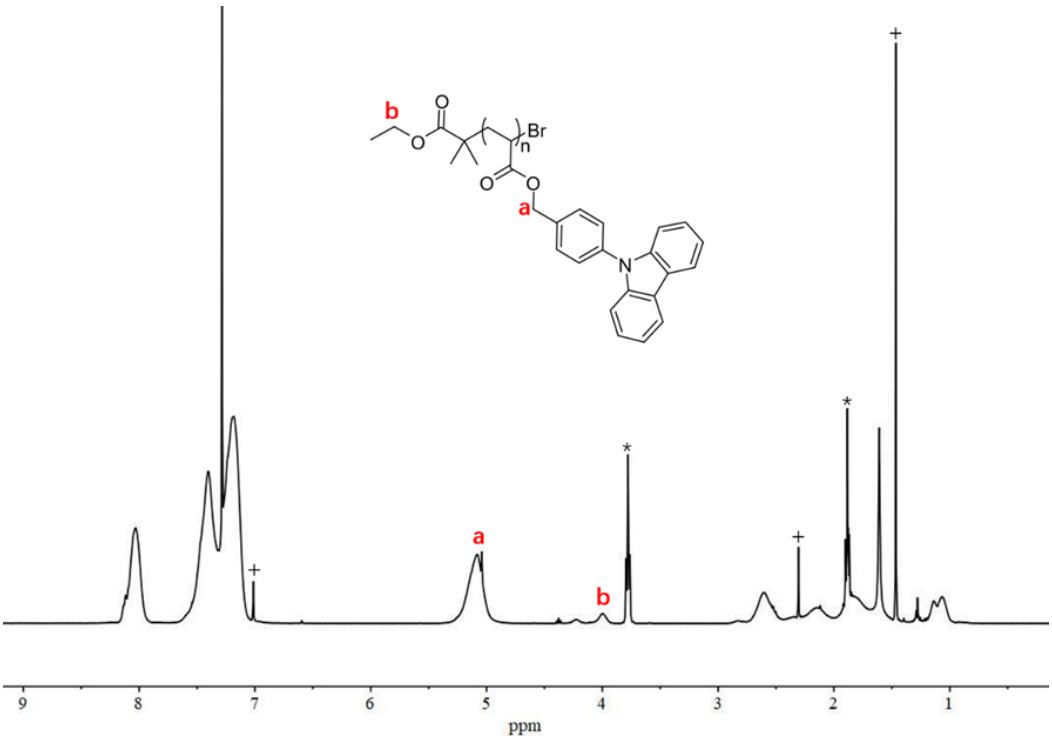

Figure 2.10. ^{1}H NMR spectrum of **poly(CzBA)$_{15}$-Br** in $CDCl_3$. * = THF; + = BHT.

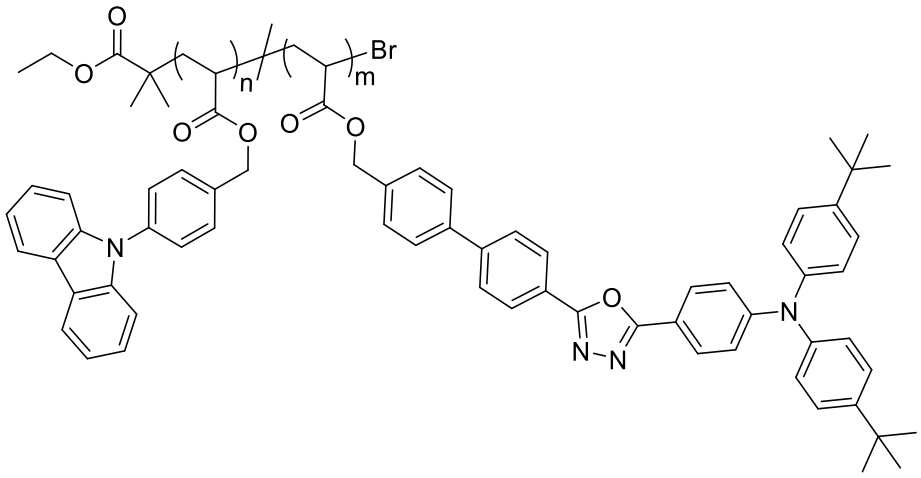

Synthesis of poly(CzBA-co-PAPOMA)$_{15}$-Br by Cu(0)-RDRP

Poly(CzBA-*co*-PAPOMA)$_{15}$-Br was synthesized in analogy with **poly(CzBA)$_{15}$-Br**. In a nitrogen atmosphere glovebox, to a 20 mL vial equipped with a magnetic stir bar was added **CzBA** (0.452 g. 1.38 mmol, 13.7 eq.), **PAPOMA** (48.8 mg, 0.0750 mmol, 0.750 eq.), 14.7 μL of a

solution of EBiB in NMP (C_{EBiB}=1.33 g mL^{-1}; EBiB: 19.5 mg, 0.100 mmol, 1.00 eq.), and 0.387 mL of a solution of $CuBr_2$/Me_6TREN in NMP (C_{Cu} = 3.75 mg mL^{-1}; $CuBr_2$: 1.5 mg, 6.5 × 10^{-3} mmol, 0.065 eq.; Me_6TREN: 1.6 mg, 6.8 x 10^{-3} mmol, 0.068 eq.). The total volume was kept to 2.9 mL of solvent. The mixture was stirred at room temperature for 10 minutes to allow all reagents to fully dissolve. A 5 cm piece of 18 gauge copper (0) wire was soaked in concentrated HCl for 10 minutes to remove surface impurities, then washed with water followed by acetone, dried *in vacuo* and taken into the glovebox. The wire was added to the mixture to initiate the polymerization. After 4 hours, a 25 μL aliquot was taken and diluted with $CDCl_3$, and the conversion monitored by ^{1}H NMR. At approximately 73 % conversion (after 7.5 hours), the polymerization was quenched by addition of water followed by filtration. The polymer was dissolved in CH_2Cl_2, dried over $MgSO_4$ and concentrated *in vacuo*. The residue was purified by preparatory SEC in THF (Bio-Rad Bio-Beads S-X1 Support) and fractions containing polymer were determined by SEC analysis. All fractions containing polymer were collected and dried in vacuo overnight. Yield = 381 mg. M_n (SEC) = 5700 Da, Đ = 1.12. ^{1}H NMR: see Figure 2.11.

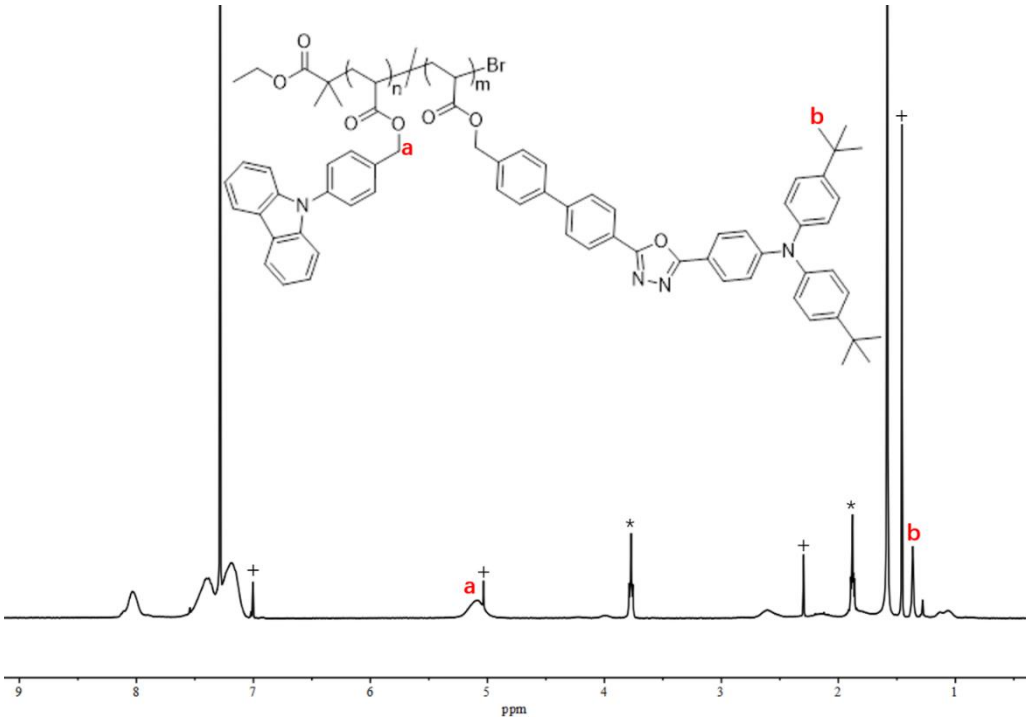

Figure 2.11. ^{1}H NMR spectrum of **poly(CzBA-*co*-PAPOMA)$_{15}$-Br** in $CDCl_3$. * = THF; + = BHT.

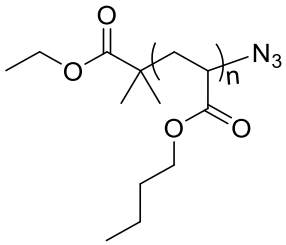

Synthesis of azido-terminated poly(nBuA)$_{40}$-N$_3$

Prepared according to a modified literature procedure.[126] To a 20 mL vial capped with a Teflon-lined lid and equipped with a magnetic stir bar was added **poly(nBuA)$_{40}$-Br** (2.40 g, 0.462 mmol, 1.00 eq.), sodium azide (60.1 mg, 0.924 mmol, 2.00 eq.), and 12 mL of dry DMF. The reaction was stirred at 25 °C in the glovebox for 24 hours. The mixture was concentrated *in vacuo*, then dissolved in CH_2Cl_2, washed 5 times with 100 mL deionized H_2O, dried over $MgSO_4$, filtered and concentrated *in vacuo.* Yield = 1.80 g. M_n (SEC) = 5300 Da (dn/dc = 0.057), Đ = 1.12. ^{1}H

NMR: see Figure 2.12.

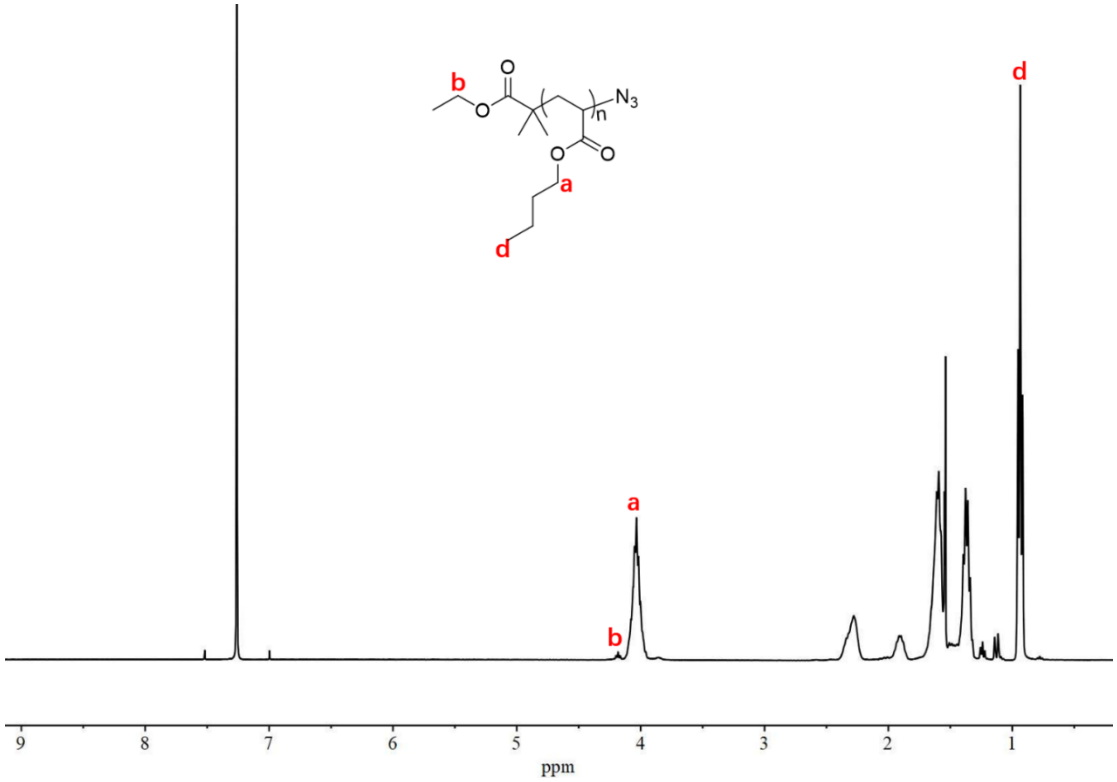

Figure 2.12. ^{1}H NMR spectrum of **poly(nBuA)$_{40}$-N$_3$** in $CDCl_3$.

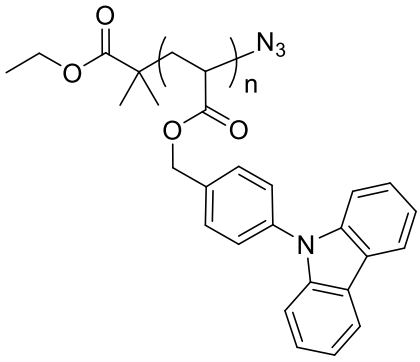

Synthesis of poly(CzBA)$_{15}$-N$_3$

To a 20 mL vial capped with a Teflon-lined lid and equipped with a magnetic stir bar was added **poly(CzBA)$_{15}$-Br** (1.67 g, 0.361 mmol, 1.00 eq.), sodium azide (46.9 mg, 0.722 mmol, 2.00 eq.) and 10 mL of dry DMF. The reaction was stirred at 25 °C in the glovebox for 24 hours. The

mixture was concentrated *in vacuo*, then dissolved in CH_2Cl_2, washed 5 times with 100 mL deionized H_2O, dried over $MgSO_4$, filtered and concentrated *in vacuo.* Yield = 1.52 g. M_n (SEC) = 5000 Da (dn/dc = 0.1946), Đ = 1.16. ^{1}H NMR: see Figure 2.13.

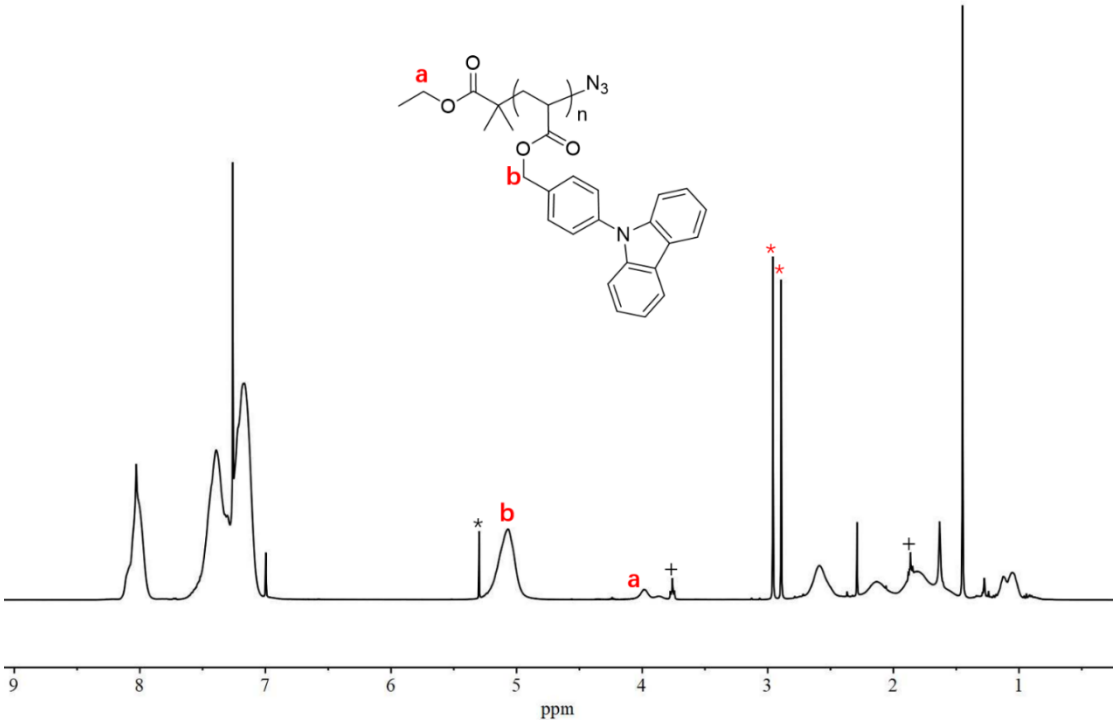

Figure 2.13. ^{1}H NMR spectrum of **poly(CzBA)$_{15}$-N$_3$** in $CDCl_3$. * = DCM; + = THF; * = DMF.

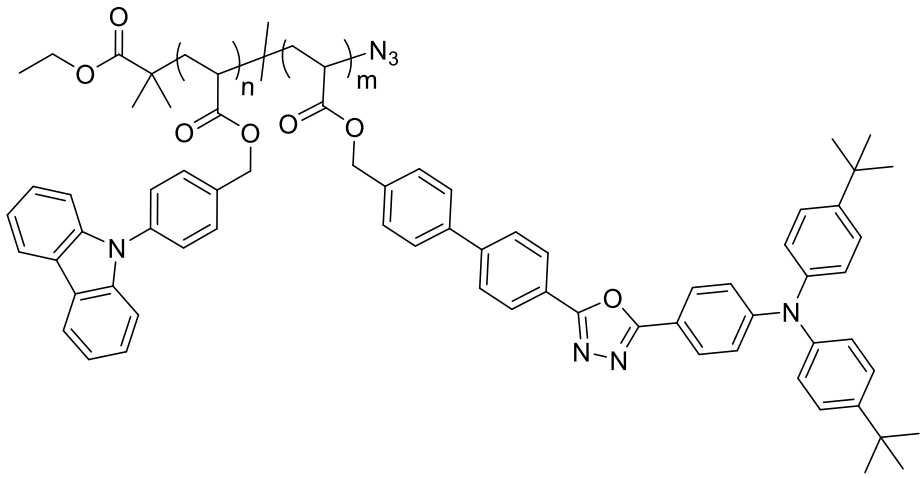

Synthesis of azido-terminated poly(CzBA-co-PAPOMA)$_{15}$-N$_3$

To a 20 mL vial capped with a Teflon-lined lid and equipped with a magnetic stir bar was added **poly(CzBA-*co*-PAPOMA)$_{15}$-Br** (381 mg, 7.50 x 10^{-2} mmol, 1.00 eq.), sodium azide (9.8 mg, 0.15 mmol, 2.0 eq.) and 2.5 mL of dry DMF. The reaction was stirred at 25 °C in the glovebox for 24 hours. The mixture was concentrated *in vacuo*, then dissolved in CH_2Cl_2, washed 5 times with 100 mL deionized H_2O, dried over $MgSO_4$, filtered and concentrated *in vacuo.* Yield = 309 mg. M_n (SEC) = 5800 Da, Đ = 1.11. ^{1}H NMR: see Figure 2.14.

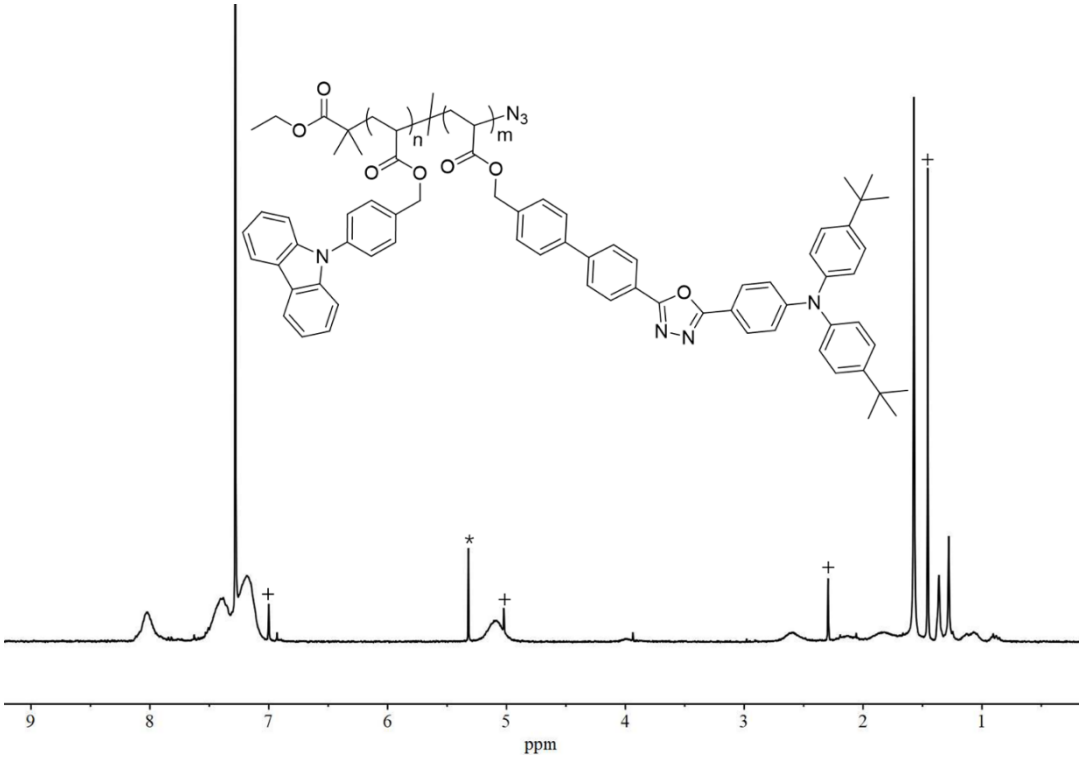

Figure 2.14. ^{1}H NMR spectrum of **poly(CzBA-co-PAPOMA)$_{15}$-N$_3$** in $CDCl_3$. * = DMF; + = BHT.

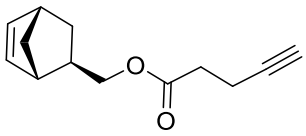

***Synthesis of exo-5-Norbornylmethylpent-4-ynoate* (1)**

A 100 mL round-bottom flask equipped with a magnetic stir bar was charged with *exo*-5-norbornene-2-methanol (1.63 g, 13.1 mmol, 1.00 eq.), 4-pentynoic acid (1.42 g, 14.5 mmol, 1.10 eq.), *N*-(3-dimethylaminopropyl)-*N′*-ethylcarbodiimide hydrochloride (3.02 g, 15.8 mmol, 1.20 eq.), and 4-dimethylaminopyridine (0.527 g, 4.31 mmol, 0.328 eq.). The flask was then degassed, and 40 mL of degassed anhydrous CH_2Cl_2 was added using a syringe under N_2. The mixture was stirred at 25 °C under N_2 for 24 hours. The reaction was extracted with CH_2Cl_2 and washed with H_2O (50 mL) and brine (50 mL), dried over $MgSO_4$, filtered and concentrated in vacuo to yield **1** as a colorless oil. Yield = 2.36 g (88%). ^{1}H NMR (400 MHz, Chloroform-*d*): δ 6.13-6.04 (m, 2H), 4.18 (dd, J =10.9, 6.5 Hz, 1H), 4.00 (dd, J = 10.9, 9.2 Hz, 1H), 2.83 (dq, J = 3.0, 1.6 Hz, 1H), 2.70 (dt, J = 2.9, 1.4 Hz, 1H), 2.62 – 2.46 (m, 4H), 1.97 (t, J = 2.5 Hz, 1H), 1.72 (dddd, J = 10.6, 8.0, 5.3, 1.3 Hz, 1H), 1.41-1.21 (m, 3H), 1.15 (ddd, J = 11.8, 4.5, 3.5 Hz, 1H) ppm; ^{13}C NMR (101 MHz, Chloroform-*d*): δ 171.80, 136.93, 136.17, 82.51, 69.02, 68.81, 44.94, 43.63, 41.58, 37.95, 33.43, 29.55, 14.43 ppm. HRMS (EI) *m/z*: [$M^{+\bullet}$] calcd for [$C_{13}H_{16}O_2{}^{23}Na$]$^\bullet$, 227.1048; found, 227.1046; difference: –0.9 ppm.

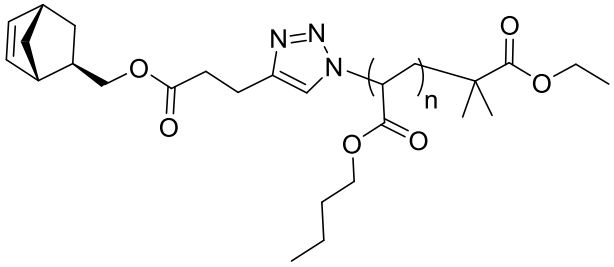

Synthesis of Macromonomer nBuA-MM via "Click" Coupling of Prepolymer and S1

Prepared according to a modified literature procedure.[126] In a nitrogen atmosphere glovebox, to a 20 mL vial capped with a Teflon-lined lid and equipped with a magnetic stir bar was added **poly(nBuA)$_{40}$ -N$_3$** (1.59 g, 0. 302 mmol, 1.00 eq.), **S1** (124 mg, 0.604 mmol, 2.00 eq.),

83 µL of a solution of CuBr/PMDETA in THF (C_{Cu} = 7.90 mg mL^{-1}; CuBr: 6.5 mg, 4.5 x 10^{-2} mmol, 0.15 eq.; PMDETA: 8.2 mg, 4.8 x 10^{-2} mmol, 0.16 eq.), 125 µL of a solution of MEHQ (C_{MEHQ} = 3.0 mg mL^{-1}; MEHQ: 0.37 mg, 3.0 x 10^{-3} mmol, 0.01 eq.), and 11 mL of THF. The mixture was stirred at 50 °C in a glovebox for 30 hours. After reaction the catalyst was removed by passing the mixture through a short neutral alumina column in THF. The residue was then purified by preparatory SEC (Bio-Rad Bio-Beads S-X1 Support) in THF and fractions containing polymer were determined by SEC analysis. All fractions containing polymer were collected and dried *in vacuo* overnight. Reprecipitation in MeOH was used to remove BHT introduced by THF after preparatory SEC. Yield = 1.40 g. M_n (SEC) = 5600 Da (dn/dc = 0.057), Đ = 1.14. ^{1}H NMR: see Figure 2.15.

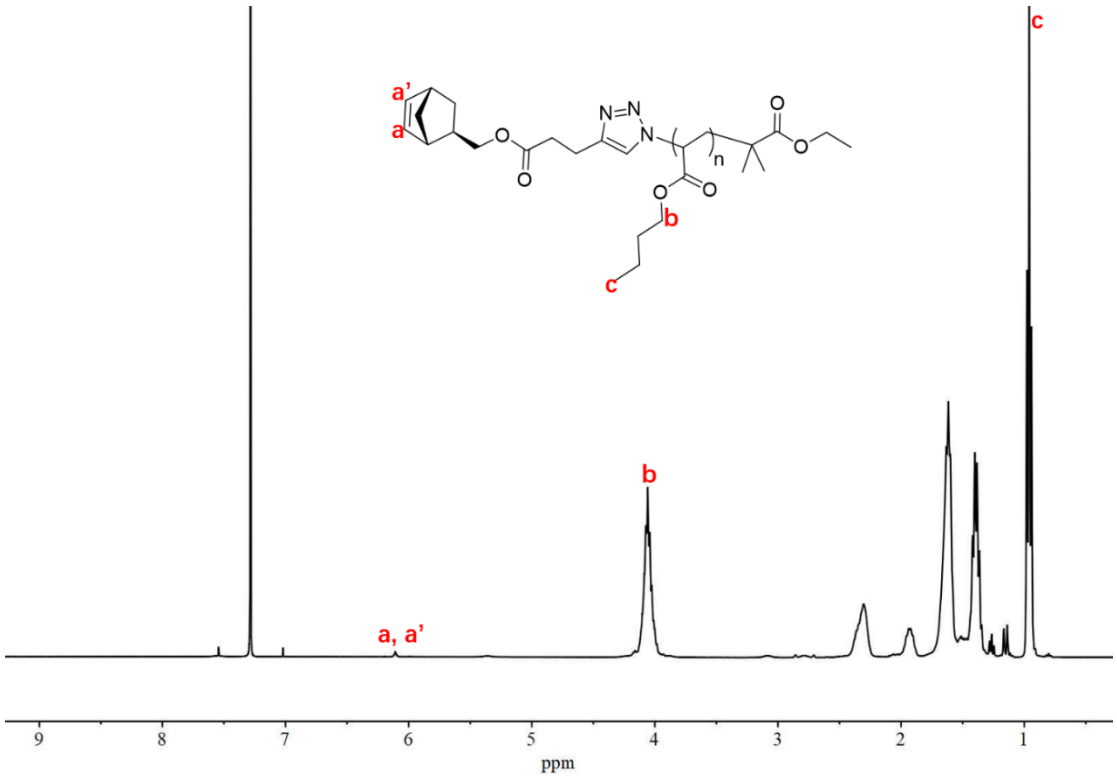

Figure 2.15. ^{1}H NMR spectrum of **nBuA-MM** in $CDCl_3$.

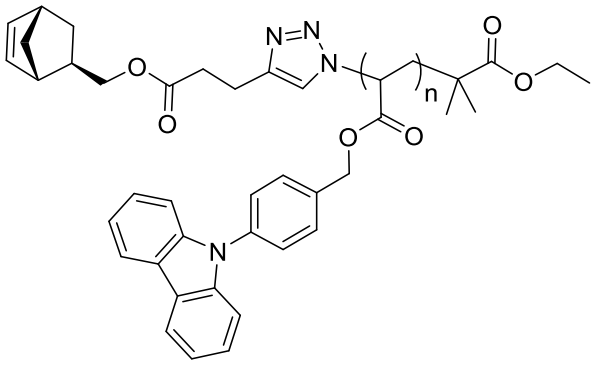

Synthesis of Macromonomer CzBA-MM via "Click" Coupling of Prepolymer and S1

In a nitrogen atmosphere glovebox, to a 20 mL vial capped with a Teflon-lined lid and equipped with a magnetic stir bar was added **poly(CzBA)$_{15}$-N$_3$** (1.41 g, 0. 281 mmol, 1.00 eq.), **1** (115 mg, 0.562 mmol, 2.00 eq.), 1 mL of a solution of CuBr/PMDETA in THF (C_{Cu} = 5.94 mg mL^{-1}; CuBr: 6.0 mg, 4.2 x 10^{-2} mmol, 0.15 eq.; PMDETA: 7.7 mg, 4.4 x 10^{-2} mmol, 0.16 eq.), 116 µL of a solution of MEHQ (C_{MEHQ} = 3.0 mg mL^{-1}; MEHQ: 0.35 mg, 2.8 x 10^{-3} mmol, 0.010 eq.), and 10 mL of THF. The mixture was stirred at 50 °C in a glovebox for 30 hours. After reaction the catalyst was removed by passing the mixture through a short neutral alumina column in THF. The residue was then purified by preparatory SEC (Bio-Rad Bio-Beads S-X1 Support) in THF and fractions containing polymer were determined by SEC analysis. All fractions containing polymer were collected and dried *in vacuo* overnight. Reprecipitation in MeOH was used to remove BHT introduced by THF after preparatory SEC. Yield = 1.35 g. M_n (SEC) = 5200 Da (dn/dc = 0.1946), Đ = 1.15. ^{1}H NMR: see Figure 2.16.

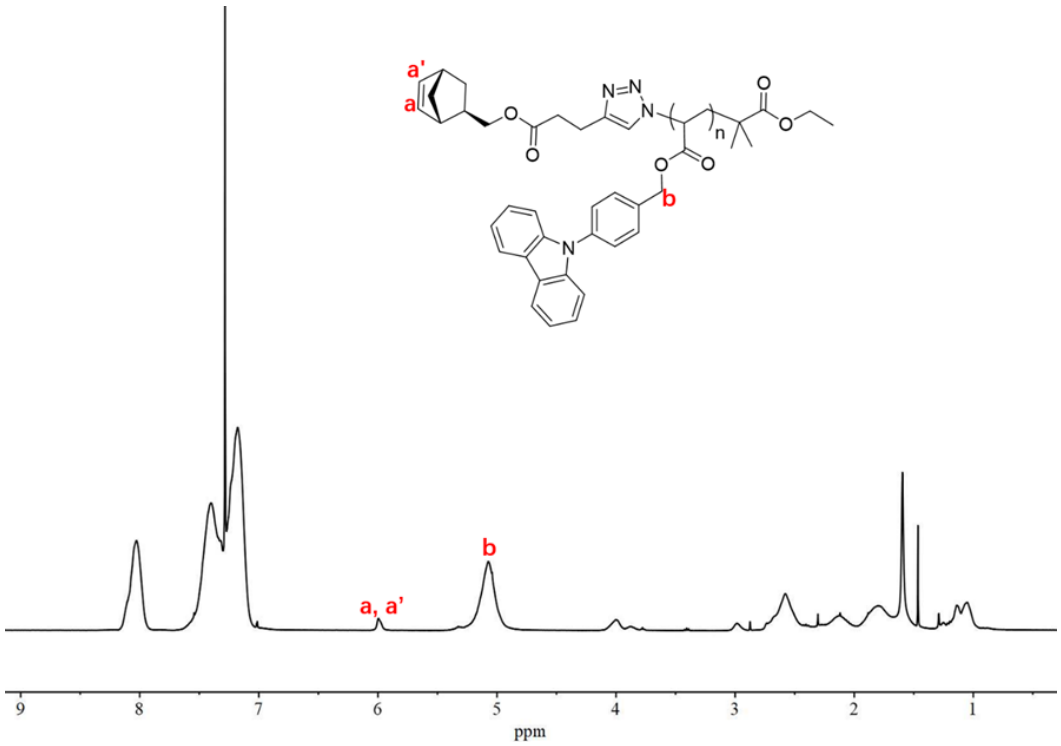

Figure 2.16. ^{1}H NMR spectrum of **CzBA-MM** in $CDCl_3$.

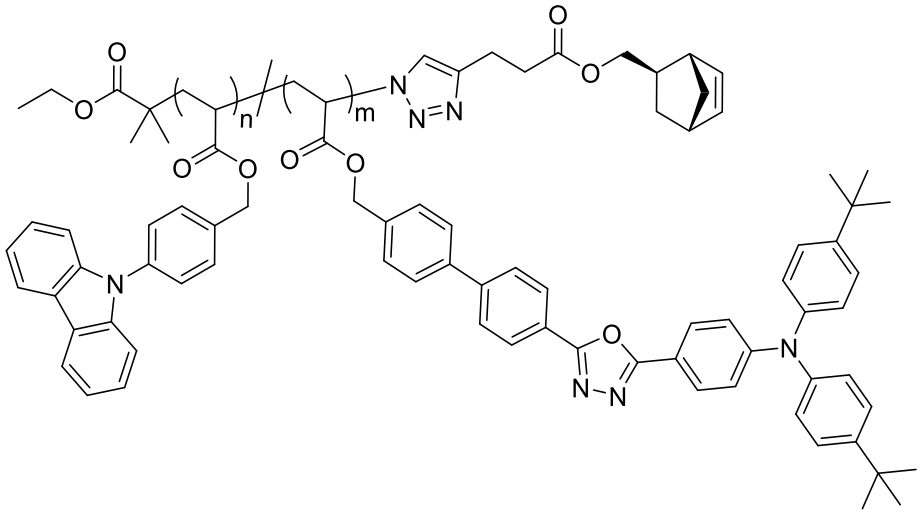

Synthesis of Macromonomer CzBA-co-PAPOMA-MM via "Click" Coupling of Prepolymer and S1

In a nitrogen atmosphere glovebox, to a 20 mL vial capped with a Teflon-lined lid and

equipped with a magnetic stir bar was added **poly(CzBA-*co*-PAPOMA)$_{15}$-N$_3$** (305 mg, 5.20 x 10^{-2} mmol, 1.00 eq.), **S1** (21.2 mg, 0.104 mmol, 2.00 eq.), 153 µL of a solution of CuBr/PMDETA in THF (C_{Cu} = 8.39 mg mL^{-1}; CuBr: 1.1 mg, 7.8 x 10^{-3} mmol, 0.15 eq.; PMDETA: 1.4 mg, 8.2 x 10^{-3} mmol, 0.16 eq.), 21 µL of a solution of MEHQ (C_{MEHQ} = 3.0 mg mL^{-1}; MEHQ: 0.064 mg, 5.2 x 10^{-4} mmol, 0.010 eq.), and 2 mL of THF. The mixture was stirred at 50 °C in a glovebox for 30 hours. After reaction the catalyst was removed by passing the mixture through a short neutral alumina column in THF. Then the residue was purified by preparatory SEC (Bio-Rad Bio-Beads S-X1 Support) in THF and fractions containing polymer were determined by SEC analysis. All fractions containing polymer were collected and dried *in vacuo* overnight. Reprecipitation in MeOH was used to remove BHT introduced by THF after preparatory SEC. Yield = 270 mg. M_n (SEC) = 6000 Da, Đ = 1.12. ^{1}H NMR: see Figure 2.17.

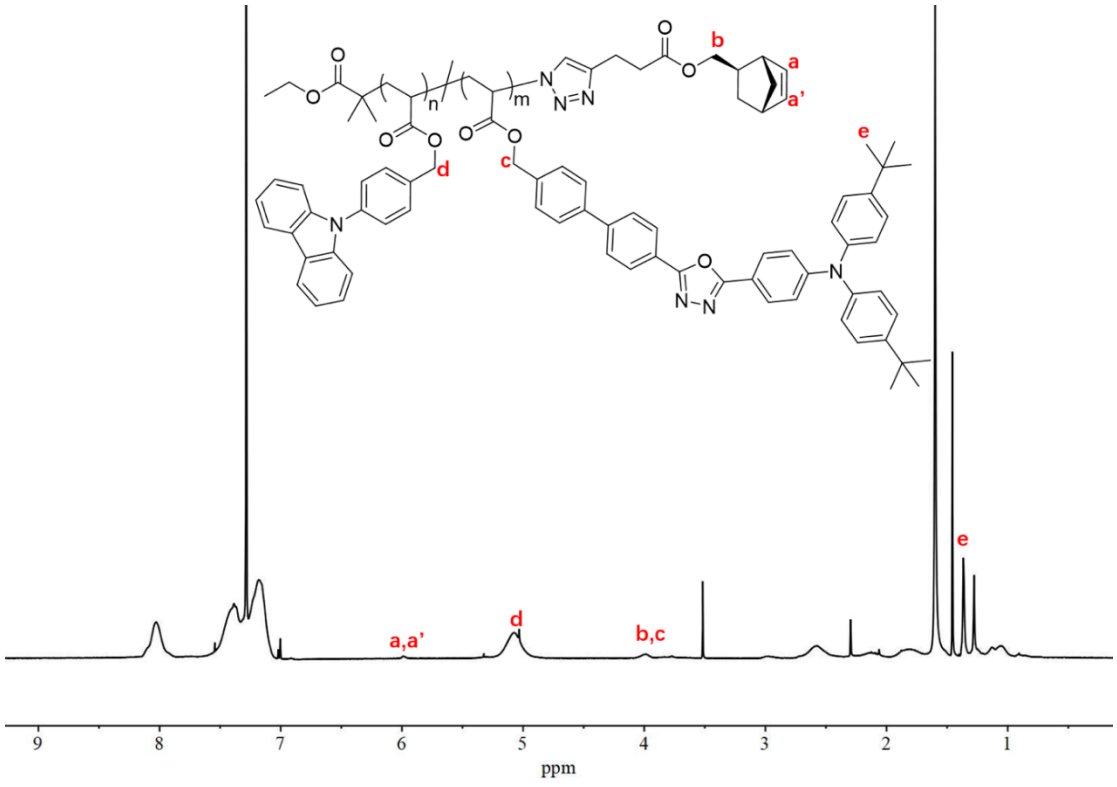

Figure 2.17. ^{1}H NMR spectrum of **(CzBA-*co*-PAPOMA)-MM** in $CDCl_3$.

2.4.3 Synthetic procedures of diblock bottlebrush copolymers

The following is the general procedure for the synthesis of (nBuA-MM)-b-(CzBA-MM) BBCPs via ROMP. Typical experiment for the preparation of (**nBuA-MM)$_{50}$-*b*-(CzBA-MM)$_{42}$**: To a 2 mL vial capped with a Teflon-lined lid and equipped with a magnetic stir bar was added **nBuA-MM** (56 mg, 9.9 × 10^{-3} mmol, 50 eq.) and 200 μL of THF (dry, degassed, filtered through basic alumina). Using a glass microsyringe, 69 μL of a solution of Grubbs' 3rd-generation ruthenium catalyst (bis(pyridine), **G3**)[33] in THF (C_{G3} = 2.0 mg mL^{-1}; G3: 0.14 mg, 2.0 x 10^{-4} mmol, 1.0 eq.) was added to the dissolved polymer rapidly in one portion. The mixture was stirred at room temperature for 1 h. Two 5 μL aliquots were taken for ^{1}H NMR and SEC analysis, before addition of **CzBA-MM** (52 mg, 9.9 x 10^{-3} mmol, 50 eq.) dissolved in 200 μL of THF. The mixture was stirred at room temperature for an additional 2 h. Two 5 μL aliquots were taken for ^{1}H NMR and SEC analysis, and the polymerization was removed from the glove box, quenched with one drop of ethyl vinyl ether, and immediately purified by preparatory SEC (Toyopearl HW-55F resin) in THF and fractions containing polymer were determined by SEC analysis. All fractions containing polymer were collected and dried *in vacuo* overnight. Reprecipitation in MeOH was used to remove BHT introduced by THF after preparatory SEC. Yield = 68 mg. The BBCPs with different block ratios were prepared as above, using 100 mg total macromonomer varying ratios of **nBuA-MM** and **CzBA-MM f**ollows: **(nBuA-MM)$_{19}$-*b*-(CzBA-MM)$_{56}$** (20:80, Yield 72 mg); **(nBuA-MM)$_{69}$-*b*-(CzBA-MM)$_{23}$ (**70:30, Yield 60 mg); **(nBuA-MM)$_{96}$-*b*-(CzBA-MM)$_{14}$** (90:10, Yield 65 mg). **(nBuA-MM)$_{41}$-*b*-(CzBA-*co*-PAPOMA-MM)$_{39}$** was prepared as above using 50 mg **nBuA-MM** and 50 mg **CzBA-*co*-PAPOMA-MM**, Yield 84 mg. ^{1}H NMR spectra for all BBCPs are shown in Figure 2.18.

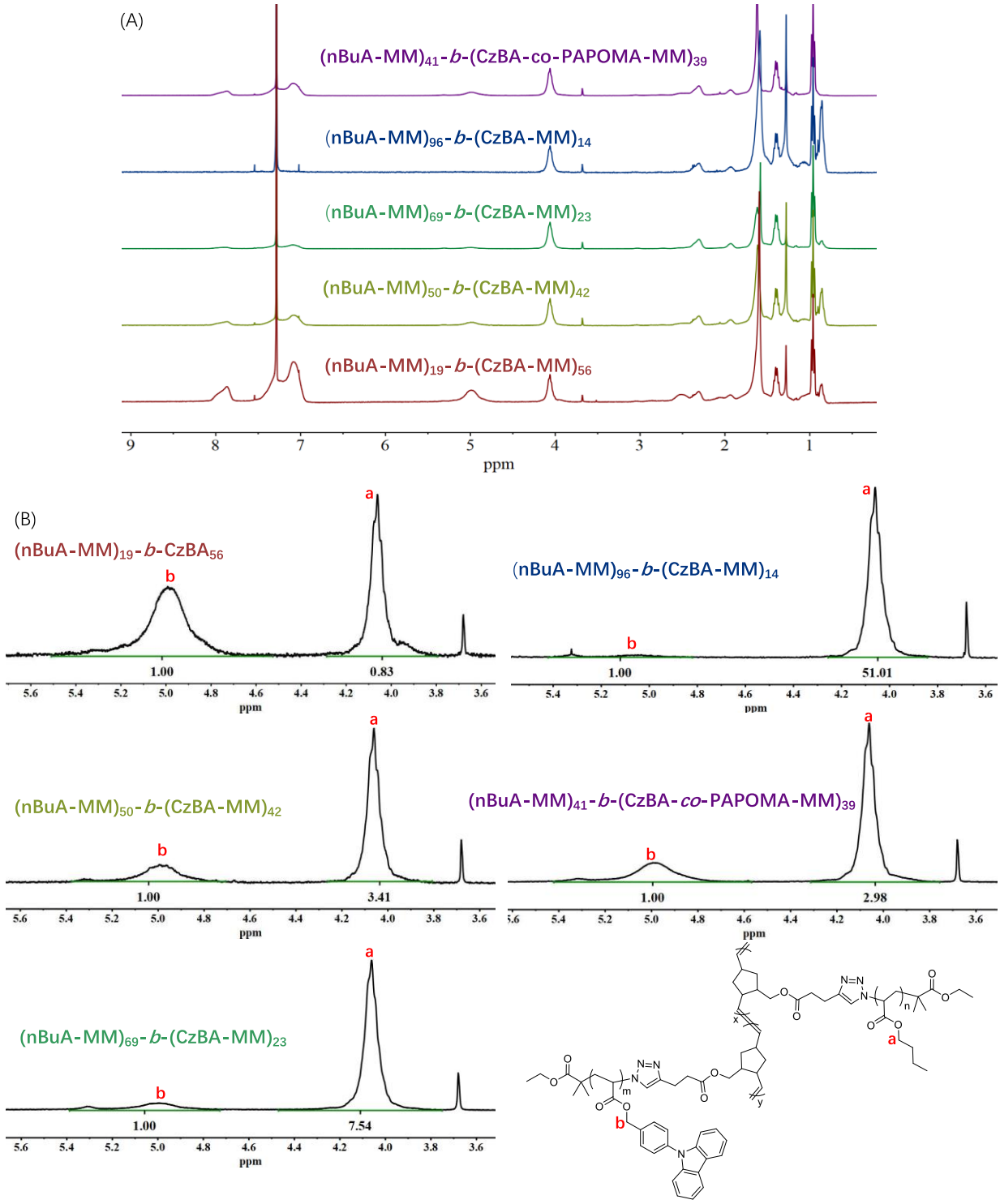

Figure 2.18. [1]H NMR spectrum of bottlebrush diblock copolymers in $CDCl_3$. The integrated areas of peaks a and b were used to determine the degree of polymerization of poly(norbornene) backbone for the **CzBA-MM** block. For the

Chapter 3: Self-assembly of bottlebrush diblock copolymers in solution and in film

This chapter describes self-assembly methods in detail using well-defined diblock bottlebrush copolymers and demonstrates the complementary use of scattering and microscopy techniques to characterize self-assembled nanostructures in solution or in film. Specifically, dynamic light scattering (DLS) was used to determine the critical micelle concentration (CMC) and micelle size distribution in solution. TEM and cryo-TEM were used to characterize the morphology and structure of self-assembled BBCPs in solution before and after being dried. Moreover, the luminescent properties were further investigated using fluorescence and UV-vis spectroscopy.

3.1 Introduction

As discussed in Chapter 1, the self-assembly of bottlebrush copolymers has attracted great attention given their unusual architectures resulting in a number of unique and potentially useful properties. These include reduced entanglement with high molecular weights, rapid self-assembly kinetics to give structures with large domains, extremely low CMCs in a selective solvent, and the ability to functionalize bottlebrush side-chains for recognition, imaging and drug delivery.[129,137,140] To understand the nanomaterials constructed from BBCP self-assembly and take full advantage of these properties, appropriate self-assembly techniques and characterization methods need to be explored first.

3.1.1 Self-assembly techniques

The self-assembly of bottlebrush copolymers can be accomplished in solution, in thin and bulk films, and at interfaces,[146] with each process requiring different self-assembly techniques. In solution, bottlebrush polymeric surfactants can be developed for encapsulation,[166] delivery,[140] signaling, and detection.[140,167] These applications require the ability to tune the size and shape of BBCPs through changes in the backbone and side-chain molecular weights, and make use of the very low CMC of BBCPs. In thin and bulk films, the self-assembly of BBCPs has been used for applications such as photonic crystals and lithographic patterning, due to their large domain sizes and rapid self-assembly kinetics.[143] This requires that the assembled domain size and lamellar spacing can be tuned by controlling brush grafting density, the degree of polymerization of the brush backbone, and the symmetry of molecular brushes. At the interface, BBCPs may be employed as compatibilizers in polymer melts and mixtures, to increase the mixing of homopolymers and maintain the order of phase-separated films by creating boundaries between individual polymer domains.[168]

Self-assembly in solution, also termed micellization, occurs in dilute solutions of bottlebrush copolymers in a selective solvent at a fixed temperature above a concentration called the critical micelle concentration (CMC), below which only molecularly dissolved unimers are present.[69] The selection of solvent depends on the solubility of each block in the BBCP, requiring a solvent which acts as a good solvent for one block and non-solvent for the other. The simplest method for preparing micelles is the direct dissolution of copolymer samples in a selective solvent with thermal treatment and/or ultrasonic agitation.[69] This procedure is recommended only for bottlebrush copolymers with low molecular weights and short side-chains. Alternatively, the copolymer is dissolved in a common solvent first, which can completely dissolve both blocks.

Subsequently, changes in the composition of the solvent or temperature can be used to cause the formation of micelles. The change of solvent composition can be achieved by the addition of a non-solvent to a common solvent, or the addition of a common solvent to a selective solvent. In addition, in order to prevent the formation of aggregates, dialysis from a good solvent for both blocks into a selective solvent can also be used to form micelles.

Self-assembly in thin and bulk films is very straightforward, and is typically performed by controlled evaporation from a common solvent or spin-coating on the substrate, followed by annealing at a temperature higher than the T_gs of all blocks. Grubbs and coworkers found that using a less volatile common solvent formed larger and better-ordered domains, since it affords improved chain mobility and allows chain rearrangement before the solvent has evaporated.[137]

Together, these studies illustrate that for a given copolymer sample, the morphology and domain size of the self-assembled structures that can be formed depend heavily on the techniques employed for the self-assembly process.

3.1.2 Characterization techniques

Dynamic light scattering (DLS)

DLS is a rapid characterization technique and can quickly provide quantitative information on micelle sizes and size distribution. DLS is often a crucial technique for screening the effects of processing techniques on block copolymer assemblies and can be used to select samples for more in-depth studies, which are more expensive and difficult to operate, such as TEM or AFM.

In solution, macromolecules are buffeted by solvent molecules, which leads to a random motion of the molecules called Brownian motion. As light scatters from the moving macromolecules, this motion imparts a randomness to the phase of the scattered light, such that

the scattered light from two or more particles is added together constructively or destructively. This results in time-dependent fluctuations in the intensity of the scattered light, which are measured by a fast photon counter[169] These fluctuations in intensity are mathematically related through the intensity autocorrelation function $G_2(\tau)$,

$$G_2(\tau) = \frac{1}{t'}\int_0^{t'} I(t)I(t+\tau)d\tau \tag{3.1}$$

where *I(t)* is the average intensity of the scattered light at time t, and τ represents the delay time.[170] The experimentally measured intensity correlation function $G_2(\tau)$ can be related to the electric field correlation function, $G_1(\tau)$ by the Siegert relationship,

$$G_2(\tau) = B[1 + \beta|G_1|^2] \tag{3.2}$$

where *B* is the baseline of the correlation function at infinite delay, β is the correlation function amplitude at zero delay. The electric field correlation function $G_1(\tau)$ describes the correlation particle movements that decay exponentially in time with a decay rate Γ, as expressed by Eq. 3.3,

$$G_1(\tau) = \exp(-\Gamma t) \tag{3.3}$$

For particles undergoing Brownian motion, the decay rate can be converted to the diffusion constant *D* for the particle via the relation:

$$\Gamma = Dq^2 \tag{3.4}$$

in which q is the magnitude of the scattering vector, and is given by the change of an incident wavevector with magnitude $2\pi/\lambda$ after it is elastically scattered by the sample particle, considering solvent-induced changes in the wavelength,[171]

$$q = \frac{4\pi n}{\lambda}\sin(\frac{\theta}{2}) \tag{3.5}$$

in which *n* is the refractive index of the solvent. This equation describes Rayleigh scattering, which requires that the particles are much smaller than the wavelength of the light. Finally, the diffusion constant can be interpreted as the hydrodynamic radius R_h of monodisperse spheres via the Stokes-Einstein equation:

$$R_h = \frac{kT}{6\pi\eta D} \tag{3.6}$$

where k is Boltzmann's constant, T is the temperature in K, and η is the solvent viscosity. Accordingly, larger particles diffuse more slowly and the autocorrelation function decays more slowly, as depicted in Figure 3.1.

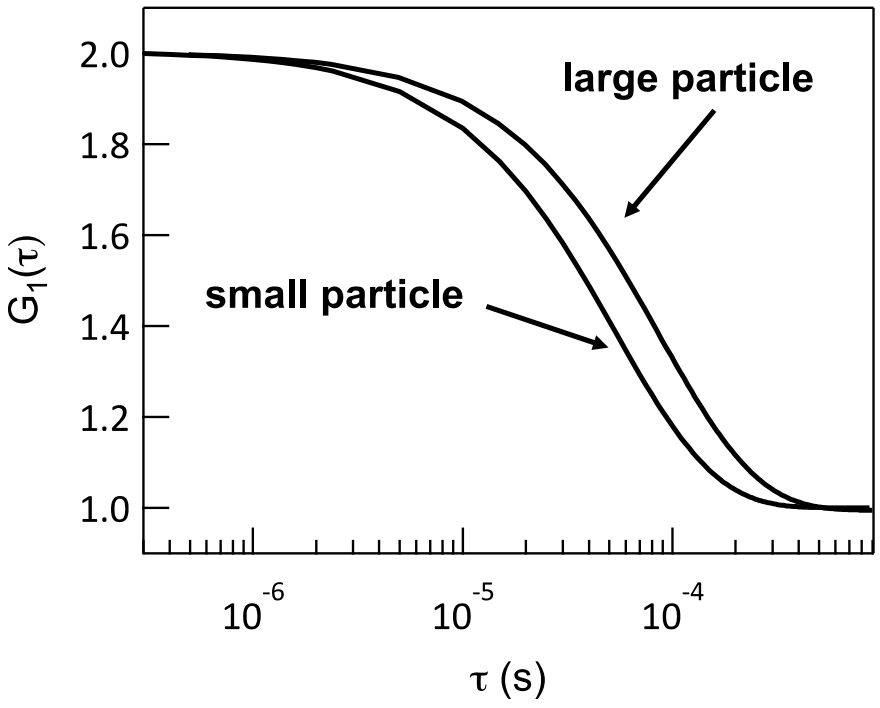

Figure 3. 1. Comparison of autocorrelation functions for small and large particles. Adapted from reference [49].

However, in most experimental systems, the particles are not perfectly monodisperse and the measured decay is the intensity-weighted sum of the individual particle decay functions,

$$G_1(\tau) = \sum_i A_i \exp(-\Gamma_i \tau) \tag{3.7}$$

in which A_i is the intensity-weight coefficient, and $A_i \propto c_i M_i P_i$ in which c_i and M_i are the concentration and molecular weight of the species, respectively, and P_i is the shape factor of the particle. There are several models to account for polydispersity in DLS data. One of the simplest models is the cumulant expansion which assumes that there is a monomodal distribution of particles that can be described by a Gaussian-like distribution.[172]

$$G_1(\tau) = \exp(-\overline{\Gamma}\tau)(1 + \frac{\mu_2}{2!}\tau^2 + \cdots) \tag{3.8}$$

in which $\overline{\Gamma}$ is the average decay constant (to calculate the average hydrodynamic radius R_h) and the higher order terms is related to the polydispersity of the sample. For samples with a broad distribution of sizes or multimodal distributions, more complex fitting functions are required, such as Dynals algorithm and the CONTIN method.[173] However, the fitted size distribution does not always provide an accurate representation of the actual size distribution of the particles in solution.[174]

In this chapter, DLS was used to understand the effects of polymer composition and solvent on the size and size distribution in BBCP micelles using Cumulant analysis and Dynals algorithm. Using DLS to measure CMC, the intensity of scattered light detected from concentrations below the CMC is similar to that obtained from pure solvent. In addition, the autocorrelation functions obtained ($G_1(\tau)$) showed very poor signal to noise ratios, and no size distribution information

could be obtained from this data. However, once the CMC was reached, the intensity of scattered light increased dramatically and proportional to micelle concentration, giving smooth autocorrelation functions with higher intercepts. By plotting the concentrations of copolymers versus the intensity of scattered light, the CMCs of self-assembled micelles were successfully determined.[175]

Transmission electron microscopy (TEM and Cryo-TEM)

TEM enables the direct visualization of self-assembled morphologies of BBCPs on nanometer length scales, and the development of cryogenic TEM makes the direct visualization of micelle morphology in solution possible.

In TEM, a sample is hit by a monochromatic electron beam, whose focus and magnification are controlled by a series of lenses, under high vacuum conditions to prevent scattering of the beam by air or other impurities.[176] Some electrons directly pass through the sample, while other electrons are scattered by the atoms in the sample, which are blocked by the objective aperture, as shown by Figure 3.2.[49] More electrons are scattered by heavier atoms (larger atomic number) or by a thicker sample, resulting in a darker image since less electrons reach the image plane. Therefore, the contrast is due to differential scattering of electrons by the material resulting from differences in composition or thickness of the material.

In polymeric samples, the TEM image contrast is generally poor since the samples are often composed of low molecular weight elements (H, C, O, and N). Sometimes heavy metal stains such as OsO_4 and RuO_4 are needed to improve the contrast for polymeric systems. However, the image contrast in cryo-TEM is enhanced by using phase contrast, which is caused by interference between the electron waves from directly passed and elastically scattered electrons and is

strengthened by imaging the sample at an underfocus.[177,178] The disadvantages of underfocus imaging are the reduced image resolution and image artifacts.[179] Although heavy metal staining is not necessary, the sample preparation for cryo-TEM is more troublesome and demanding. It requires the ultra-fast freezing of the sample in a thin layer of solvent, and solvent volatility can be a problem if organic solvents are used.

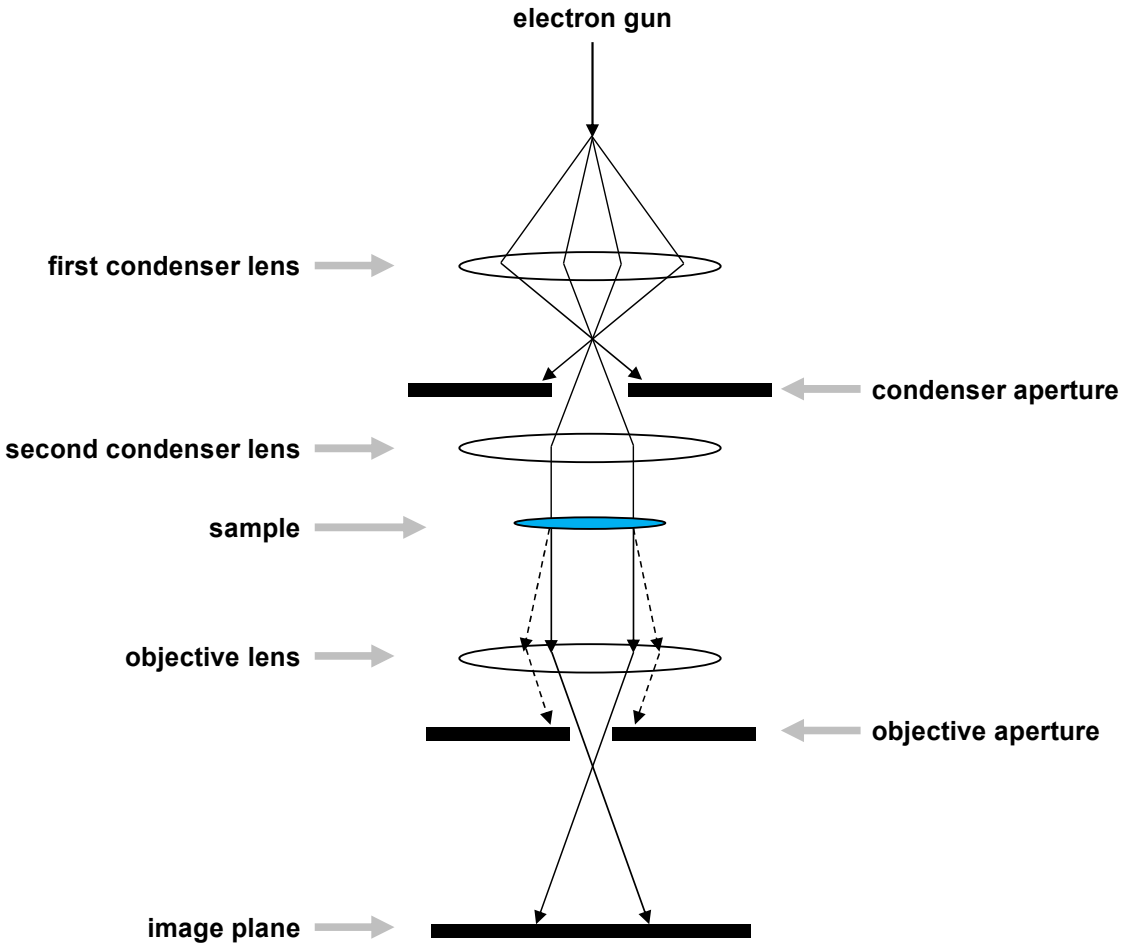

Figure 3. 2. A simplified TEM with important components. The condenser lenses and aperture focus and align the beam. The objective lens and aperture refocus and filter the bean after it passes through the sample. Adapted from reference [20].

Cryo-TEM images can suffer from several potential artifacts, and representative images are presented in Figure 3.3.[49] Sometimes sample grids are poorly vitrified, which results in poorly spread samples and cracks in the thin ice layer (Figure 3.3 a-c). Hexagonal and vitreous ice contamination is possible for cryo-TEM images (Figure 3.3 d). Samples can also experience radiolysis by the electron beam (Figure 3.3 e). An uneven film can also result, which leads to the aggregation of micelles (Figure 3.3 e) or size segregation (Figure 3.4), where large particles are located at the edge with thickest ice.

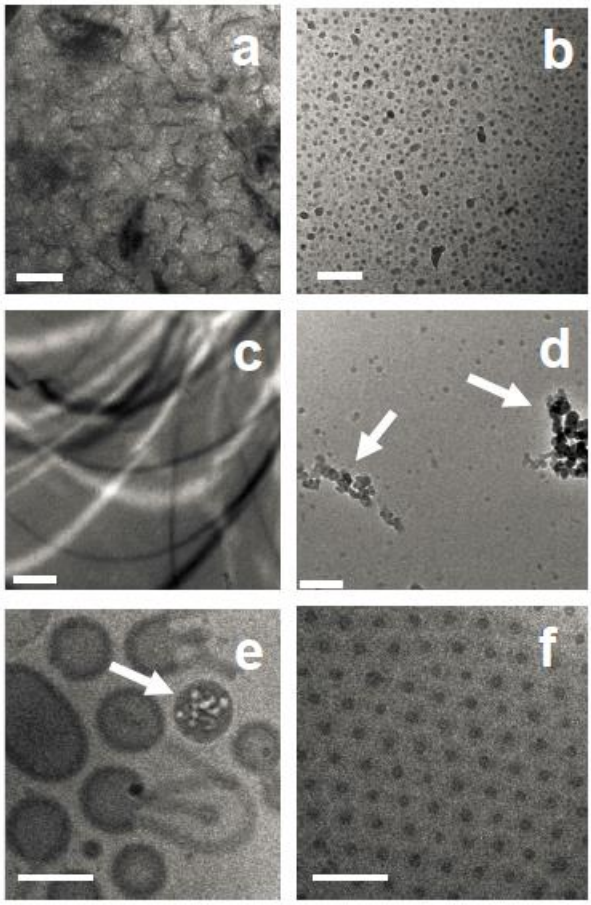

Figure 3.3. Common artifacts in cryo-TEM: (a-c) poorly vitrified samples, (d) water crystals, (e) beam damage, (f) micelle aggregation. Adapted from reference, scale bar = 100 nm [20].

Figure 3.4. Schematic representation of size segregation of particles due to sample preparation, with larger particles at the edges of the holes and smaller particles in the center. Adapted from reference [20].

3.2 Results and Discussion

3.2.1 Self-assembly in solution of bottlebrush diblock copolymers (nBuA-MM)x-*b*-(CzBA-MM)y

The **nBuA** block provides excellent solubility in a variety of common organic solvents, and acetone and 2,2,2-trifluoroethanol (TFE) were identified as suitable selective solvents for self-assembly of these BBCPs. Self-assembly experiments were performed by dropwise addition of 100 µL of a 50 mg/mL solution of BBCP in THF into either acetone or TFE, followed by brief sonication to aid in dispersing the BBCPs and standing for 24 hours (Figure 3.5). By dynamic light scattering (DLS), remarkably low CMCs of < 50 µg/mL were determined for all four BBCPs, corresponding to molar concentrations of 3.0 nM to 54 nM in TFE and 2.3 nM to 8.2 nM in acetone (Figure 3.6 and Figure 3.7). Specifically, for each micelle sample, the CMC in acetone was lower than the CMC in TFE. Consistent with the results of Rzayev,[180] this indicates that these semiconductor-based bottlebrush surfactants are capable of forming stable micellar structures at extremely low concentrations, which is advantageous in applications such as intravenous drug delivery or fluorescent sensing where high dilution may be required. As expected, the highest CMC in both solvents was observed for **(nBuA-MM)$_{96}$-*b*-(CzBA-MM)$_{14}$**, the BBCP with the longest solvophilic block.[181]

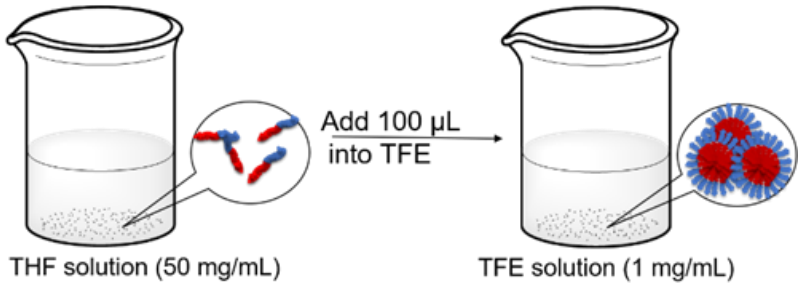

Figure 3. 5. Schematic illustrations of self-assembly of diblock copolymers in TFE.

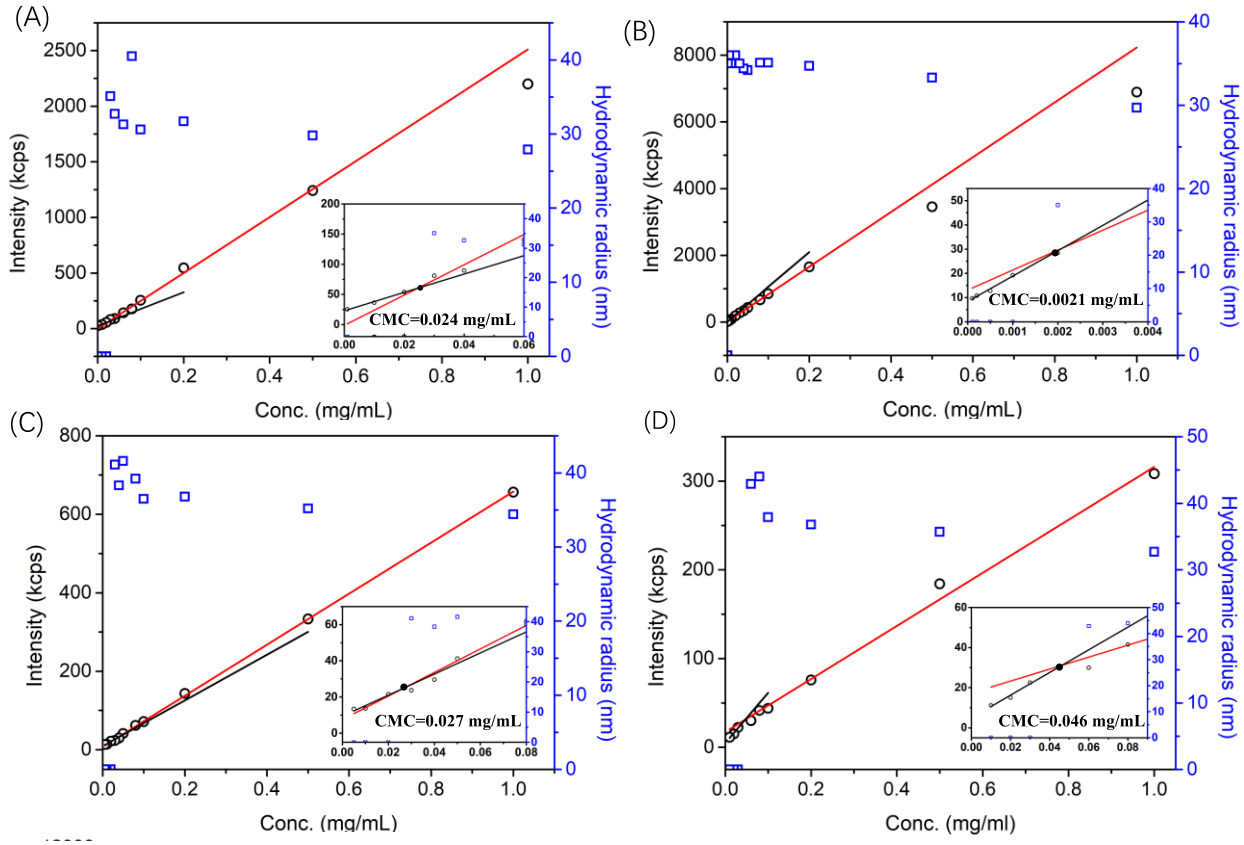

Figure 3.6. Dynamic light scattering plots of intensity of scattered light (black circle) and hydrodynamic radius (blue square) obtained for bottlebrush diblock copolymers (A) **(nBuA-MM)$_{19}$-*b*-(CzBA-MM)$_{56}$,** (B) **(nBuA-MM)$_{50}$-*b*-(CzBA-MM)$_{42}$,** (C) **(nBuA-MM)$_{69}$-*b*-(CzBA-MM)$_{23}$,** (D) **(nBuA-MM)$_{96}$-*b*-(CzBA-MM)$_{14}$,**at various concentrations in trifluoroethanol. The intersection of the two lines in the intensity data corresponds to the critical micelle concentration (CMC).

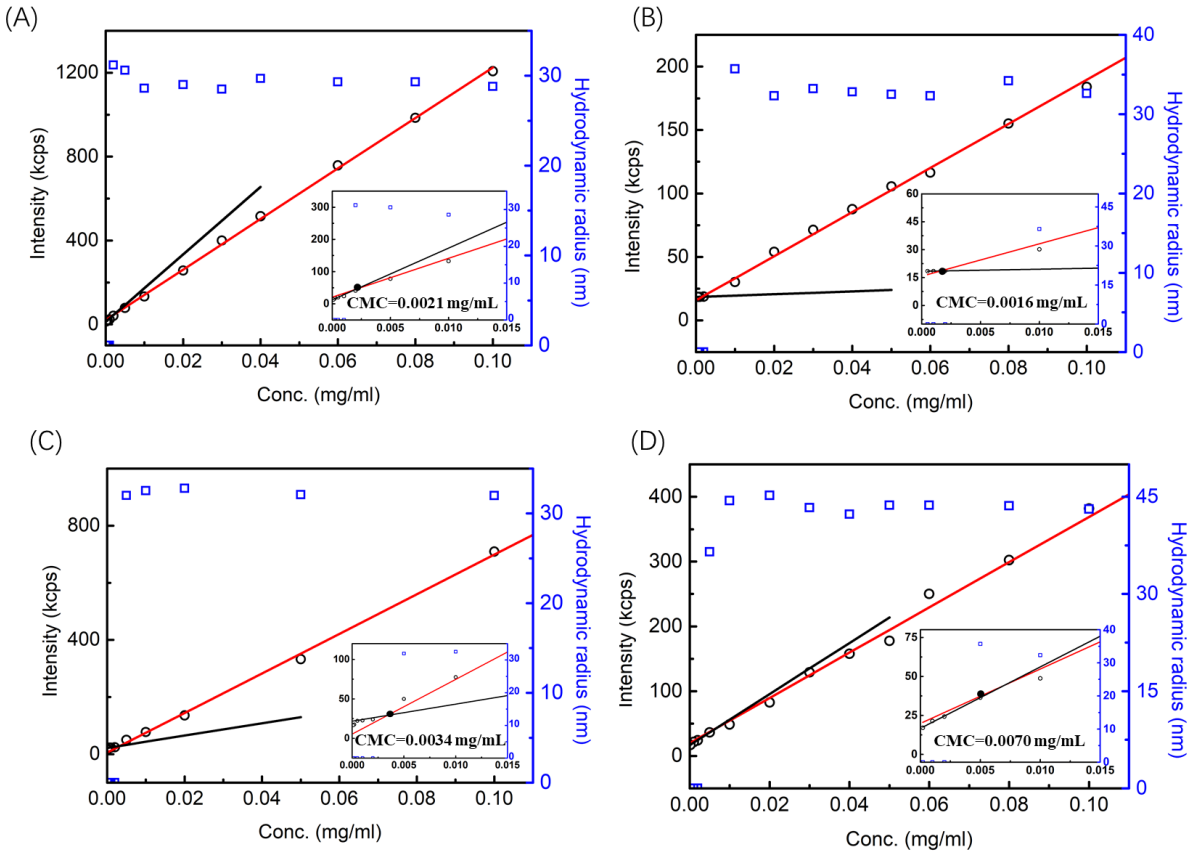

Figure 3.7. Dynamic light scattering plots of intensity of scattered light (black circle) and hydrodynamic radius (blue square) obtained for bottlebrush diblock copolymers (A) **(nBuA-MM)$_{19}$-*b*-(CzBA-MM)$_{56}$,** (B) **(nBuA-MM)$_{50}$-*b*-(CzBA-MM)$_{42}$,** (C) **(nBuA-MM)$_{69}$-*b*-(CzBA-MM)$_{23}$**, (D) **(nBuA-MM)$_{96}$-*b*-(CzBA-MM)$_{14}$,** at various concentrations in acetone. The intersection of the two lines in the intensity data corresponds to the critical micelle concentration (CMC).

The self-assembly process can also be readily observed with the aid of a handheld laser pointer, as assembly to form micelles gives rise to strong Tyndall scattering observable to the naked eye (Figure 3.8 b). By TEM, the BBCPs were found to self-assemble into narrowly-dispersed spherical micelles for all block ratios investigated here, remaining stable in solution for several months without flocculation (Figure 3.9). For our cryo-TEM images, we observed the size

segregation and micelle aggregation in trifluoroethanol (TFE) (Figure 3.10 a). In acetone, hardly any sample was seen and the film appeared damaged by the beam (Figure 3.10 b-c). Micelles showed a remarkably consistent diameter in the range of 63 - 86 nm by DLS for all samples despite significant differences in the volume fraction of the core, indicating that the overall length of the bottlebrush chains was more critical in determining the micelle size. The dispersity of the micelle samples was also relatively narrow at 9.8-23.8% in TFE and at 5.5-21.8% in acetone. Specifically, for each micelle sample, the dispersity of micelle sizes in acetone was narrower than the corresponding one in TFE. For both solvents, the narrowest distribution was obtained for the micelles with the **nBuA-MM:CzBA-MM** block ratio closest to 1:1, and the broadest distribution was obtained for micelles with the longest **nBuA-MM** blocks (Figures 3.11 and Figure 3.12). From this phenomenon, we concluded that the symmetry of the two blocks of bottlebrush copolymers and the nature of the selective solvent influenced the quality of self-assembled micelles, such as dispersity and CMC. Each micelle sample showed the characteristic absorbance and purple fluorescence of the **CzBA** polymer,[163] with a fluorescence quantum yield of 0.46 (Figure 3.13 and Table 3.1), which means that the self-assembly process and the block length variation did not influence the fluorescent properties of the **CzBA** polymer.

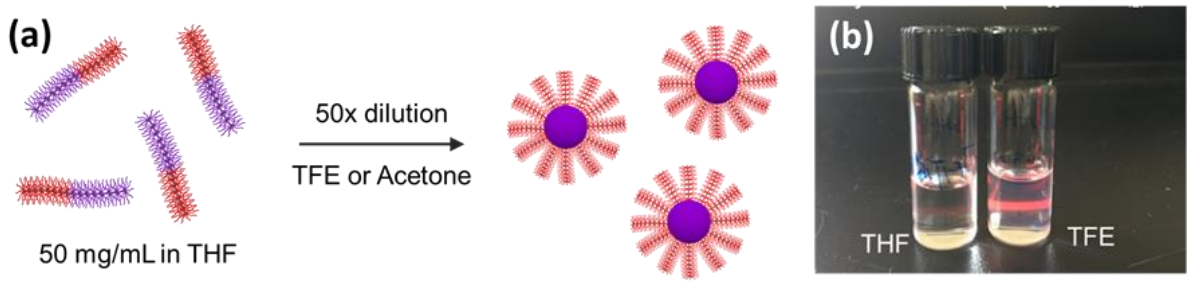

Figure 3.8. (a) Schematic representation of the assembly of **(nBuA-MM)-*b*-(CzBA-MM)** BBCPs to form micelles (red: **nBuA**, purple: **CzBA**). (b) Tyndall scattering observed in a 0.1 mg/mL solution of **(nBuA-MM)$_{50}$-*b*-(CzBA-MM)$_{42}$** micelles in TFE.

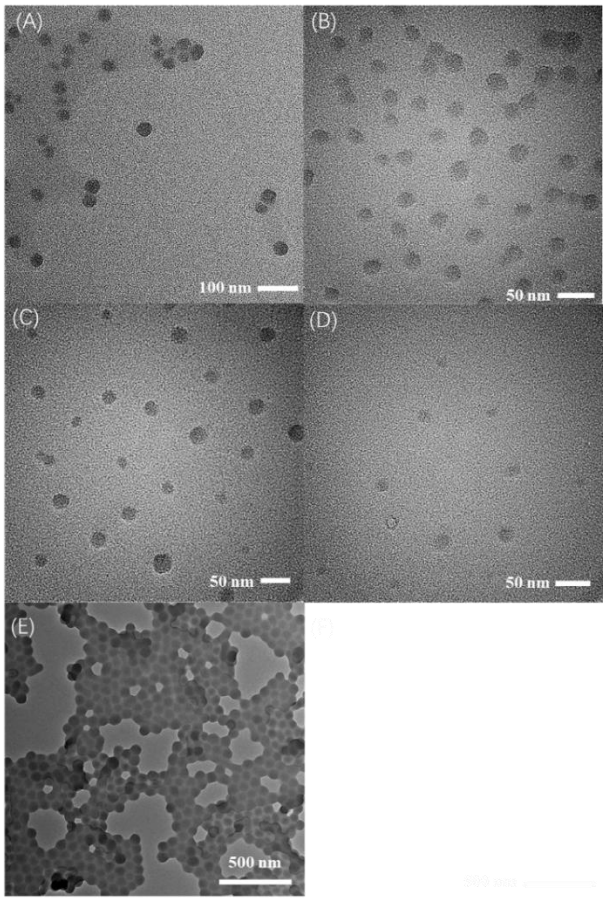

Figure 3.9. TEM images of micelles (A) **(nBuA-MM)$_{19}$-*b*-(CzBA-MM)$_{56}$,** (B) **(nBuA-MM)$_{50}$-*b*-(CzBA-MM)$_{42}$,** (C) **(nBuA-MM)$_{69}$-*b*-(CzBA-MM)$_{23}$**, (D) **(nBuA-MM)$_{96}$-*b*-(CzBA-MM)$_{14}$,** (E) **(nBuA-MM)$_{19}$-*b*-(CzBA-MM)$_{56}$** . For A-D, micelles were formed at 0.06 mg/ml in trifluoroethanol and dried for TEM imaging. For E, samples were directly dissolved in acetone at 1 mg/ mL and dried for TEM imaging.

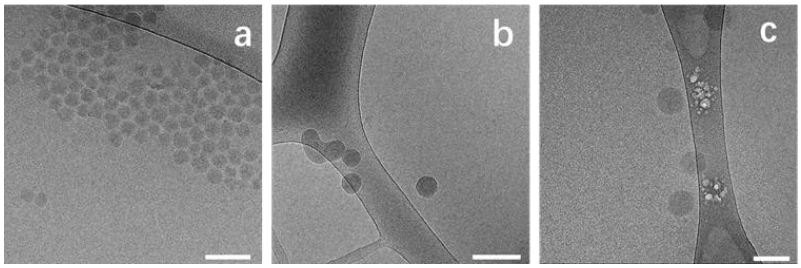

Figure 3.10. Cryo-TEM images of **(nBuA-MM)$_{19}$-*b*-(CzBA-MM)$_{56}$** in TFE (a) and **(nBuA-MM)$_{50}$-*b*-(CzBA-MM)$_{42}$** in acetone (b-c)**,** scale bar = 100 nm for a and b, = 50 nm for c.

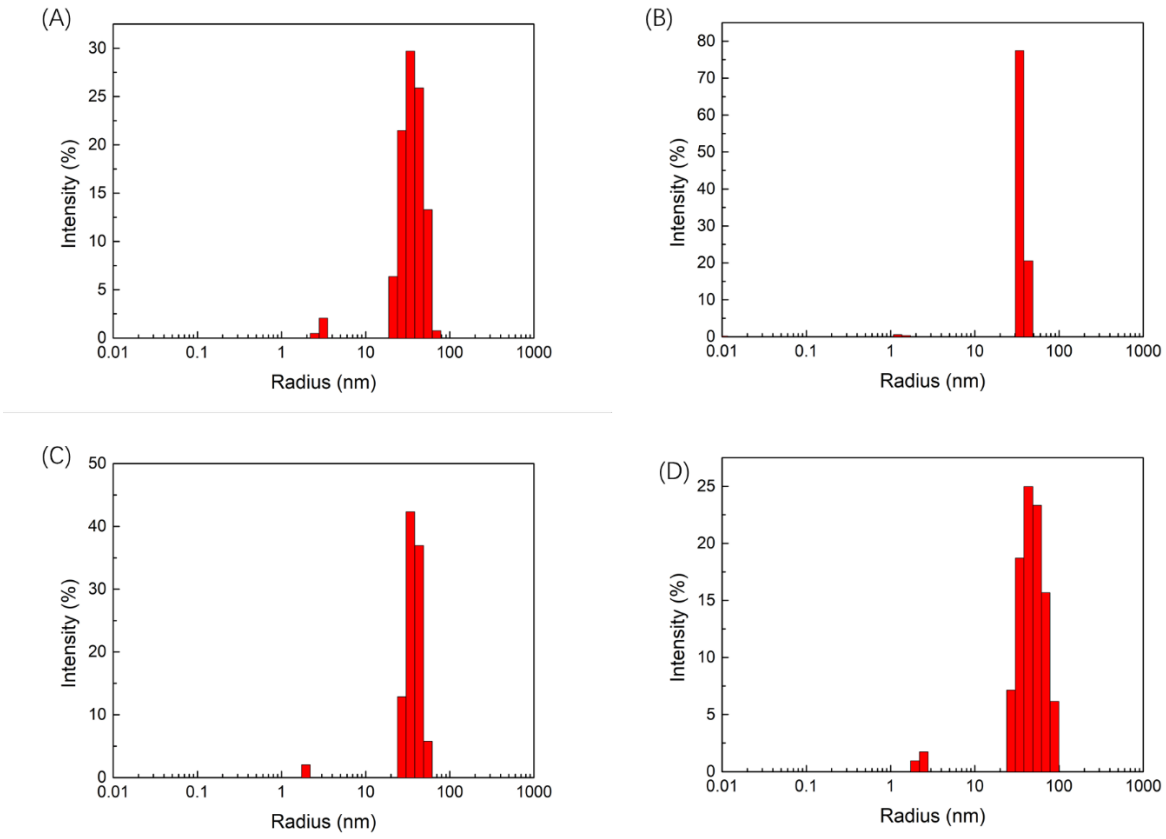

Number	R (nm)	Polydispersity (%)
A	31.3	17.9
B	34.3	9.8
C	33.2	15.7
D	42.9	23.8

Figure 3.11. Size distribution by dynamic light scattering for micelles of bottlebrush diblock copolymers (A) (**nBuA-MM)$_{19}$-*b*-(CzBA-MM)$_{56}$**, (B) **(nBuA-MM)$_{50}$-*b*-(CzBA-MM)$_{42}$**, (C) **(nBuA-MM)$_{69}$-*b*-(CzBA-MM)$_{23}$**, (D) **(nBuA-MM)$_{96}$-*b*-(CzBA-MM)$_{14}$** at 0.06 mg/mL in trifluoroethanol.

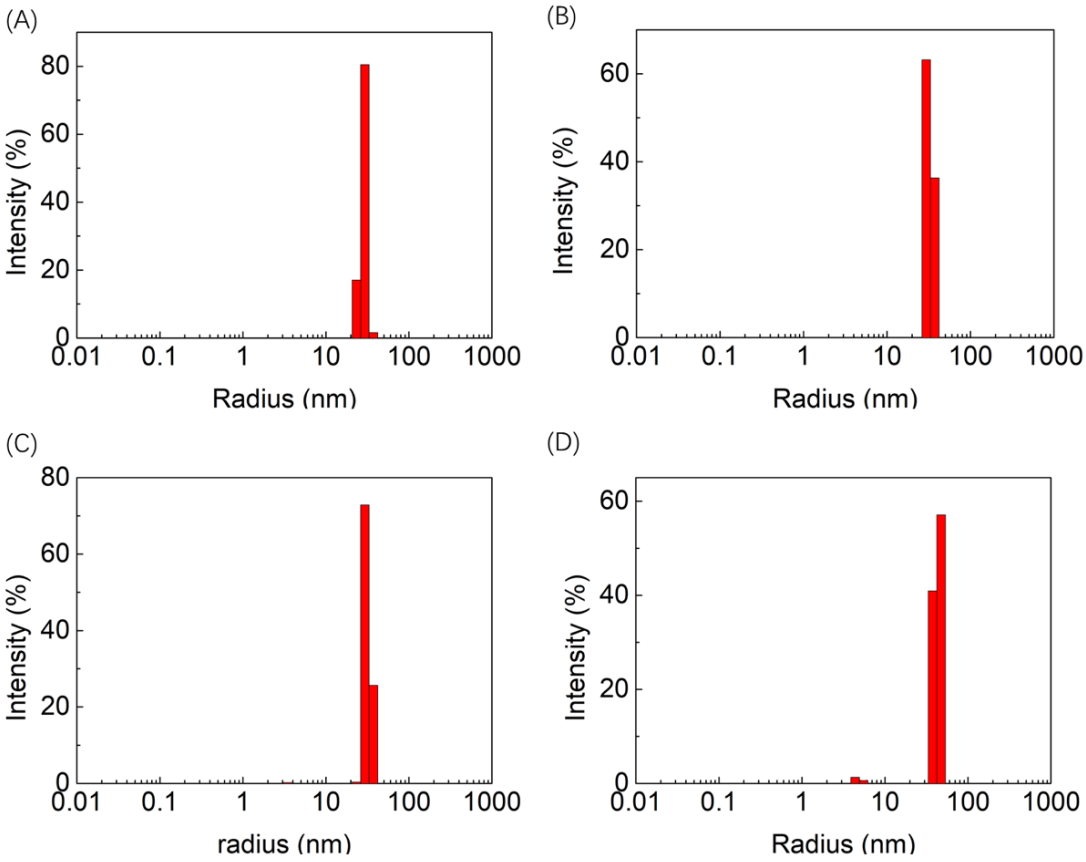

Number	R (nm)	Polydispersity (%)
A	28.4	6.9
B	32.1	5.5
C	31.1	6.8
D	43.5	21.8

Figure 3.12. Size distribution by dynamic light scattering for micelles of bottlebrush diblock copolymers (A) **(nBuA-MM)$_{19}$-*b*-(CzBA-MM)$_{56}$**, (B) **(nBuA-MM)$_{50}$-*b*-(CzBA-MM)$_{42}$**, (C) **(nBuA-MM)$_{69}$-*b*-(CzBA-MM)$_{23}$**, (D) **(nBuA-MM)$_{96}$-*b*-(CzBA-MM)$_{14}$**, at 0.06 mg/mL in acetone.

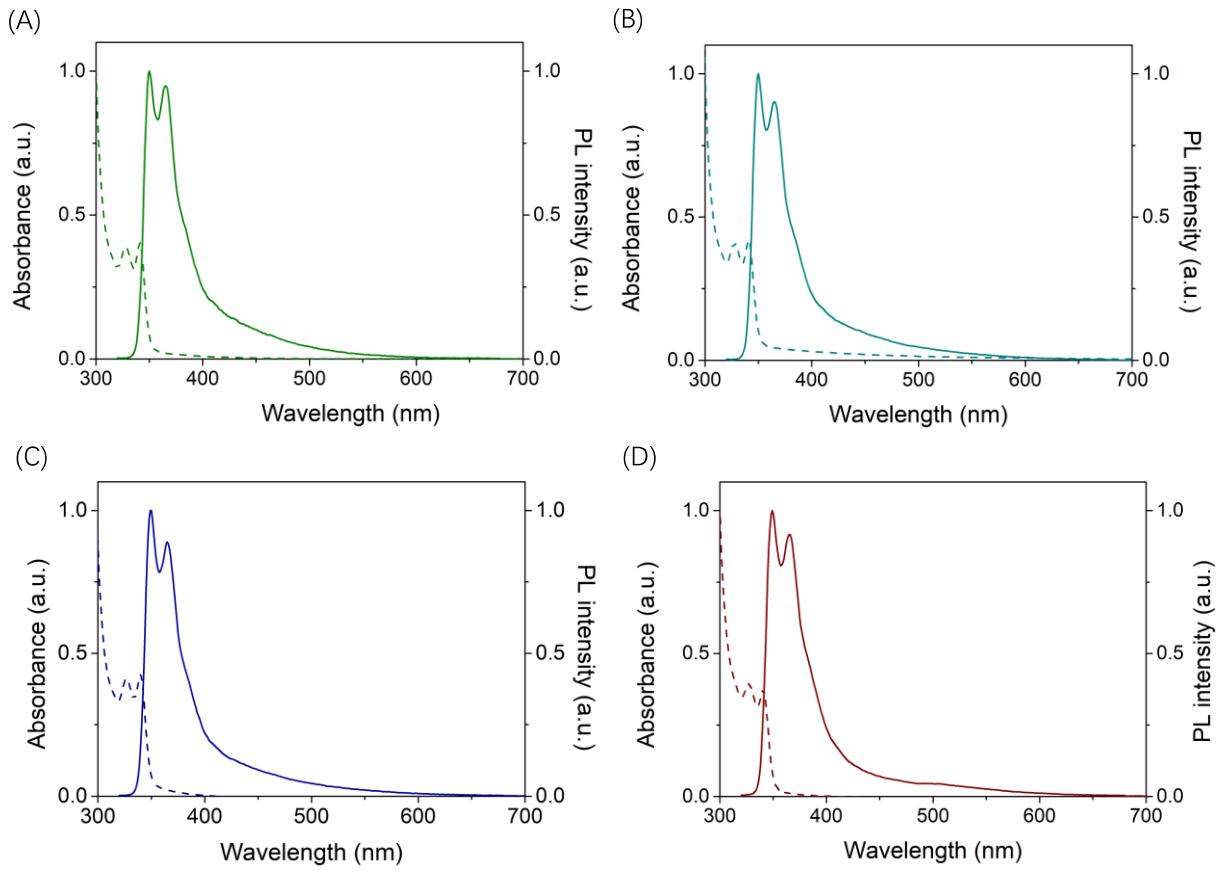

Figure 3.13. Normalized absorbance (dashed) and photoluminescence (solid) spectra for micelles of bottlebrush diblock copolymers (A) **(nBuA-MM)$_{19}$-*b*-(CzBA-MM)$_{56}$,** (B) **(nBuA-MM)$_{50}$-*b*-(CzBA-MM)$_{42}$,** (C) **(nBuA-MM)$_{69}$-*b*-(CzBA-MM)$_{23}$,** (D) **(nBuA-MM)$_{96}$-*b*-(CzBA-MM)$_{14}$,** in trifluoroethanol at 0.1 mg/mL. λ_{ex} = 300 nm.

Table 3. 1. Polymer photophysical properties.

Entry	$\lambda_{max,\ abs}$[a]	$\lambda_{max,\ em}$[a]	$\lambda_{max,\ em,\ before\ annealing}$	$\lambda_{max,\ em,\ after\ annealing}$
(nBuA-MM)$_{19}$-*b*-(CzBA-MM)$_{56}$	293	350	349	351
(nBuA-MM)$_{50}$-*b*-(CzBA-MM)$_{42}$	293	350	349	368
(nBuA-MM)6$_{9}$-*b*-(CzBA-MM)$_{23}$	293	350	349	348
(nBuA-MM)$_{96}$-*b*-(CzBA-MM)$_{14}$	293	349	348	362

Concentrations = 0.1 mg mL^{-1}. [a]Measured in TFE.

3.2.2 Self-assembly in solution of functionalized bottlebrush diblock copolymer (nBuA-MM)$_{41}$-*b*-(CzBA-*co*-PAPOMA-MM)$_{39}$

For (**nBuA-MM)$_{41}$-*b*-(CzBA-*co*-PAPOMA-MM)$_{39}$**, the same self-assembly methods and characterization techniques were used to analyze the self-assembly behaviors of this functionalized diblock bottlebrush copolymer functionalized with a fluorescent dye (Figure 3.14).

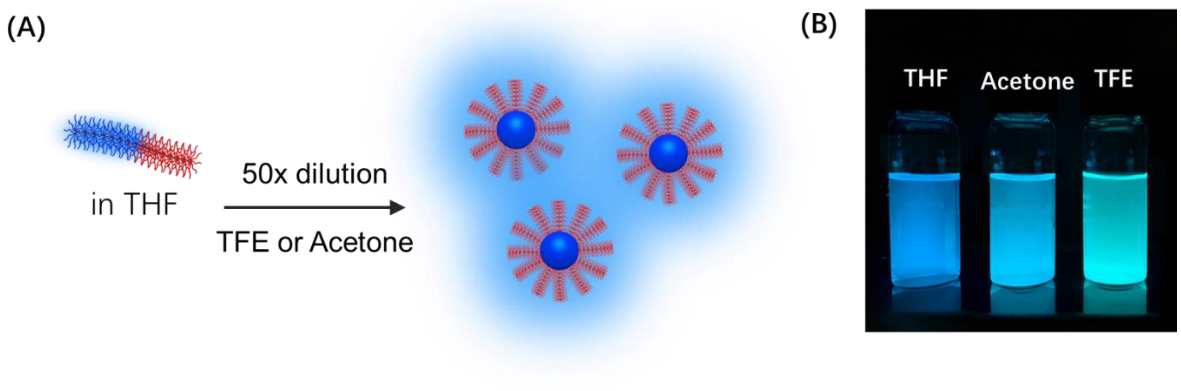

Figure 3.14. (A) Schematic representation of the self-assembly of luminescent BBCPs into spherical micelles. (B) Photographs of **(nBuA-MM)$_{41}$-*b*-((CzBA-*co*-PAPOMA)-MM)$_{39}$** BBCPs at 0.1 mg/mL in THF (left), acetone (center), and TFE (right) under 365 nm irradiation.

As previously, self-assembly in TFE gave spherical micelles with diameters of 61 nm and dispersities of 12.9% (Figure 3.15 b and Figure 3.16), though the sample now exhibited strong fluorescence with λ_{max} = 484 nm (Figure 3.17 a). Importantly, no emission was observed from the **CzBA** host following self-assembly despite its relatively high quantum yield, indicating that rapid and efficient energy transfer was occurring to the dopant. This is in contrast to the emission spectrum of the BBCP in THF prior to self-assembly (Figure 3.17 b) in which some host emission can still be observed, indicating that the collapse of the **CzBA-*co*-PAPOMA** block into a micellar

core improves energy transfer substantially. Most remarkably, the quantum efficiency of these micelles in solution was measured to be 1.04 ± 0.05, representing an emission quantum yield of unity for a self-assembled structure with a CMC below 10 nM.

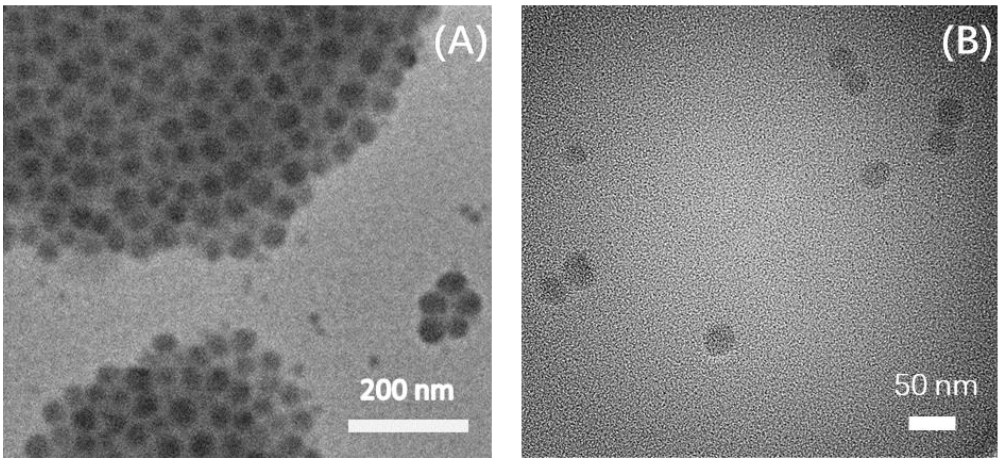

Figure 3.15. TEM images of micelles of **(nBuA-MM)$_{41}$-*b*-((CzBA-*co*-PAPOMA)-MM)$_{39}$** in acetone (A) and in TFE (B). For A, samples were directly dissolved in acetone at 1 mg/ mL and dried for TEM imaging. For B, micelles were formed at 0.06 mg/ml in trifluoroethanol and dried for TEM imaging.

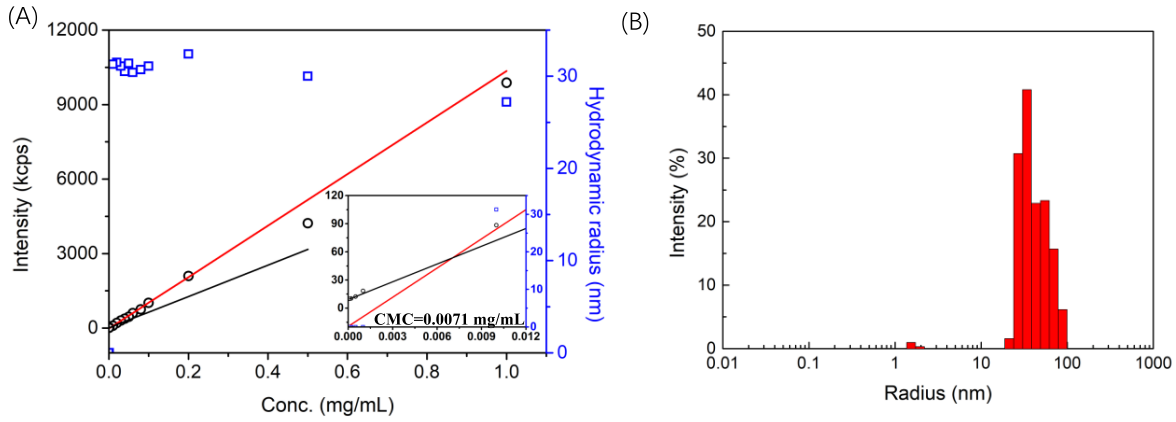

Figure 3.16. (A) Dynamic light scattering plots of intensity of scattered light (black circle) and hydrodynamic radius (blue square) obtained for functionalized bottlebrush diblock copolymer **(nBuA-MM)$_{41}$-*b*-((CzBA-*co*-PAPOMA)-MM)$_{39}$,** at various concentrations in trifluoroethanol. The intersection of the two lines in the intensity data corresponds

to the critical micelle concentration (CMC). (B) Size distribution by dynamic light scattering for micelles of **(nBuA-MM)$_{41}$-*b*-((CzBA-*co*-PAPOMA)-MM)$_{39}$** at 0.06 mg/mL in trifluoroethanol.

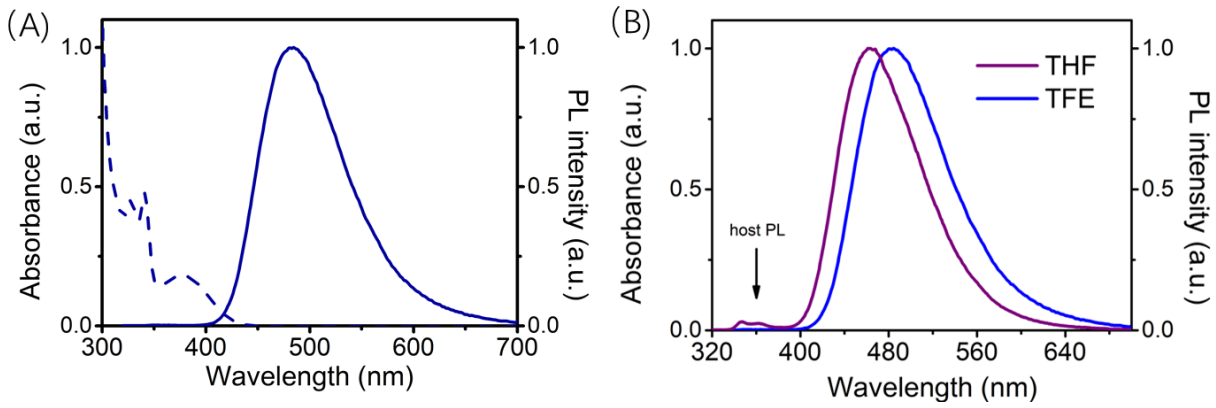

Figure 3.17. (A) Absorption and emission spectra of micelles of (**nBuA-MM)$_{41}$-*b*-(CzBA-*co*-PAPOMA-MM)$_{39}$** in TFE. (B) Emission spectra for (**nBuA-MM)$_{41}$-*b*-(CzBA-*co*-PAPOMA-MM)$_{39}$** at 0.1 mg/mL in THF and TFE. λ_{ex} = 300 nm.

3.2.3 Self-assembly in films

Self-assembly of bottlebrush block copolymers in films has been used to fabricate one-dimensional photonic crystals, which consist of alternating layers of high- and low-refractive-index materials and have the periodicity comparable to the wavelength of light.[137,143] Due to the refractive index contrast of the **nBuA** and **CzBA** blocks, we then reasoned that similar one-dimensional photonic crystals could be developed by the self-assembly of our bottlebrush diblock copolymers. A series of films was prepared by spin-coating the solution of bottlebrush diblock copolymer **(nBuA-MM)-*b*-(CzBA-MM)** or (**nBuA-MM)-*b*-(CzBA-*co*-nBuA-MM)** in THF on the surface of prewashed quartz slides (Figure 3.20 A). As observed by TEM, these films exhibited disordered lamella morphologies with a lack of well-defined domains (Figure 3.18). Further

studies on improving the periodicity of these films and charactering domain sizes using small-angle X-ray scattering (SAXS) or small-angle neutron scattering (SANS) are required. The fluorescent properties of these films were also investigated. Interestingly, the peaks in the emission spectrum of BBCPs in films were broader than the previous ones in solution (Figure 3.19 and Figure 3.13), although the λ_{max} didn't change (Table 3.1). The annealing process influenced the emission spectrum to different extents, with more influence for the less symmetric (**nBuA-MM)$_{19}$-*b*-(CzBA-MM)$_{56}$** and **(nBuA-MM)$_{96}$-*b*-(CzBA-MM)$_{14}$**.

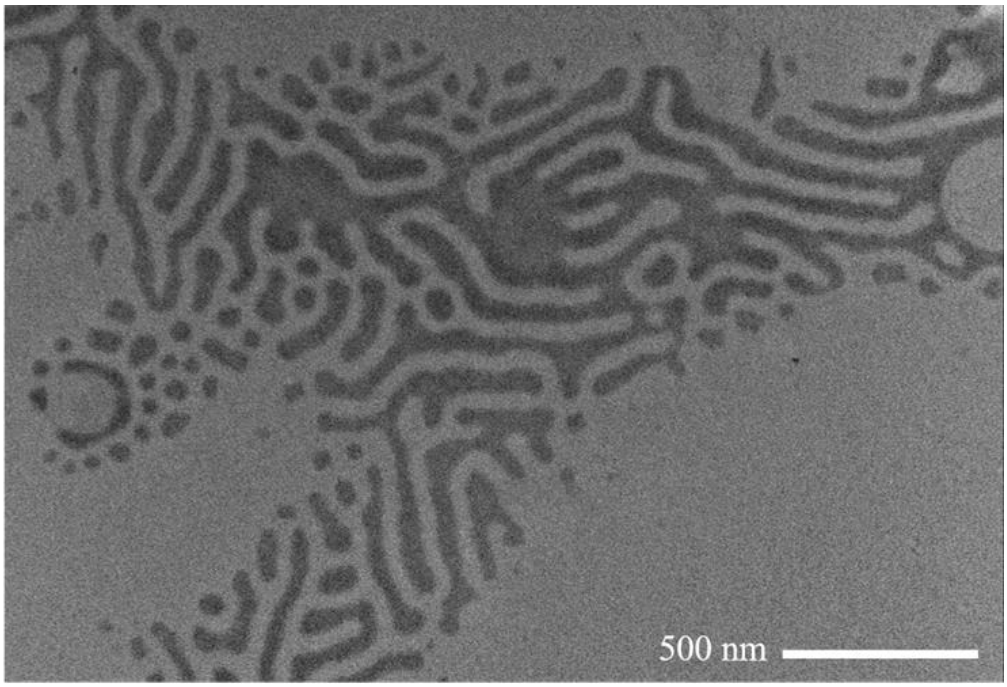

Figure 3.18. TEM image for (**nBuA-MM)$_{50}$-b-(CzBA-MM)$_{42}$** film. A film was spin-coated on a Formvar-coated TEM grid using 1 mg/mL THF solution.

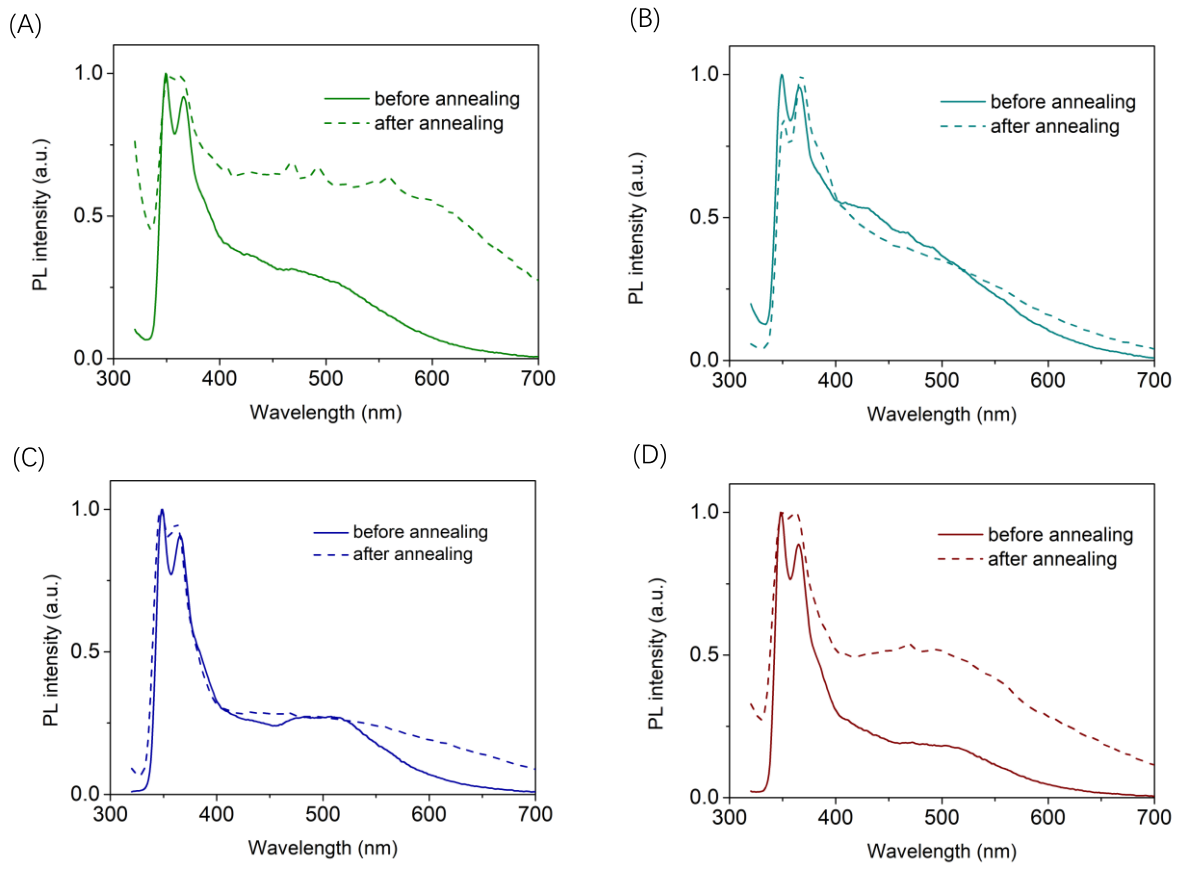

Figure 3.19. Solid state photoluminescence spectra of bottlebrush diblock copolymers (A) **(nBuA-MM)$_{19}$-*b*-(CzBA-MM)$_{56}$,** (B) **(nBuA-MM)$_{50}$-*b*-(CzBA-MM)$_{42}$,** (C) **(nBuA-MM)$_{69}$-*b*-(CzBA-MM)$_{23}$,** (D) **(nBuA-MM)$_{96}$-b-(CzBA-MM)$_{14}$,** before (solid) and after (dashed) annealing. Spin-coated on quartz glass substrates. Annealed at 150 °C. λ_{ex} = 293 nm.

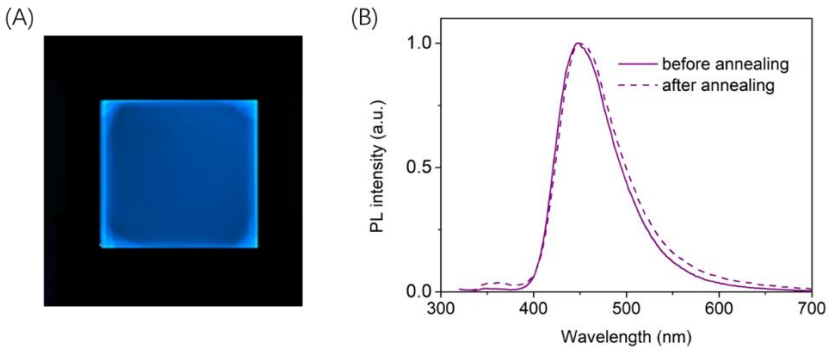

Figure 3.20. (A) Photographs of **(nBuA-MM)$_{41}$-*b*-((CzBA-*co*-PAPOMA)-MM)$_{39}$** BBCPs as a thin film in the solid state under 365 nm irradiation. (B) Solid state photoluminescence spectra of **(nBuA-MM)$_{41}$-*b*-((CzBA-*co*-**

PAPOMA)-MM)$_{39}$ before (solid) and after (dashed) annealing. Spin-coated on quartz glass substrates. Annealed at 150 °C. λex = 293 nm.

3.3 Conclusions

Bottlebrush copolymers composed of a soluble **nBuA** block and a carbazole-based organic semiconductor block successfully self-assembled into narrowly dispersed spherical micelles in selective solvent, which could potentially be functionalized further for use as giant amphiphilic surfactants in applications such as bioimaging and drug delivery. The sizes of these micelles ranged from 60 nm to 90 nm, which perfectly fit in the range of effective sizes of enhanced permeability and retention (EPR) effect[99] - large enough to accumulate inside the tissues such as tumors. Other advantages of these self-assembled micelles are their extremely low CMCs (below 54 nM) and stability over periods of months.

Moreover, the incorporation of a blue fluorescent acrylic dye **PAPOMA** didn't influence the self-assembly behaviour of bottlebrush diblock copolymers, maintaining a narrow dispersity and low CMC at 10 nM), although it introduced strong fluorescence into the self-assembled micelles resulting in a quantum yield of ~100%. This provides opportunities to incorporate higher-order function into the organic semiconductor block to give functional micelles with large sizes, narrow dispersities and very low CMCs.

3.4 Experimental details

3.4.1 General considerations

Dynamic Light Scattering (DLS)

DLS experiments were performed with a DynaPro Titan DLS instrument (Wyatt Technology Corporation) equipped with a 60 mW helium-neon laser (λ=832.15 nm) and

thermoelectric temperature controller. Measurements were taken at a 90° scattering angle in a 3 × 3 mm quartz cuvette on solutions that had been equilibrated to 25 °C. The laser power was controlled to 8-10%. The sample solutions were diluted in 2,2,2-trifluoroethanol (TFE) or acetone and filtered prior to analysis (syringe filter, 0.2 μm pore size, PTFE filter membrane, Fisher Scientific). The concentrations of the analyzed sample solutions were from 1 mg mL^{-1} to 0.0001 mg mL^{-1}. The lowest analyzed concentration of each sample varied depending on its critical micelle concentration (CMC). Dispersity by DLS was determined as a percentage, as:

$$\text{Dispersity} = \left(\frac{\text{standard deviation}}{\text{mean radius}}\right)^2$$

The software packages are DYNAMIC versions 6.10.0 with analysis methods using Dynals algorithm and cumulant expansion.

Transmission Electron Microscopy (TEM)

TEM images were collected at the UBC BioImaging Facility on a FEI Tecnai G2 TEM (200 kV LaB6 filament) equipped with a high-speed AMT 2K side mount CCD camera, and a high-resolution FEI Eagle 4K bottom mount CCD camera for capturing digital images. The sample solutions were deposited on a Formvar-coated TEM grid and allowed to evaporate to dryness before imaging.

Fluorescence and Absorbance Measurements

Absorbance measurements were made on a Cary 60 spectrometer and fluorescence measurements were performed on an Edinburgh Instruments FS5 spectrometer. Absolute photoluminescence quantum yields were determined using an Edinburgh Instruments SC-30

Integrating Sphere Module; toluene was used as the solvent and spectra obtained at concentrations of 0.01 mg mL^{-1}.[182]

3.4.2 Self-assembly methods

Self-assembly of BBCPs in 2,2,2-trifluoroethanol (TFE)

A concentrated solution of **(nBuA-MM)-*b*-(CzBA-MM)** or (**nBuA-MM)-*b*-(CzBA-*co*-PAPOMA-MM)** in THF (50 mg/mL) was prepared. 100 μL of this solution was then added into 4.9 mL of TFE to form micelles driven by phase separation, followed by 2 minutes of sonication in an ultrasonic bath and standing for 24 hours. A red laser pointer can be conveniently used to monitor the formation of diblock copolymer micelles via the Tyndall effect.

Preparation of Films Based on nBuA-b-CzBA or nBuA-b-(CzBA-co-nBuA)

Quartz slides (25 × 25 × 1 mm, Chemglass) were sonicated with deionized water, acetone and isopropyl alcohol in sequence and then dried *in vacuo*. 30 μL of a **nBuA-*b*-CzBA** (or **nBuA-*b*-(CzBA-*co*-nBuA)**) solution in THF (5 mg mL^{-1}) was spin-coated on the surface of the quartz glass. The glass was left for 1 hour at room temperature under air to allow the solvent to evaporate. The dried film was then annealed on a hot plate at 150 °C for two hours. A film on a quartz slide before and after annealing was utilized for solid-state fluorescence analysis.

Chapter 4: Conclusion and Future work

4.1 Conclusion

This dissertation focuses on the development of giant amphiphilic surfactants synthesized from bottlebrush copolymers composed of a soluble **nBuA** block and a carbazole-based organic semiconductor block (**CzBA**), of which the self-assembled structures exhibit spherical morphologies and can be stable over periods of months with CMCs below 54 nM.

By taking advantage of recent advances in controlled living radical polymerization and ring opening metathesis polymerization techniques, we have successfully applied an efficient and facile "grafting through" strategy to synthesis a series of well-defined bottlebrush diblock copolymers with different backbone length ratios. Carbazole moieties are found in many of the most common host materials used in OLEDs, capable of efficient energy transfer to a wide range of luminescent dopant molecules.[21] Based on this principle, we then proved the accessibility of incorporating a deep-blue dye **PAPOMA** with bright luminescence into the carbazole segment of our BBCPs without losing control over their composition and structure, giving giant polymer micelles with a quantum yield of unity after self-assembly. These macromonomers can also be 'doped' with a small amount of other semiconductor materials, if their functional groups are compatible with the Grubbs' catalysts, such as iridium-based and platinum-based compounds with emissions of tunable wavelengths.[183,184] Details about the design and realization of the "grafting through" synthetic route can be found in **Chapter 2.**

In **Chapter 3**, we have demonstrated a simple process that assembles these bottlebrush diblock copolymers into narrowly dispersed spherical micelles with very low CMCs (2.1 nM – 54 nM), although we disproved the hypothesis that the morphologies of micelles would be influenced by the backbone length ratios of BBCPs. These micelles showed a remarkably consistent diameter

in the range of 63 - 90 nm by DLS despite significant differences in the volume fraction of the core, indicating that the overall length of the bottlebrush chains was more critical in determining the micelle size. For the self-assembly of these BBCPs in films, disordered lamella morphologies were observed by TEM. More studies on improving the periodicity of these films and charactering their domain sizes using small-angle X-ray scattering (SAXS) or small-angle neutron scattering (SANS) are required. If good control over the ordering and domain sizes of these films can be realized, they can be further used as photonic crystals.

Above results demonstrate that organic semiconductors can be incorporated into soft-matter nanostructures formed from bottlebrush copolymers, taking advantage of their reduced chain entanglement to give highly regular self-assembled structures. Furthermore, it is possible to incorporate higher-order function into the organic semiconductor block to give functional micelles which remain self-assembled even at very low concentration, making these structures promising candidates for further studies in high-dilution applications such as drug delivery and bioimaging.

4.2 Future work

For the self-assembly of BBCPs in solution, additional factors to influence the morphologies of the micelles obtained should be investigated, such as the use of different self-assembly techniques (e.g. dialysis) and variations in the lengths of side-chains. Future studies will also examine the applications of self-assembled bottlebrush micelles formed from optoelectronic materials, as well as the hierarchical assembly of multiblock bottlebrushes to give higher-order nanoscale assemblies.

For example, bottlebrush diblock copolymers can be expanded to triblocks, into which another block such as polystyrene can be introduced. This will increase the complexity of

macromolecular architectures, leading to hierarchical self-assembled nanostructures. Further exploration on appropriate self-assembly techniques are required, such as the choice of selective solvents for different blocks.

For the self-assembly of BBCPs in films, methods to improve the lamellar order and more characterization techniques to measure the domain sizes can be further explored. For example, a more quantitative understanding with the influence of side chain length and backbone length on controlling the domain sizes can be further investigated.

References:

(1) Gennis, R. B. *Biomembranes Molecular Structure and Function*: Springer-Verlag, Heidelberg, 1989.
(2) Sinden, R. R. *DNA structure and Function*: Academic Press, San Diego, 2012.
(3) Timmermans, S. B. P. E.; van Hest, J. C. M. Self-Assembled Nanoreactors Based on Peptides and Proteins. *Curr. Opin. Colloid Interface Sci.* **2018,** *35*, 26.
(4) Ulijn, R. V.; Jerala, R. Peptide and Protein Nanotechnology into the 2020s: Beyond Biology. *Chem. Soc. Rev.* **2018,** *47* (10), 3391.
(5) Roy, S. S.; Dasgupta, R.; Bagchi, A. A Review on Phylogenetic Analysis: A Journey through Modern Era. *Comput. Mol. Biosci.* **2014,** *4* (3), 7.
(6) Ingber, D. E. Biological Design Principles that Guide Self-Organization, Emergence, and Hirerarchical Assembly: From Complexity to Tensegerity. *Unifying Themes In Complex Systems* **2000,** *1*, 269.
(7) Fong, C.; Le, T.; Drummond, C. J. Lyotropic Liquid Crystal Engineering–Ordered Nanostructured Small Molecule Amphiphile Self-Assembly Materials by Design. *Chem. Soc. Rev.* **2012,** *41* (3), 1297.
(8) Capito, R. M.; Azevedo, H. S.; Velichko, Y. S.; Mata, A.; Stupp, S. I. Self-Assembly of Large and Small Molecules into Hierarchically Ordered Sacs and Membranes. *Science* **2008,** *319* (5871), 1812.
(9) Israelachvili, J. N.; Mitchell, D. J.; Ninham, B. W. Theory of Self-Assembly of Hydrocarbon Amphiphiles into Micelles and Bilayers. *J. Chem. Soc. Faraday Trans.* **1976,** *72* (0), 1525.
(10) Israelachvili, J. N.; Mitchell, D. J.; Ninham, B. W. Theory of Self-Assembly of Lipid Bilayers and Vesicles. *Biochimica et Biophysica Acta (BBA) - Biomembranes* **1977,** *470* (2), 185.
(11) Nagarajan, R.; Ruckenstein, E. Theory of Surfactant Self-Assembly: A Predictive Molecular Thermodynamic Approach. *Langmuir* **1991,** *7* (12), 2934.
(12) Xie, E.; Cook, C. A.; Grayson, W. L.; Benkoski, J. J. Novel Surfactant Self-Assembly Process Generates Multi-Scale Surface Topographies for Stem Cell Growth and Differentiation. *Hemijska Industrija* **2018,** *72* (2), 69.
(13) Zhao, Y.; Yang, W.; Chen, C.; Wang, J.; Zhang, L.; Xu, H. Rational Design and Self-Assembly of Short Amphiphilic Peptides and Applications. *Curr. Opin. Colloid Interface Sci.* **2018,** *35*, 112.
(14) Wang, L.; Dong, S.; Hao, J. Recent Progress of Magnetic Surfactants: Self-Assembly, Properties and Functions. *Curr. Opin. Colloid Interface Sci.* **2018,** *35*, 81.
(15) Drummond, C. J.; Fong, C. Surfactant Self-Assembly Objects as Novel Drug Delivery Vehicles. *Curr. Opin. Colloid Interface Sci.* **1999,** *4* (6), 449.
(16) Mai, Y.; Eisenberg, A. Self-Assembly of Block Copolymers. *Chem. Soc. Rev.* **2012,** *41* (18), 5969.
(17) Morris, M. A. Directed Self-Assembly of Block Copolymers for Nanocircuitry Fabrication. *Microelectron. Eng.* **2015,** *132*, 207.
(18) Li, Z.; Loh, X. J. Water Soluble Polyhydroxyalkanoates: Future Materials for Therapeutic Applications. *Chem. Soc. Rev.* **2015,** *44* (10), 2865.

(19) Edrington, A. C.; Urbas, A. M.; DeRege, P.; Chen, C. X.; Swager, T. M.; Hadjichristidis, N.; Xenidou, M.; Fetters, L. J.; Joannopoulos, J. D.; Fink, Y.et al. Polymer-Based Photonic Crystals. *Adv. Mater.* **2001,** *13* (6), 421.
(20) Rösler, A.; Vandermeulen, G. W. M.; Klok, H.-A. Advanced Drug Delivery Devices via Self-Assembly of Amphiphilic Block Copolymers. *Adv. Drug Deliv. Rev.* **2012,** *64*, 270.
(21) Yan, K.; Li, H.; Li, P.; Zhu, H.; Shen, J.; Yi, C.; Wu, S.; Yeung, K. W. K.; Xu, Z.; Xu, H.et al. Self-Assembled Magnetic Fluorescent Polymeric Micelles for Magnetic Resonance and Optical Imaging. *Biomaterials* **2014,** *35* (1), 344.
(22) McKenzie, B. E.; Friedrich, H.; Wirix, M. J. M.; de Visser, J. F.; Monaghan, O. R.; Bomans, P. H. H.; Nudelman, F.; Holder, S. J.; Sommerdijk, N. A. J. M. Controlling Internal Pore Sizes in Bicontinuous Polymeric Nanospheres. *Angew. Chem. Int. Ed.* **2015,** *54* (8), 2457.
(23) Otulakowski, Ł.; Gadzinowski, M.; Slomkowski, S.; Basinska, T.; Forys, A.; Dworak, A.; Trzebicka, B. Micellisation of Polystyrene-*b*-Polyglycidol Copolymers in Water Solution. *Eur. Polym. J.* **2018,** *99*, 72.
(24) Zhang, Q.; Lin, J.; Wang, L.; Xu, Z. Theoretical Modeling and Simulations of Self-Assembly of Copolymers in Solution. *Prog. Polym. Sci.* **2017,** *75*, 1.
(25) Jia, L.; Albouy, P.-A.; Di Cicco, A.; Cao, A.; Li, M.-H. Self-Assembly of Amphiphilic Liquid Crystal Block Copolymers Containing a Cholesteryl Mesogen: Effects of Block Ratio and Solvent. *Polymer* **2011,** *52* (12), 2565.
(26) Yu, W.; Inam, M.; Jones, J. R.; Dove, A. P.; O'Reilly, R. K. Understanding the CDSA of Poly(lactide) Containing Triblock Copolymers. *Polym. Chem.* **2017,** *8* (36), 5504.
(27) Bates, F. S.; Fredrickson, G. H. Block Copolymer Thermodynamics: Theory and Experiment. *Annu. Rev. Phys. Chem.* **1990,** *41* (1), 525.
(28) Bates, F. S.; Fredrickson, G. H. Block Copolymers-Designer Soft Materials. *Physics Today* **2000,** *52*.
(29) Stadler, R.; Auschra, C.; Beckmann, J.; Krappe, U.; Voight-Martin, I.; Leibler, L. Morphology and Thermodynamics of Symmetric Poly(A-block-B-block-C) Triblock Copolymers. *Macromolecules* **1995,** *28* (9), 3080.
(30) Bates, F. S. Polymer-Polymer Phase Behavior. *Science* **1991,** *251* (4996), 898.
(31) Matsen, M. W. Thin Films of Block Copolymer. *J. Chem. Phys.* **1997,** *106* (18), 7781.
(32) Hamley, I. W. Ordering in Thin Films of Block Copolymers: Fundamentals to Potential Applications. *Prog. Polym. Sci.* **2009,** *34* (11), 1161.
(33) Leibler, L. Theory of Microphase Separation in Block Copolymers. *Macromolecules* **1980,** *13* (6), 1602.
(34) Fredrickson, G. H.; Helfand, E. Fluctuation Effects in the Theory of Microphase Separation in Block Copolymers. *J. Chem. Phys.* **1987,** *87* (1), 697.
(35) Han, C. D.; Baek, D. M.; Kim, K. J.; Ogawa, T.; Sakamoto, N.; Hashimoto, T. Effect of Volume Fraction on the Order-Disorder Transition in Low Molecular Weight Polystyrene-block-Polyisoprene Copolymers. 1. Order-Disorder Transition Temperature Determined by Rheological Measurements. *Macromolecules* **1995,** *28* (14), 5043.
(36) Shull, K. R. Mean-Field Theory of Block Copolymers: Bulk Melts, Surfaces, and Thin Films. *Macromolecules* **1992,** *25* (8), 2122.
(37) Vavasour, J. D.; Whitmore, M. D. Self-Consistent Mean Field Theory of the Microphases of Diblock Copolymers. *Macromolecules* **1992,** *25* (20), 5477.

(38) Almdal, K.; Koppi, K. A.; Bates, F. S.; Mortensen, K. Multiple Ordered Phases in a Block Copolymer Melt. *Macromolecules* **1992,** *25* (6), 1743.
(39) Helfand, E.; Wasserman, Z. R. Block Copolymer Theory. 5. Spherical Domains. *Macromolecules* **1978,** *11* (5), 960.
(40) Helfand, E.; Wasserman, Z. Block Copolymer Theory. 6. Cylindrical Domains. *Macromolecules* **1980,** *13* (4), 994.
(41) Hasegawa, H.; Tanaka, H.; Yamasaki, K.; Hashimoto, T. Bicontinuous Microdomain Morphology of Block Copolymers. 1. Tetrapod-Network Structure of Polystyrene-Polyisoprene Diblock Polymers. *Macromolecules* **1987,** *20* (7), 1651.
(42) Atanase, L.; Riess, G. Self-Assembly of Block and Graft Copolymers in Organic Solvents: An Overview of Recent Advances. *Polymers* **2018,** *10* (1), 62.
(43) Choucair, A.; Elsenberg, A. Control of Amphiphilic Block Copolymer Morphologies Using Solution Conditions. *Eur. Phys. J. E* **2003,** *10* (1), 37.
(44) Di Cola, E.; Lefebvre, C.; Deffieux, A.; Narayanan, T.; Borsali, R. Micellar Transformations of Poly(Styrene-*b*-Isoprene) Block Copolymers in Selective Solvents. *Soft Matter* **2009,** *5* (5), 1081.
(45) He, Y.; Li, Z.; Simon, P.; Lodge, T. P. Self-Assembly of Block Copolymer Micelles in an Ionic Liquid. *J. Am. Chem. Soc.* **2006,** *128* (8), 2745.
(46) Alexandridis, P.; Lindaman, B. *Amphiphilic Block Copolymers: Self-Assembly and Applications* Elsevier Science B. V., Amsterdam, 2000.
(47) Jain, S.; Bates, F. S. On the Origins of Morphological Complexity in Block Copolymer Surfactants. *Science* **2003,** *300* (5618), 460.
(48) Lund, R.; Willner, L.; Richter, D. *Kinetics of Block Copolymer Micelles Studied by Small-Angle Scattering Methods*: Springer-Verlag, Heidelberg, 2013.
(49) Kelley, E. G. *Synthesis, Solution Self-Assembly, and Characterization of Amphiphilic Block Polymers*: ProQuest LLC, Ph. D Thesis, University of Delaware, 2014.
(50) Shusharina, N. P.; Zhulina, E. B.; Dobrynin, A. V.; Rubinstein, M. Scaling Theory of Diblock Polyampholyte Solutions. *Macromolecules* **2005,** *38* (21), 8870.
(51) Svensson, B.; Olssen, U.; Alexandridis, P. Self-Assembly of Block Copolymers in Selective Solvents: Influence of Relative Block Size on Phase Behavior. *Langmuir* **2000,** *16* (17), 6839.
(52) Willner, L.; A., P.; Allgaier, J.; Monkenbush, M.; Lindner, P.; Richter, D. Micellization of Amphiphilic Diblock Copolymers: Corona Shape and Mean-Field to Scaling Crossover. *Europhys. Lett.* **2002,** *51* (6), 628.
(53) Zhang, L.; Eisenberg, A. Multiple Morphologies and Characteristics of "Crew-Cut" Micelle-like Aggregates of Polystyrene-*b*-Poly(acrylic acid) Diblock Copolymers in Aqueous Solutions. *J. Am. Chem. Soc.* **1996,** *118* (13), 3168.
(54) Cui, H.; Chen, Z.; Zhong, S.; Wooley, K. L.; Pochan, D. J. Block Copolymer Assembly via Kinetic Control. *Science* **2007,** *317* (5838), 647.
(55) Won, Y.-Y.; Davis, H. T.; Bates, F. S. Molecular Exchange in PEO−PB Micelles in Water. *Macromolecules* **2003,** *36* (3), 953.
(56) Jain, S.; Bates, F. S. Consequences of Nonergodicity in Aqueous Binary PEO−PB Micellar Dispersions. *Macromolecules* **2004,** *37* (4), 1511.
(57) Choi, S.-H.; Bates, F. S.; Lodge, T. P. Molecular Exchange in Ordered Diblock Copolymer Micelles. *Macromolecules* **2011,** *44* (9), 3594.

(58) Rharbi, Y. Fusion and Fragmentation Dynamics at Equilibrium in Triblock Copolymer Micelles. *Macromolecules* **2012,** *45* (24), 9823.
(59) Lund, R.; Willner, L.; Richter, D.; Dormidontova, E. E. Equilibrium Chain Exchange Kinetics of Diblock Copolymer Micelles: Tuning and Logarithmic Relaxation. *Macromolecules* **2006,** *39* (13), 4566.
(60) Murphy, R. P.; Kelley, E. G.; Rogers, S. A.; Sullivan, M. O.; Epps, T. H. Unlocking Chain Exchange in Highly Amphiphilic Block Polymer Micellar Systems: Influence of Agitation. *ACS Macro Lett.* **2014,** *3* (11), 1106.
(61) Ma, Y.; Lodge, T. P. Chain Exchange Kinetics in Diblock Copolymer Micelles in Ionic Liquids: The Role of χ. *Macromolecules* **2016,** *49* (24), 9542.
(62) Wang, E.; Lu, J.; Bates, F. S.; Lodge, T. P. Effect of Corona Block Length on the Structure and Chain Exchange Kinetics of Block Copolymer Micelles. *Macromolecules* **2018,** *51* (10), 3563.
(63) Zhao, D.; Ma, Y.; Lodge, T. P. Exchange Kinetics for a Single Block Copolymer in Micelles of Two Different Sizes. *Macromolecules* **2018,** *51* (6), 2312.
(64) Zinn, T.; Willner, L.; Pipich, V.; Richter, D.; Lund, R. Molecular Exchange Kinetics of Micelles: Corona Chain Length Dependence. *ACS Macro Lett.* **2016,** *5* (7), 884.
(65) Prhashanna, A.; Dormidontova, E. E. Tadpole and Mixed Linear/Tadpole Micelles of Diblock Copolymers: Thermodynamics and Chain Exchange Kinetics. *Macromolecules* **2017,** *50* (4), 1740.
(66) Dormidontova, E. E. Micellization Kinetics in Block Copolymer Solutions: Scaling Model. *Macromolecules* **1999,** *32* (22), 7630.
(67) Sun, X.-L.; Liu, D.-M.; Wang, P.; Tan, J.-L.; Li, K.-K.; Deng, L.; Wan, W.-M. Expanding the Morphology Library of Block Copolymer Self-Assemblies with Clews of Tubules. *Chem. Commun.* **2017,** *53* (36), 5005.
(68) Ren, K.; Perez-Mercader, J. Light-induced Evolution of Microaggregates: Transformation to Vesicles, Cyclic Growth and Collapse and Vesicle Fusion. *Polym. Chem.* **2018,** *9* (26), 3594.
(69) Riess, G. Micellization of Block Copolymers. *Prog. Polym. Sci.* **2003,** *28* (7), 1107.
(70) Cruz, M.; Xu, J.; Guerin, G.; Manners, I.; Winnik, M. A. Visualizing Nanoscale Coronal Segregation in Rod-Like Micelles Formed by Co-Assembly of Binary Block Copolymer Blends. *Macromol. Rapid Commun.* **2018,** *39* (22), 1800397.
(71) Zhang, L. Multiple Morphologies of "Crew-Cut" Aggregates of Polystyrene-b-poly(acrylic acid) Block Copolymers. *Science* **1995,** *268* (5218), 1728.
(72) Takahashi, R.; Narayanan, T.; Yusa, S.-i.; Sato, T. Kinetics of Morphological Transition between Cylindrical and Spherical Micelles in a Mixture of Anionic–Neutral and Cationic–Neutral Block Copolymers Studied by Time-Resolved SAXS and USAXS. *Macromolecules* **2018,** *51* (10), 3654.
(73) Chen, Q.; Wang, J.; Shao, L. Nanoparticle-Loaded Cylindrical Micelles from Nanopore Extrusion of Block Copolymer Spherical Micelles. *Macromol. Rapid Commun.* **2013,** *34* (23-24), 1850.
(74) Kinning, D. J.; Winey, K. I.; Thomas, E. L. Structural Transitions from Spherical to Nonspherical Micelles in Blends of Poly(styrene-butadiene) Diblock Copolymer and Polystyrene Homopolymers. *Macromolecules* **1988,** *21* (12), 3502.

(75) Liu, G.; Lv, L.; Chen, C.; Hu, X.; Ji, J. Biocompatible Poly(D,L-lactide)-block-Poly(2-methacryloyloxyethylphosphorylcholine) Micelles for Drug Delivery. *Macromol. Chem. Phys.* **2011,** *212* (6), 643.
(76) Lü, J.; Liu, B.; Shi, B.; Lü, C. Coordination-induced Assemblies of Quantum Dots in Amphiphilic Thermo-Responsive Block Copolymer Micelles: Morphologies, Optical Properties and Applications. *Polym. Chem.* **2018,** *9* (22), 3158.
(77) Blanazs, A.; Armes, S. P.; Ryan, A. J. Self-Assembled Block Copolymer Aggregates: From Micelles to Vesicles and their Biological Applications. *Macromol. Rapid Commun.* **2009,** *30* (4-5), 267.
(78) Qiu, H.; Hudson, Z. M.; Winnik, M. A.; Manners, I. Multidimensional Hierarchical Self-Assembly of Amphiphilic Cylindrical Block Comicelles. *Science* **2015,** *347* (6228), 1329.
(79) Hudson, Z. M.; Qian, J.; Boott, C. E.; Winnik, M. A.; Manners, I. Fluorous Cylindrical Micelles of Controlled Length by Crystallization-Driven Self-Assembly of Block Copolymers in Fluorinated Media. *ACS Macro Lett.* **2015,** *4* (2), 187.
(80) Majdanski, T. C.; Pretzel, D.; Czaplewska, J. A.; Vitz, J.; Sungur, P.; Höppener, S.; Schubert, S.; Schacher, F. H.; Schubert, U. S.; Gottschaldt, M. Spherical and Worm-Like Micelles from Fructose-Functionalized Polyether Block Copolymers. *Macromolecular Bioscience* **2018,** *18* (4), 1700396.
(81) Pawar, K.; Kutcherlapati, S. N. R.; Yeole, N.; Hundiwale, D.; Jana, T. Vesicular and Micellar Self-Assembly of Stimuli-Responsive Poly(N-isopropyl acrylamide-b-9-anthracene methyl methacrylate) Amphiphilic Diblock Copolymers. *J. Appl. Polym. Sci.* **2018,** *135* (28), 46474.
(82) Voevodin, A.; Campos, L. M.; Roy, X. Multifunctional Vesicles from a Self-assembled Cluster-Containing Diblock Copolymer. *J. Am. Chem. Soc.* **2018,** *140* (16), 5607.
(83) Du, J.; Tang, Y.; Lewis, A. L.; Armes, S. P. pH-Sensitive Vesicles Based on a Biocompatible Zwitterionic Diblock Copolymer. *J. Am. Chem. Soc.* **2005,** *127* (51), 17982.
(84) Hu, Y.; Chen, Y.; Du, J. Evolution of Diverse Higher-order Membrane Structures of Block Copolymer Vesicles. *Polym. Chem.* **2019**.
(85) Tyrrell, Z. L.; Shen, Y.; Radosz, M. Fabrication of Micellar Nanoparticles for Drug Delivery Through the Self-Assembly of Block Copolymers. *Prog. Polym. Sci.* **2010,** *35* (9), 1128.
(86) Bouix, M.; Guozi, J.; Charleux, B.; Vairon, J.-P.; Philippe, P. Synthesis of Amphiphilic Polyelectrolyte Block Copolymers using "Living" Radical Polymerization. Application as Stabilizers in Emulsion Polymerization. *Macromol. Rapid Commun.* **1998,** *19* (4), 209.
(87) Vriezema, D. M.; Aragonès, M. C.; Elemans, J. A. A. W.; Cornelissen, J. J. L. M.; Rowan, A. E.; Nolte, R. J. M. Self-Assembled Nanoreactors. *Chem. Rev.* **2005,** *105* (4), 1445.
(88) Taylor, K. C.; Nasr-EI-Din, H. A. Water-Soluble Hydrophobically Associating Polymers for Improved Oil Recovery: A Literature Review. *J Petrol. Sci. Eng.* **1998,** *19* (3-4), 265.
(89) Kim, J. K.; Yang, S. Y.; Lee, Y.; Kim, Y. Functional Nanomaterials Based on Block Copolymer Self-Assembly. *Prog. Polym. Sci.* **2010,** *35* (11), 1325.
(90) Choudhury, S.; Fischer, D.; Formanek, P.; Stamm, M.; Ionov, L. Phase Inversion Strategy to Fabricate Porous Carbon for Li-S Batteries via Block Copolymer Self-Assembly. *ADV MATER INTERFACES* **2018,** *5* (5), 1701116.
(91) Tamate, R.; Hashimoto, K.; Ueki, T.; Watanabe, M. Block Copolymer Self-Assembly in Ionic Liquids. *PCCP* **2018,** *20* (39), 25123.

(92) Strebhardt, K. Paul Ehrlich's Magic Bullet Concept: 100 Years of Progress. *Nat. Rev. Cancer* **2008,** *8* (6), 473.
(93) Cabral, H.; Miyata, K.; Osada, K.; Kataoka, K. Block Copolymer Micelles in Nanomedicine Applications. *Chem. Rev.* **2018,** *118* (14), 6844.
(94) Sharma, A.; Sharma, U. S. Liposomes in Drug Delivery: Progress and Limitations. *Int. J. Pharm.* **1997,** *154* (2), 123.
(95) Kabanov, A. V.; Nazarova, I. R.; Astafieva, I. V.; Batrakova, E. V.; Alakhov, V. Y.; Yaroslavov, A. A.; Kabanov, V. A. Micelle Formation and Solubilization of Fluorescent Probes in Poly(oxyethylene-b-oxypropylene-b-oxyethylene) Solutions. *Macromolecules* **1995,** *28* (7), 2303.
(96) Harada, A.; Kataoka, K. Novel Polyion Complex Micelles Entrapping Enzyme Molecules in the Core: Preparation of Narrowly-Distributed Micelles from Lysozyme and Poly(ethylene glycol)−Poly(aspartic acid) Block Copolymer in Aqueous Medium. *Macromolecules* **1998,** *31* (2), 288.
(97) Wang, J.; Mao, W.; Lock, L. L.; Tang, J.; Sui, M.; Sun, W.; Cui, H.; Xu, D.; Shen, Y. The Role of Micelle Size in Tumor Accumulation, Penetration, and Treatment. *ACS Nano* **2015,** *9* (7), 7195.
(98) Tang, L.; Yang, X.; Yin, Q.; Cai, K.; Wang, H.; Chaudhury, I.; Yao, C.; Zhou, Q.; Kwon, M.; Hartman, J. A.et al. Investigating the Optimal Size of Anticancer Nanomedicine. *Proc. Natl. Acad. Sci.* **2014,** *111* (43), 15344.
(99) Matsumoto, Y.; Nichols, J. W.; Toh, K.; Nomoto, T.; Cabral, H.; Miura, Y.; Christie, R. J.; Yamada, N.; Ogura, T.; Kano, M. R.et al. Vascular Bursts Enhance Permeability of Tumour Blood Vessels and Improve Nanoparticle Delivery. *Nat. Nanotech.* **2016,** *11*, 533.
(100) Adams, M. L.; Lavasanifar, A.; Kwon, G. S. Amphiphilic Block Copolymers for Drug Delivery. *J. Pharm. Sci.* **2003,** *92* (7), 1343.
(101) Zalipsky, S. Chemistry of Polyethylene Glycol Conjugates with Biologically Active Molecules. *Adv. Drug Deliv. Rev.* **1995,** *16* (2-3), 157.
(102) Kainthan, R. K.; Hester, S. R.; Levin, E.; Devine, D. V.; Brooks, D. E. In Vitro Biological Evaluation of High Molecular Weight Hyperbranched Polyglycerols. *Biomaterials* **2007,** *28* (31), 4581.
(103) Ravin, H. A.; Seligman, A. M.; Fine, J. Polyvinyl Pyrrolidone as a Plasma Expander. *N Engl J Med* **1952,** *247* (24), 921.
(104) Takeuchi, H.; Kojima, H.; Yamamoto, H.; Kawashima, Y. Evaluation of Circulation Profiles of Liposomes Coated with Hydrophilic Polymers Having Different Molecular Weights in Rats. *J. Controlled Release* **2001,** *75* (1-2), 83.
(105) Torchilin, V. P.; Shtilman, M. I.; Trubetskoy, V. S.; Whiteman, K.; Milstein, A. M. Amphiphilic Vinyl Polymers Effectively Prolong Liposome Circulation Time in Vivo. *Biochimica et Biophysica Acta (BBA) - Biomembranes* **1994,** *1195* (1), 181.
(106) Whiteman, K. R.; Subr, V.; Ulbrich, K.; Torchilin, V. P. Poly(HPMA)-Coated Liposomes Demonstrate Prolonged Circulation in Mice. *J. Liposome Res.* **2001,** *11* (2-3), 153.
(107) Hoogenboom, R. Poly(2-oxazoline)s: A Polymer Class with Numerous Potential Applications. *Angew. Chem. Int. Ed.* **2009,** *48* (43), 7978.
(108) Inoue, T.; Chen, G.; Nakamae, K.; Hoffman, A. S. An AB Block Copolymer of Oligo(methyl methacrylate) and Poly(acrylic acid) for Micellar Delivery of Hydrophobic Drugs. *J. Controlled Release* **1998,** *51* (2), 221.

(109) Cai, S.; Thati, S.; Bagby, T. R.; Diab, H.-M.; Davies, N. M.; Cohen, M. S.; Forrest, M. L. Localized Doxorubicin Chemotherapy with a Biopolymeric Nanocarrier Improves Survival and Reduces Toxicity in Xenografts of Human Breast Cancer. *J. Controlled Release* **2010,** *146* (2), 212.
(110) Kabanov, A. V.; Chekhonin, V. P.; Alakhov, V. Y.; Batrakova, E. V.; Lebedev, A. S.; Melik-Nubarov, N. S.; Arzhakov, S. A.; Levashov, A. V.; Morozov, G. V.; Severin, E. S.et al. The Neuroleptic Activity of Haloperidol Increases After its Solubilization in Surfactant Micelles. Micelles as Microcontainers for Drug Targeting. *FEBS Lett.* **1898,** *258* (2), 343.
(111) Yokoyama, M.; Inoue, S.; Kataoka, K.; Yui, N.; Okano, T.; Sakurai, Y. Molecular Design for Missile Drug: Synthesis of Adriamycin Conjugated with Immunoglobulin G using Poly (ethylene glycol) - block - Poly (aspartic acid) as Intermediate Carrier. *Die Makromolekulare Chemie* **1989,** *190* (9), 2041.
(112) Klingelhöfer, S.; Heitz, W.; Greiner, A.; Oestreich, S.; Förster, S.; Antonietti, M. Preparation of Palladium Colloids in Block Copolymer Micelles and Their Use for the Catalysis of the Heck Reaction. *J. Am. Chem. Soc.* **1997,** *119* (42), 10116.
(113) Yu, W.-Y.; Liu, H.-F.; Tao, Q. Modification of Metal Cations to Metal Clusters in Liquid Medium. *Chem. Commun.* **1996,** *0* (15), 1773.
(114) Wu, B.; Zhang, J.; Wei, Z.; Cai, S.; Liu, Z. Chemical Alignment of Oxidatively Shortened Single-Walled Carbon Nanotubes on Silver Surface. *J. Phys. Chem. B* **2001,** *105* (22), 5075.
(115) Broz, P.; Driamov, S.; Ziegler, J.; Ben-Haim, N.; Marsch, S.; Meier, W.; Hunziker, P. Toward Intelligent Nanosize Bioreactors: A pH-Switchable, Channel-Equipped, Functional Polymer Nanocontainer. *Nano Lett.* **2006,** *6* (10), 2349.
(116) Cummins, C.; Morris, M. A. Using Block Copolymers as Infiltration Sites for Development of Future Nanoelectronic Devices: Achievements, Barriers, and Opportunities. *Microelectron. Eng.* **2018,** *195*, 74.
(117) Böhme, S.; Arias-Zapata, J.; Garnier, J.; Girardot, C.; Legrain, A.; Zelsmann, M. Annealing Treatments of Cylindrical Siloxane-Based Block Copolymers Optimized for Nanomanufacturing. *Micro and Nano Engineering* **2018,** *1*, 56.
(118) Krishnan, M. R.; Lu, K.-Y.; Chiu, W.-Y.; Chen, I.-C.; Lin, J.-W.; Lo, T.-Y.; Georgopanos, P.; Avgeropoulos, A.; Lee, M.-C.; Ho, R.-M. Directed Self-Assembly of Star-Block Copolymers by Topographic Nanopatterns through Nucleation and Growth Mechanism. *Small* **2018,** *14* (16), 1704005.
(119) Jeong, S.-J.; Kim, J. Y.; Kim, B. H.; Moon, H.-S.; Kim, S. O. Directed Self-Assembly of Block Copolymers for Next Generation Nanolithography. *Mater. Today* **2013,** *16* (12), 468.
(120) Park, M.; Harrison, C.; Chaikin, P. M.; Register, R. A.; Adamson, D. H. Block Copolymer Lithography: Periodic Arrays of ~10^{11} Holes in 1 Square Centimeter. *Science* **1997,** *276* (5317), 1401.
(121) Rempp, P.; Lutz, P.; Masson, P.; Chaumont, P. Macromonomers: A New Class of Polymeric Intermediates in Macromolecular Synthesis - II - Homo- and Copolymerization. *Die Makromolekulare Chemie* **1985,** *13* (s19851), 47.
(122) Börner, H. G.; Duran, D.; Matyjaszewski, K.; da Silva, M.; Sheiko, S. S. Synthesis of Molecular Brushes with Gradient in Grafting Density by Atom Transfer Polymerization. *Macromolecules* **2002,** *35* (9), 3387.
(123) Bolton, J.; Rzayev, J. Synthesis and Melt Self-Assembly of PS–PMMA–PLA Triblock Bottlebrush Copolymers. *Macromolecules* **2014,** *47* (9), 2864.

(124) Gadwal, I.; Rao, J.; Baettig, J.; Khan, A. Functionalized Molecular Bottlebrushes. *Macromolecules* **2014,** *47* (1), 35.
(125) De, S. Efficient Synthesis of Multifunctional Polymers via Thiol–Epoxy "Click" Chemistry. *Chem. Commun.* **2012,** *48* (25), 3130.
(126) Xia, Y.; Kornfield, J. A.; Grubbs, R. H. Efficient Synthesis of Narrowly Dispersed Brush Polymers via Living Ring-Opening Metathesis Polymerization of Macromonomers. *Macromolecules* **2009,** *42* (11), 3761.
(127) Choi, T.-L.; Grubbs, R. H. Controlled Living Ring‐Opening‐Metathesis Polymerization by a Fast‐Initiating Ruthenium Catalyst. *Angew. Chem.* **2003,** *115* (15), 1785.
(128) Wu, D.; Yang, Y.; Cheng, X.; Liu, L.; Tian, J.; ZhaO, H. Mixed Molecular Brushes with PLLA and PS Side Chains Prepared by AGET ATRP and Ring-Opening Polymerization. *Macromolecules* **2006,** *39* (22), 7513.
(129) Miki, K.; Kimura, A.; Oride, K.; Kuramochi, Y.; Matsuoka, H.; Harada, H.; Hiraoka, M.; Ohe, K. High-Contrast Fluorescence Imaging of Tumors In Vivo Using Nanoparticles of Amphiphilic Brush-Like Copolymers Produced by ROMP. *Angew. Chem.* **2011,** *50* (29), 6567.
(130) Sankaran, N. B.; Rys, A. Z.; Nassif, R.; Nayak, M. K.; Metera, K.; Chen, B.; Bazzi, H. S.; Sleiman, H. F. Ring-Opening Metathesis Polymers for Biodetection and Signal Amplification: Synthesis and Self-Assembly. *Macromolecules* **2010,** *43* (13), 5530.
(131) Moad, G.; Rizzardo, E.; Thang, S. H. Radical Addition–Fragmentation Chemistry in Polymer Synthesis. *Polymer* **2008,** *49* (5), 1079.
(132) Matyjaszewski, K. Atom Transfer Radical Polymerization (ATRP): Current Status and Future Perspectives. *Macromolecules* **2012,** *45* (10), 4015.
(133) Matyjaszewski, K.; Xia, J. Atom Transfer Radical Polymerization. *Chem. Rev.* **2001,** *101* (9), 2921.
(134) Konkolewicz, D.; Wang, Y.; Zhong, M.; Krys, P.; Isse, A. A.; Gennaro, A.; Matyjaszewski, K. Reversible-Deactivation Radical Polymerization in the Presence of Metallic Copper. A Critical Assessment of the SARA ATRP and SET-LRP Mechanisms. *Macromolecules* **2013,** *46* (22), 8749.
(135) Bielawski, C. W.; Grubbs, R. H. Living Ring-Opening Metathesis Polymerization. *Prog. Polym. Sci.* **2007,** *32* (1), 1.
(136) Zhou, L. Well-Defined Molecular Brushes: Synthesis by a "Grafting Through" Strategy and Self Assembly into Complicated Hierarchical Nanostructures. *All Theses and Dissertations (ETDs). 212., PhD Thesis, Washington University in St. Louis* **2011**.
(137) Sveinbjörnsson, B. R.; Weitekamp, R. A.; Miyake, G. M.; Xia, Y.; Atwater, H. A.; Grubbs, R. H. Rapid Self-Assembly of Brush Block Copolymers to Photonic Crystals. *Proc. Natl. Acad. Sci.* **2012,** *109* (36), 14332.
(138) Trefonas, P.; Thackeray, J. W.; Sun, G.; Cho, S.; Clark, C.; Verkhoturov, S. V.; Eller, M. J.; Li, A.; Pavia-Sanders, A.; Schweikert, E. A.et al. Bottom-up/Top-down, High-Resolution, High-Throughput Lithography using Vertically Assembled Block Bottle Brush Polymers. *J Micro Nanolithogr MEMS MOEMS* **2013,** *12* (4), 043006.
(139) Miki, K.; Kimura, A.; Oride, K.; Kuramochi, Y.; Matsuoka, H.; Harada, H.; Hiraoka, M.; Ohe, K. High-Contrast Fluorescence Imaging of Tumors In Vivo Using Nanoparticles of Amphiphilic Brush-Like Copolymers Produced by ROMP. *Angew. Chem.* **2011,** *50* (29), 6567.

(140) Johnson, J. A.; Lu, Y. Y.; Burts, A. O.; Xia, Y.; Durrell, A. C.; Tirrell, D. A.; Grubbs, R. H. Drug-Loaded, Bivalent-Bottle-Brush Polymers by Graft-through ROMP. *Macromolecules* **2010,** *43* (24), 10326.
(141) Lin, S. Y.; Fleming, J. G.; Hetherington, D. L.; Smith, B. K.; Biswas, R.; Sigalas, K. M. H., M. M. ; Zubrzycki, W.; Kurtz, S. R.; Bur, J. A Three-Dimensional Photonic Crystal Operating at Infrared Wavelengths. *Nature* **1998,** *394* (6690), 251.
(142) Masuda, H.; Ohya, M.; Asoh, H.; Nakao, M.; Nohtomi, M.; Tamamura, T. Photonic Crystal Using Anodic Porous Alumina. *Jpn. J. Appl. Phys* **1999,** *38* (12a), L1403.
(143) Liberman-Martin, A. L.; Chu, C. K.; Grubbs, R. H. Application of Bottlebrush Block Copolymers as Photonic Crystals. *Macromol. Rapid Commun.* **2017,** *38* (13), 1700058.
(144) Xia, Y.; Olsen, B. D.; Kornfield, J. A.; Grubbs, R. H. Efficient Synthesis of Narrowly Dispersed Brush Copolymers and Study of Their Assemblies: The Importance of Side Chain Arrangement. *J. Am. Chem. Soc.* **2009,** *131* (51), 18525.
(145) Miyake, G. M.; Weitekamp, R. A.; Piunova, V. A.; Grubbs, R. H. Synthesis of Isocyanate-Based Brush Block Copolymers and Their Rapid Self-Assembly to Infrared-Reflecting Photonic Crystals. *J. Am. Chem. Soc.* **2012,** *134* (34), 14249.
(146) Pelras, T.; Mahon, C. S.; Müllner, M. Synthesis and Applications of Compartmentalised Molecular Polymer Brushes. *Angew. Chem.* **2018,** *57* (24), 6982.
(147) Sankaran, N. B. Ring-Opening Metathesis Polymers for Biodetection and Signal Amplification: Synthesis and Self-Assembly. *Macromolecules* **2010,** *43* (13), 5530.
(148) Tonge, C. M.; Sauvé, E. R.; Cheng, S.; Howard, T. A.; Hudson, Z. M. Multiblock Bottlebrush Nanofibers from Organic Electronic Materials. *J. Am. Chem. Soc.* **2018,** *140* (37), 11599.
(149) Sivula, K.; Ball, Z. T.; Watanabe, N.; Fréchet, J. M. J. Amphiphilic Diblock Copolymer Compatibilizers and Their Effect on the Morphology and Performance of Polythiophene:Fullerene Solar Cells. *Adv. Mater.* **2006,** *18* (2), 206.
(150) Teo, Y. C.; Xia, Y. Importance of Macromonomer Quality in the Ring-Opening Metathesis Polymerization of Macromonomers. *Macromolecules* **2015,** *48* (16), 5656.
(151) Hein, J. E.; Fokin, V. V. Copper-Catalyzed Azide–Alkyne Cycloaddition (CuAAC) and Beyond: New Reactivity of Copper(i) Acetylides. *Chem. Soc. Rev.* **2010,** *39* (4), 1302.
(152) Song, D.-P.; Cheng, L.; Nicholas, C. S.; Xie, W.; Li, S.; Lu, X.; Gido, S.; Lee, J.-H.; Watkins, J. J. Large-Volume Self-Organization of Polymer/Nanoparticle Hybrids with Millimeter-Scale Grain Sizes Using Brush Block Copolymers. *J. Am. Chem. Soc.* **2015,** *137* (39), 12510.
(153) Vougioukalakis, G. C.; Grubbs, R. H. Ruthenium-Based Olefin Metathesis Catalysts Coordinated with Unsymmetrical N-Heterocyclic Carbene Ligands: Synthesis, Structure, and Catalytic Activity. *Chem. Eur. J* **2008,** *14* (25), 7545.
(154) Love, J. A.; Morgan, J. P.; Trnka, T. M.; Grubbs, R. H. A Practical and Highly Active Ruthenium‐Based Catalyst that Effects the Cross Metathesis of Acrylonitrile. *Angew. Chem.* **2002,** *114* (21), 4207.
(155) Vougioukalakis, G. C.; Grubbs, R. H. Ruthenium-Based Heterocyclic Carbene-Coordinated Olefin Metathesis Catalysts. *Chem. Rev.* **2010,** *110* (3), 1746.
(156) Kaeser, A.; Fischer, I.; Abbel, R.; Besenius, P.; Dasgupta, D.; Gillisen, M. A. J.; Portale, G.; Stevens, A. L.; Herz, L. M.; Schenning, A. P. H. J. Side Chains Control Dynamics and Self-Sorting in Fluorescent Organic Nanoparticles. *ACS Nano* **2013,** *7* (1), 408.

(157) Radzinski, S. C.; Foster, J. C.; Chapleski Jr, R. C.; Troya, D.; Matson, J. B. Bottlebrush Polymer Synthesis by Ring-Opening Metathesis Polymerization: The Significance of the Anchor Group. *J. Am. Chem. Soc.* **2016,** *138* (22), 6998.
(158) Cheng, C.; Khoshdel, E.; Karen, W. L. ATRP from a Norbornenyl-Functionalized Initiator: Balancing of Complementary Reactivity for the Preparation of α-Norbornenyl Macromonomers/ω-Haloalkyl Macroinitiators. *Macromolecules* **2005,** *38* (23), 9455.
(159) Patton, D. L.; Advincula, R. C. A Versatile Synthetic Route to Macromonomers via RAFT Polymerization. *Macromolecules* **2006,** *39* (25), 8674.
(160) Tamoto, N.; Adachi, C.; Nagai, K. Electroluminescence of 1,3,4-Oxadiazole and Triphenylamine-Containing Molecules as an Emitter in Organic Multilayer Light Emitting Diodes. *Chem. Mater.* **1997,** *9* (5), 1077.
(161) Tao, Y.; Wang, Q.; Shang, Y.; Yang, C.; Ao, L.; Qin, J.; Ma, D.; Shuai, Z. Multifunctional Bipolar Triphenylamine/Oxadiazole Derivatives: Highly Efficient Blue Fluorescence, Red Phosphorescence Host and Two-Color Based White OLEDs. *Chem. Commun.* **2009,** (1), 77.
(162) Sanford, M. S.; Love, J. A.; Grubbs, R. H. A Versatile Precursor for the Synthesis of New Ruthenium Olefin Metathesis Catalysts. *Organometallics* **2001,** *20* (25), 5314.
(163) Sauvé, E. R.; Tonge, C. M.; Paisley, N. R.; Cheng, S.; Hudson, Z. M. Cu(0)-RDRP of Acrylates Based on P-type Organic Semiconductors. *Polym. Chem.* **2018,** *9* (12), 1397.
(164) Tonge, C. M.; Hudson, Z. M. manuscript in preparation. **2018**.
(165) Samanta, S. R.; Levere, M. E.; Percec, V. SET-LRP of Hydrophobic and Hydrophilic Acrylates in Trifluoroethanol. *Polym. Chem.* **2013,** *4* (11), 3212.
(166) Huang, K.; Jacobs, A.; Rzayev, J. De Novo Synthesis and Cellular Uptake of Organic Nanocapsules with Tunable Surface Chemistry. *Biomacromolecules* **2011,** *12* (6), 2327.
(167) Fouz, M. F.; Mukumoto, K.; Averick, S.; Molinar, O.; McCartney, B. M.; Matyjaszewski, K.; Armitage, B. A.; Das, S. R. Bright Fluorescent Nanotags from Bottlebrush Polymers with DNA-Tipped Bristles. *ACS Cent. Sci.* **2015,** *1* (8), 431.
(168) Macfarlane, R. J.; Kim, B.; Lee, B.; Weitekamp, R. A.; Bates, C. M.; Lee, S. F.; Chang, A. B.; Delaney, K. T.; Fredrickson, G. H.; Atwater, H. A.et al. Improving Brush Polymer Infrared One-Dimensional Photonic Crystals via Linear Polymer Additives. *J. Am. Chem. Soc.* **2014,** *136* (50), 17374.
(169) Xu, R. Light scattering: A Review of Particle Characterization Applications. *Particuology* **2015,** *18*, 11.
(170) Berne, B. J.; Pecora, R. *Dynamic Light Scattering with Applications to Chemistry, Biology, and Physics.* : Dover Publications Inc., Minneola, 2000.
(171) Goldburg, W. I. Dynamic Light Scattering. *Am. J. Phys.* **1999,** *67* (12), 1152.
(172) Frisken, B. J. Revisiting the Method of Cumulants for the Analysis of Dynamic Light-Scattering Data. *Appl. Opt.* **2001,** *40* (24), 4087.
(173) Fesenko, O.; Yatsenko, L. *Nanophysics, Nanomaterials, Interface Studies, and Applications*: Springer, Gewerbestrasse, 2016.
(174) Schmitz, K. S. *Introduction to Dynamic Light Scattering by Macromolecules*: Academic Press Inc., San Diego, 1990.
(175) Kim, S. H.; Tan, J. P. K.; Nederberg, F.; Fukushima, K.; Colson, J.; Yang, C.; Nelson, A.; Yang, Y.-Y.; Hedrick, J. L. Hydrogen Bonding-Enhanced Micelle Assemblies for Drug Delivery. *Biomaterials* **2010,** *31* (31), 8063.

(176) Williams, D. B.; Carter, C. B. *Transmission Electron Microscopy: Basics*: Springer, San Diego, 1996.
(177) Danino, D. Cryo-TEM of Soft Molecular Assemblies. *Curr. Opin. Colloid Interface Sci.* **2012,** *17* (6), 316.
(178) Smith, M. F.; Langmore, J. P. Quantitation of Molecular Densities by Cryo-electron Microscopy: Determination of the Radial Density Distribution of Tobacco Mosaic Virus. *J. Mol. Biol.* **1992,** *226* (3), 763.
(179) Crassous, J. J.; Ballauff, M.; Drechsler, M.; Schmidt, J.; Talmon, Y. Imaging the Volume Transition in Thermosensitive Core−Shell Particles by Cryo-Transmission Electron Microscopy. *Langmuir* **2006,** *22* (6), 2403.
(180) Fenyves, R.; Schmutz, M.; Horner, I. J.; Bright, F. V.; Rzayev, J. Aqueous Self-Assembly of Giant Bottlebrush Block Copolymer Surfactants as Shape-Tunable Building Blocks. *J. Am. Chem. Soc.* **2014,** *136* (21), 7762.
(181) Hsiao, L.; Dunning, H. N.; Lorenz, P. B. Critical Micelle Concentrations of Polyoxyethylated Non-ionic Detergents. *The Journal of Physical Chemistry* **1956,** *60* (5), 657.
(182) Tonge, C. M.; Sauvé, E. R.; Paisley, N. R.; Heyes, J. E.; Hudson, Z. M. Polymerization of Acrylates Based on N-Type Organic Semiconductors using Cu(0)-RDRP. *Polym. Chem.* **2018,** *9* (24), 3359.
(183) Mayder, D. M.; Thompson, K. A.; Christopherson, C. J.; Paisley, N. R.; Hudson, Z. M. An Efficient Room-Temperature Synthesis of Highly Phosphorescent Styrenic Pt(ii) Complexes and Their Polymerization by ATRP. *Polym. Chem.* **2018,** *9* (45), 5418.
(184) Christopherson, C. J.; Hackett, Z. S.; Sauvé, E. R.; Paisley, N. R.; Tonge, C. M.; Mayder, D. M.; Hudson, Z. M. Synthesis of Phosphorescent Iridium-Containing Acrylic Monomers and Their Room-Temperature Polymerization by Cu(0)-RDRP. *J. Polym. Sci., Part A: Polym. Chem.* **2018,** *56* (22), 2539.